Purification of Human Recombinant Naglu from Sf9 cells and Uptake Studies with MPS IIIB Fibroblasts

by

Rhea Ashmead
B.Sc., University of Victoria, 2016

A Thesis Submitted in Partial Fulfillment
of the Requirements for the Degree of

MASTER OF SCIENCE

in the Department of Biology

Supervisory Committee

Purification of Human Recombinant Naglu from Sf9 cells and Uptake Studies with MPS IIIB Fibroblasts

by

Rhea Ashmead
B.Sc., University of Victoria, 2016

Supervisory Committee

Dr. Francis Choy, (Department of Biology)
Supervisor

Dr. Raad Nashmi, (Deparment of Biology)
Departmental Member

Dr. Patrick Walter, (Deparment of Biology)
Departmental Member

Abstract

Supervisory Committee
Dr. Francis Choy
Supervisor
Dr. Raad Nashmi
Departmental Member
Dr. Patrick Walter
Departmental Member

Mucopolysaccharidosis IIIB (MPS IIIB) is a rare, metabolic disorder that results from a deficiency in the lysosomal hydrolase, α-N-acetylglucosaminidase (Naglu). Naglu is a housekeeping enzyme involved in the degradation pathway of heparan sulfate. A deficiency in active Naglu leads to an accumulation of heparan sulfate within the lysosome, initiating a pathological cascade within the cell. Patients with MPS IIIB experience progressive central nervous system degeneration and die within the first few decades of life. Presently, enzyme replacement therapy, which is a standard of care for other lysosomal storage disorders, is an ineffective treatment for MPS IIIB. This is due to impermeability of the blood-brain barrier (BBB) to exogenous recombinant enzymes. A promising approach to this therapeutic obstacle is protein transduction domains. Protein transduction domains have been shown to facilitate the delivery of active enzyme across the BBB in mice.

Previously, our laboratory used *Spodoptera frugiperda* (Sf9) insect cell system to express human recombinant Naglu fused to a synthetic protein transduction domain (PTD4). The purpose was to use PTD4 to the facilitate the delivery of Naglu across biological membranes, including the blood-brain barrier. However, a missing stop codon following PTD4 limited its transducibility. The stop codon was re-introduced and the improved fusion enzyme, Naglu-PTD4X, was stably expressed in Sf9 cells. The overarching goal of this project is to create a large-scale production of human recombinant Naglu that has the potential to be used to treat the neuropathology of patients with MPS IIIB.

This project used a three-step purification system to purify Naglu-PTD4X. Uptake of Naglu-PTD4X was assessed in MPS IIIB fibroblasts using a fluorogenic activity assay, immunoblotting, and immunocytochemistry. Our purification system was successful at purifying Naglu-PTD4X to homogeneity with a 26% yield and specific activity of 84,000 units/mg. An increase in Naglu activity was detected in MPS IIIB fibroblasts following incubation with Naglu-PTD4X. Future directions will focus on optimizing immunodetection and conducting BBB penetration studies in murine models.

Table of Contents

List of Tables

List of Figures

List of Abbreviations

%	percent
°C	degrees Celsius
4MU-Naglu	4-methyl-umbelliferyl-N-acetyl-α-D-glucosaminide
His	hexahistidine
AAV	adeno-associated virus
AFU	arbitrary fluorescence unit
AMT	absorptive-mediated transcytosis
BBB	blood-brain barrier
BBBD	blood-brain barrier disruption
BEC	brain endothelial cell
BSA	bovine serum albumin
bp	base pair
cDNA	complimentary DNA
CED	convection-enhanced diffusion
CiPP	capture, intermediate purification, polishing
CHO	Chinese hamster ovary
CNS	central nervous system
CON-A	concanavalin A
CPP	cell penetrating peptide
CSF	cerebral spinal fluid
CV	column volume
DNA	deoxyribonucleic acid

DTT	dithiothreitol
ECM	extracellular matrix
EDTA	ethylenediaminetetracaacetic acid
ER	endoplasmic reticulum
ERT	enzyme replacement therapy
FBS	fetal bovine serum
FPLC	fast protein liquid chromatography
GAG	glycosaminoglycan
GM01426	MPS IIIB skin fibroblast cell line
GM02391	MPS IIIB skin fibroblast cell line
HIC	hydrophobic interaction chromatography
HIR	human insulin receptor
HIRMAb	monoclonal antibody against human insulin receptor
HRP	horseradish peroxidase
HS	heparan sulfate
HSPG	heparan sulfate proteoglycan
IDS	iduronate 2-sulfatase
IDUA	iduronidase
IEX	ion exchange chromatography
IT	intrathecal
kb	kilobase pair
kDa	kilo Dalton
LAD	lipoamide dehydrogenase

LSD	lysosomal storage disorder
M	molar
M6P	mannose-6-phosphate
MCH064	normal skin fibroblast cell line
µg	microgram
µL	microlitre
min	minute
mg	milligram
mM	millimolar
mL	millilitre
MMC	multi-modal chromatography
MPS	Mucopolysaccharidosis
MPS III	Mucopolysaccharidosis type III
MPS IIIB	Mucopolysaccharidosis type IIIB
MTH	molecular trojan horse
Naglu	N-α-D-acetylglucosaminidase
NEAA	non-essential amino acids
nm	nanometre
nM	nanomolar
nmol	nanomole
NNSS	native Naglu secretion signal
NVU	neurovascular unit
PAGE	polyacrylamide gel electrophoresis

PBS	phosphate buffered saline
PBST	PBS with Tween 20
PTD	protein transduction domain
PTD4	synthetically optimized protein transduction domain
PVDF	polyvinylidene fluoride
RER	rough endoplasmic reticulum
rhIDU	recombinant human α-L-iduronidase
RMT	receptor-meditated transcytosis
RNA	ribonucleic acid
rpm	revolutions per minute
SDS	sodium dodecyl sulfate
Sf9	*Spodoptera frugiperda* 9 cells
TAT	trans-activator of transcription
TfR	transferrin receptor
UTR	untranslated region
UV	ultra-violet
v/v	volume to volume ratio
V	volts
w/v	weight to volume ratio
xg	times the force of gravity

Acknowledgments

I am deeply grateful to Dr. Choy for his mentorship throughout my undergraduate and graduate program. Dr. Choy continually inspired me with his unfailing passion for science and 'elegant' research as well as his joy in teaching others. I would like to express my appreciation to my committee members for their valued insights for this project. There are also many members in the Biology and Biochemistry Department to whom I owe a huge thank you. Thank you to Dr. Chow for the time he devoted in training me on the confocal microscope. Thank you to Dr. Ehlting and Dr. Howard for use of their lab equipment. Thank you to Laura and Michelle in Biology Office for their cheerful and valued help with answering my many questions and queries. Thank you to the 'Excel guy' who taught me the drop-down function in Excel during ecology lab. I am indebted to my lab mates, the 'Choy's Angels', who have aided me in the progress of this project: Chloe Christensen, Emma Wells-Durand, Laura Wotton, Samuel Chu and other past Choy lab members. In particular, I am deeply grateful to Chloe Christensen, 'lab mom', who was enduring in her encouragement, ingenious in her troubleshooting, and continual in her support.

Dedication

To my family, who celebrated with me in the good times and supported me in the hard times.

My dreams came true because of their support, guidance, and love.

Go ‘Team Rhea’!

1. Introduction

1.1 Lysosomal storage disorders

1.1.1 Overview

Lysosomes are membrane-bound organelles that are responsible for the degradation of specific intra and extracellular materials. Intracellular wastes are primarily transported through autophagy to the lysosome whereas extracellular wastes are transported through various endocytic pathways, including phagocytosis, macropinocytosis, and caveolin-mediated endocytosis (Settembre *et al.*, 2013). Degradation in the lysosome is accomplished by an array of proteins that exist within the acidified lumen as well as within the membrane of the lysosome. These proteins enable the lysosome to break down a large selection of biological substrates, including glycosaminoglycans, proteins, and sphingolipids. Within the lumen alone, there are over 50 distinct acid hydrolases that are capable of breaking down a vast repertoire of biological substrates (Schroder *et al.*, 2010). Lysosomal storage disorders (LSDs) are a family of over 50 rare diseases with an approximate collectively prevalence of 1 in 5,000 to 8,000 in the general population (Parenti *et al.*, 2015; Platt, 2017). LSDs arise from genetic mutations that perturb the degradative function of the lysosome. These mutations occur in genes that encode proteins involved in the catabolism or the transport machinery of the lysosome. This results in an ineffective break down of cellular wastes and their subsequent accumulation or "storage" within the lysosome. This accumulation leads to lysosomal engorgement and dysfunction, which initializes a pathological cascade of cellular dysfunction.

1.1.2 Overview of Mucopolysaccharidosis III

Mucopolysaccharidosis III (MPS III), also known as Sanfilippo Syndrome, is an autosomal recessive LSD that was first described by the pediatrician Sylvester Sanfilippo

(Andrade *et al.*, 2015). MPS III results from the ineffective degradation of the glycosaminoglycan, heparan sulfate (HS). HS is broken down in the lysosome by four different enzymes. A deficiency in each of these enzymes corresponds to the four subtypes of MPS III: heparan N-sulfatase (MPS IIIA, OMIM 252900), α-N-acetylglucosaminidase (MPS IIIB, OMIM 252920), Acetyl CoA:α-glucosaminide N-acetyltransferase (MPS IIIC, OMIM 252930), and N-acetylglucosamine 6-sulfatase (MPS IIID, 252940). The most common forms of MPS III are MPS IIIA and B whereas MPS IIIC and D are significantly rarer.

MPS IIIB has an approximate incidence of 1 in 200,000 to 400,000 in the general population (Andrade *et al.*, 2015; Clark *et al.*, 2018). It arises from mutations in the α-N-acetylglucosaminidase (*NAGLU*) gene that encode the lysosomal acid hydrolase, Naglu. Naglu is responsible for the hydrolysis of the $\alpha 1 \rightarrow 4$ linkage between N-acetylglucosamine and uronic acid during the break down of HS (Valstar *et al.*, 2008). Mutations in *NAGLU* can result in a functional deficiency of Naglu in the lysosome and the subsequent accumulation of partially degraded HS The progressive accumulation of HS leads to the clinical onset of MPS IIIB.

1.1.3 Molecular genetics of MPS IIIB

In 1996, *NAGLU* was identified and mapped to chromosome 17q21.1(Zhao *et al.*, 1996). The gene spans 8.5 kb and contains 6 exons. To date, over 150 mutations have been reported that cause MPS IIIB; the majority of these mutations being missense mutations (70.6%) (Andrade *et al.*, 2015). These mutations are often private mutations and occur with a very low allelic frequency. This heterogeneity likely contributes to the broad spectrum of clinical severity of MPS IIIB.

R297X is the most frequent mutation in MPS IIIB patients. It has a reported allelic frequency of 11.5% (Yogalingam and Hopwood, 2001). This nonsense mutation results in a

truncated 34kDa polypeptide that is rapidly degraded, likely before reaching the lysosome. Fibroblasts from a patient homozygous for this mutation expressed no detectable levels of Naglu activity and significantly elevated levels of accumulated glycosaminoglycans. This mutation is associated with the severe form of MPS IIIB. For example, a patient with the R297X/ R297X genotype exhibited severe dementia at the age of 13 despite bone marrow transplants.

Common missense mutations are Y140C, R674H, R643C, R565W, and P521L (Yogalingam and Hopwood, 2001; Valstar *et al.*, 2010; Birrane *et al.*, 2019). Their reported frequency is 5.4%, 4.7% 3.4%, 3.4%, 4.1% respectively. These mutations result in residual Naglu activity within the lysosome and are associated with the attenuated form of MPS IIIB.

1.1.4 MPS IIIB at the biochemical level

α-N-Acetylglucosaminidase

In humans, Naglu is a house-keeping enzyme present in all cell types. There are several different tissue specific isozymes, ranging from 73 to 86kDa in size. The optimal pH for activity of purified Naglu is 4.5 and its isoelectric point is 5.1. Naglu can be easily inactivated by increases in pH and heat.

In vivo, Naglu was synthesized in the rough endoplasmic reticulum (RER) as a precursor polypeptide of about 743 amino acid in length (Weber, 1996; Zhao *et al.*, 1996). A signal peptide of 20-23 amino acids at the N-terminus is removed and results in the mature Naglu protein of 720 amino acid (Zhao *et al.*, 1996). In the lumen of the RER, Naglu is folded and glycosylated. Naglu undergoes N-glycosylation at potentially six putative asparagine residues at sites: 261, 272, 435, 503, 526, and 532 (Weber, 1996; Birrane *et al.*, 2019). Through vesicular transport, Naglu is trafficked to the Golgi where it undergoes additional post-translational modification. In the Golgi, two enzymes work in series, N-acetylglucosaminylphosphotransferase and N-

acetylglucosamine-1-phosphodiester α-N-acetylglucosaminidase respectively, to modify Naglu and add a recognition marker in the form of phosphomannosyl residues (Kornfeld, 1986). This recognition marker is bound by mannose-6-phosphate receptors and Naglu is translocated into a pre-lysosomal compartment. The low pH of this compartment encourages the dissociation of Naglu from its receptor and thereafter Naglu is packaged into a mature lysosome.

In 2008, a homology model of human Naglu was constructed based on the crystal structure of *Cp*GH89, a bacterial glycoside hydrolase from *Clostridium perfringens* (Ficko-Blean *et al.*, 2008). These two enzymes shared approximately 30% sequence identity. The homology model allowed for the mapping of known MPS IIIB mutations and revealed that these mutations were randomly scattered throughout the protein. This suggested that these mutations likely reduced the stability of newly synthesized Naglu and impaired its trafficking to the lysosome. In addition, only four were found in the active site and none of the catalytic residues were mutated. Mutations of the catalytic residues were proposed to be so severe as to be perinatally lethal.

In 2019, the first paper was published that depicted the crystal structure of human recombinant Naglu (Figure 1.1; Birrane *et al.*, 2019). This work demonstrated that human recombinant Naglu, expressed from CHO cells, exists as a homogenous trimer. The three monomers interact through hydrophobic interactions and hydrogen bonds to form a symmetrical, propeller-like shaped enzyme with multiple catalytic sites facing outwards. In addition to fully elucidating the 3D structure of human Naglu, this work also provided a greater insight into the effects that known MPS IIIB mutations have on its functionality. This is particularly true for mutations further from active sites that are in regions that shared low homology with *Cp*GH89. For example, this work mapped a cluster of mutations associated with severe MPS IIIB pathology (R520W, P521L, R674C/H, R676P, E705K and Q706X) and, based on the 3D crystal

structure, determined that these mutations would disrupt the hydrogen bond network of domain III and destabilize the active site.

Heparan Sulfate

HS is characterized as a glycosaminoglycan (GAG), which is a linear, negatively charged polysaccharide. The base structure of HS consists of a repeating disaccharide units of glucosamine and uronic acid but various tissue specific modifications that occur during biosynthesis make HS highly heterogenous (Shriver *et al.*, 2012). HS, like other GAGs, is typically found covalently attached to a protein core in the form of a HS proteoglycan (HSPG). There are four major groups of HSPGs, which are defined based on their core protein. They are syndecans; glypicans; secreted HSPGs, which include perlecan, agrin, and collagen XVIII; and serglycin (Li and Kusche-Gullberg, 2016). These HSPGs are located primarily at the cell surface and within the extracellular matrix. They are involved in regulating various cellular processes through interactions with various ligands, including cytokines, ECM proteins, proteases, lipases, and growth factors (Whitelock and Iozzo, 2005). In the CNS, HSPGs play a role in: neurogenesis, axonal guidance, and synaptogenesis (Yamaguchi, 2001).

HS breakdown occurs via the intracellular lysosomal degradation route. The half-life range for HSPGs on the cell surface is between 4hrs to 24hrs with the majority being turned over by 48hrs (Whitelock and Iozzo, 2005). In the first step of degradation, intracellular endoglycosidases, known as heparanases, cleave the HS oligosaccharides from the protein core (Bame, 2001). These oligosaccharides are transported to the lysosome to be broken down in a stepwise fashion involving heparan N-sulfatase, Naglu, Acetyl CoA:α-glucosaminide N-acetyltransferase, and then N-acetylglucosamine 6-sulfatase (Figure 1.2; Valstar *et al.*, 2008).

In MPS IIIB, this pathway is disrupted by the deficiency of Naglu which leads to the accumulation of HS fragments in the lysosome. This accumulation negatively affects lysosomal function, resulting in secondary accumulation of GM2 and GM3 gangliosides and free cholesterol (McGlynn *et al.*, 2004). This secondary accumulation has been proposed to affect signal transduction since these are important constituents of lipid rafts. In addition to HS sequestering in the lysosome, several studies investigating MPS IIIB have found increased levels of HS, particularly highly sulfated HS, in the Golgi, on the cell surface and in the ECM (Wilkinson *et al.*, 2012; Watson *et al.*, 2014). In the Golgi, this accumulation of HS leads to enlargement and defects in the sorting of the Golgi network (Roy *et al.*, 2012). On the cell surface and in the ECM, the increased presence of these highly sulfated HS oligosaccharides has also been shown to result in alterations in cell signaling pathways (Watson *et al.*, 2014; De Pasquale *et al.*, 2018).

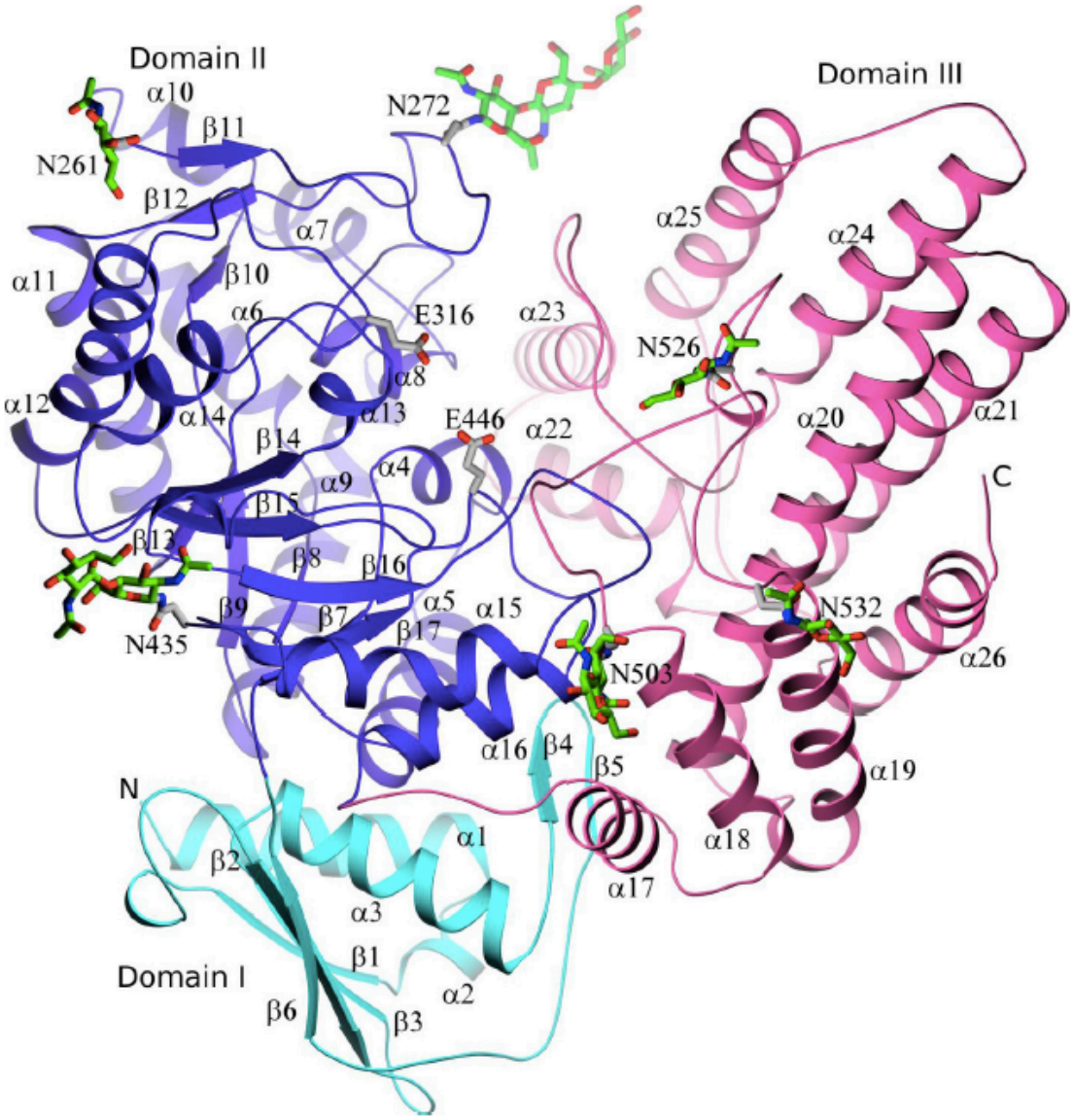

Figure 1.1 Stick-and-ribbon representation of the crystal structure of human Naglu

The tertiary structure of human Naglu contains three distinct domains: Domain I (cyan), Domain II (purple), and Domain III (pink). The catalytic structures are depicted by the green and grey sticks. Figure from Birrane *et al.* 2019.

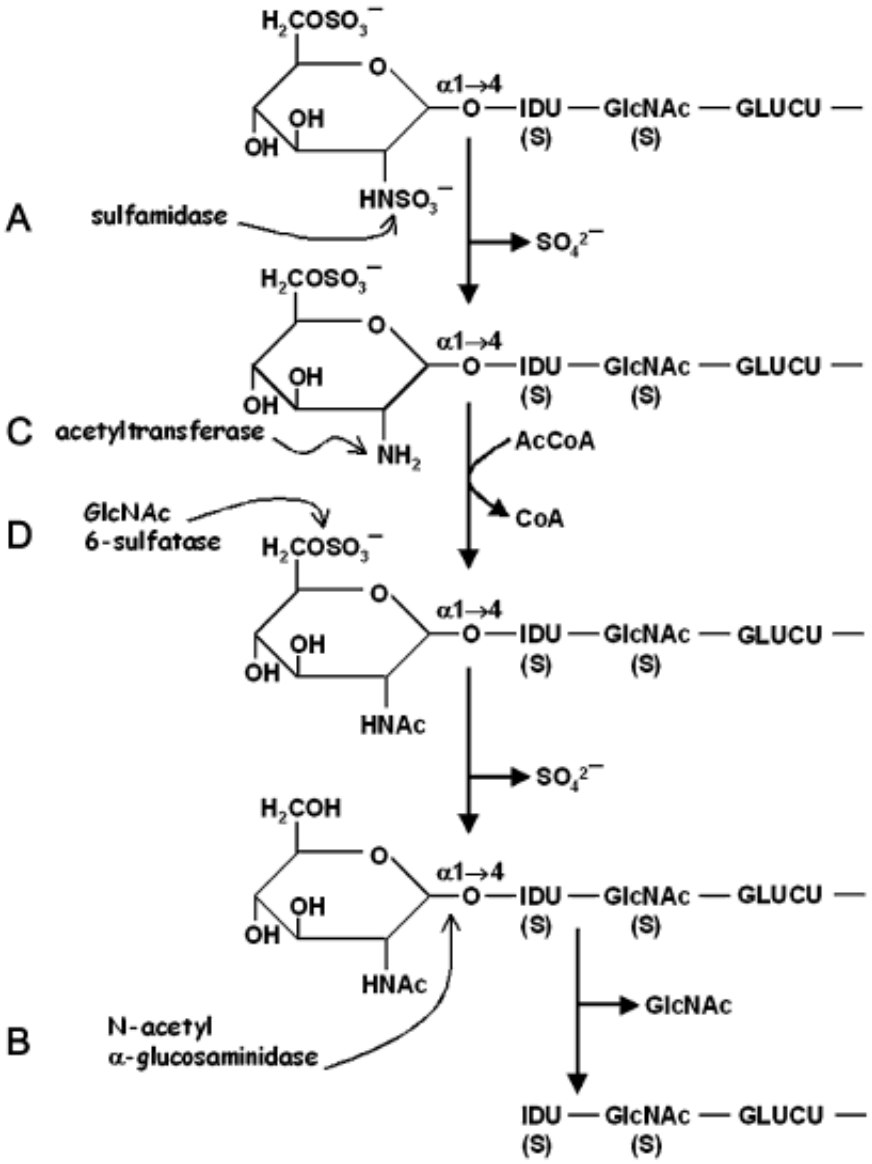

Figure 1.2 Heparan sulfate degradation pathway

During the first degradative step, the sulfate group linked to the amino group of glucosamine are removed by sulfamidase. Acetylation of the free amino groups of glucosamine is catalyzed by α-glucosaminide N-acetyltransferase and then the sulfate group from N-acetylglucosamine residues is removed by N-acetylglucosamine 6-sulfatase. Lastly, α-N-acetylglucosaminidase hydrolyses the α1→ 4 linkage between N-acetylglucosamine and uronic acid. Deficiency in each of these enzymes results in MPS IIIA, MPS IIIC, MPS IIID, and MPS IIIB respectively. Figure from Valstar *et al.* 2008.

1.1.4 General clinical signs and symptoms of MPS IIIB

Children with MPS IIIB appear normal at birth. The first signs of clinical disorder present between 1 and 4 years of age (Truxal *et al.*, 2016). These patients experience developmental delay, particularly speech delay. Around the age of 4, regression in cognition and behaviour become evident. Common features at this stage are aggressive behaviour, hyperactivity, convulsions and sleep disturbances. Physical presentations include coarse facial features, enlargement of spleen, heart, and liver, hirsutism, alterations in the respiratory tract, deafness, and pigmentary retinopathy (Andrade *et al.*, 2015). In the later stages of the disease, progressive neurodegeneration results in the onset of severe dementia and the decline of motor skills, eventually resulting in a vegetative state.

There is a broad range of clinical severity for MPS IIIB, which can be roughly delineated into two phenotypes: classic and attenuated phenotype (Valstar *et al.*, 2010; Andrade *et al.*, 2015). The classic phenotype is more severe, and the disease progresses more rapidly. These patients become fully dependent on external care in their adolescent years and typically die within the second to third decade of life. The attenuated phenotype, which is suggested to be more common, progresses more slowly. Although clinical symptoms arise for this phenotype around the age of 4, these patients experience intellectual stagnation and remain with a stable intellectual disability for many years. The loss of motor skills does not typically occur until they reach 30s or 40s. For patients with the severe phenotype, diagnosis occurs in early childhood whereas attenuated phenotype often goes undiagnosed until the second or third decade of life (Valstar *et al.*, 2010).

1.1.5 Neuropathology of MPS IIIB

As previously mentioned, the initial pathology of MPS IIIB involves the incomplete breakdown and resulting accumulation of HS oligosaccharides in the lysosome within all tissue of the body,

including the central nervous system (CNS). In the CNS, this accumulation is found in neuronal and non-neuronal cell types (Li *et al.*, 2002; Ausseil *et al.*, 2008; Wilkinson *et al.*, 2012). Beyond this, the precise mechanism of CNS pathology of MPS IIIB is not well understood. Number studies have revealed that there are many complex secondary events, such as oxidative stress, autoimmune response, metabolic disturbances, autophagy, neuroinflammation, and neurodegeneration, involved in the neuropathology of MPSIIIB (Ausseil *et al.*, 2008; Settembre *et al.*, 2008; Villani *et al.*, 2009; Killedar *et al.*, 2010; Fu, Meadows, Pineda, *et al.*, 2017). Recent studies have demonstrated that neuropathology is not limited to the CNS but affects the peripheral nervous system (PNS) as well (Fu *et al.*, 2012).

Oxidative stress is a factor that may contribute to the progression of MPS IIIB. Oxidative stress has been implicated as having a role in neurodegeneration (Uttara *et al.*, 2009). In an MPS IIIB mouse model, the expression of several genes related to oxidative stress were analyzed and an upregulation was seen in several of these genes (Villani *et al.*, 2007). This increase in expression, particularly of NADPH oxidase, was hypothesized to lead to an increase in superoxide ions. A later study by Villani *et al.* (2009), measured the superoxide ion production in different regions of the MPS IIIB brain in one-month old mice and found increased levels of protein oxidation. Based on these results, it was suggested that oxidative stress and the resulting damage to cellular macromolecules may play an important role in the early pathology of MPS IIIB disease (Villani *et al.*, 2009).

In addition to measuring oxidative stress in MPS IIIB, Villani *et al.* (2009) also investigated the expression of apoptosis-related genes. A detectable increase was noted in proteins involved in granule-dependent killing mediated by cytotoxic T lymphocytes and natural killer cells. It was theorized that an autoimmune response may be causing neuronal cell injury

and potentially apoptosis. Previous data examining mouse MPS IIIB models had not found evidence of increased levels of apoptosis in the brain (Li *et al.*, 2002; Villani *et al.*, 2007). However, further research using adoptively transferred MPS IIIB T lymphocytes into naïve wildtype mice, supported this theory that MPS IIIB primes an autoimmune response (Killedar *et al.*, 2010). In addition, they found that the MPS IIIB T lymphocytes led to a significant increase in activated glial cells and expression of cytokines, IL2, IL4, IL5, IL17, and IFNγ, in the wildtype brain. They proposed that this alteration in brain homeostasis could impair neuronal function without causing cell death.

Profound metabolic disturbances have also been observed in MPS IIIB. A study analyzed the global metabolomic profile of serum samples from 7-month-old MPS IIIB mice using mass spectroscopy(Fu, Meadows, Ware, *et al.*, 2017). The findings indicated that there was wide-spread impairment of virtually all metabolic pathways for amino acids, peptides, lipids, carbohydrates, energy, nucleotides, vitamins and cofactors, and xenobiotics. Furthermore, the majority of significantly altered serum metabolite were greatly reduced (97.4%). Following this study, Fu *et al.* (2017) analyzed serum samples from MPS IIIA and MPS IIIB patients and compared them to controls. The global metabolite profile findings were similar to those found in mice in that all metabolic pathways were affected. Notably, there were metabolite decreases in key amino acids, all major neurotransmitter pathways, and broad neuroprotective compounds (Fu, Meadows, Pineda, *et al.*, 2017).

The accumulation of HS oligosaccharides in MPS IIIB also impairs autophagy. A microscopy analysis of brain section of MPS IIIB mice showed that there was an accumulation of subunit c of mitochondrial ATP synthase along with GAGs in neurons. This data suggested that there was an impairment in autophagy in the MPS IIIB brain (Ryazantsev *et al.*, 2007). A

different study investigated the impairment of autophagy in mouse models of mucopolysaccharidoses type II and IIIA (MPSII and MPSIIIA, respectively) and of multiple sulfatase deficiency (Settembre *et al.*, 2008). Their findings indicated that the accumulation of storage products (GAGs) blocked the fusion of autophagosomes and lysosomes. As a result, cellular wastes, such as toxic proteins and dysfunctional mitochondria, would accumulate. This could lead to direct apoptosis or apoptosis through induction of chronic inflammation and cytokine release.

Numerous studies have demonstrated that neuroinflammation occurs in MPS IIIB. Studies with MPS IIIB mouse models, have shown increased levels of reactive astrocytes and activated microglial cells in the brain, which are hallmarks for neuroinflammation (Li *et al.*, 2002; Ohmi *et al.*, 2003). It has been observed that abnormal, undigested HS oligosaccharides in MPS IIIB mice lead to microglial priming (Ausseil *et al.*, 2008). Additionally, gene expression analysis indicated an upregulation of inflammatory molecules in the MPS IIIB brain (Wilkinson *et al.*, 2012). A microarray of genes associated with chemokines, cytokines, and their receptors showed that 16 of the 17 genes were upregulated (Villani *et al.*, 2007). In particular, MIP-1α, which is a crucial for macrophage recruitment, was increased 5-fold over the wild-type. Although it has been established that neuroinflammation occurs in MPS IIIB, the link between neuroinflammation and the progression of this disease is unclear. A study observed the early neurodegeneration in MPS IIIB mice still occurred in the absence of microglial priming, which indicated the neuroinflammation was not causative of early neurodegeneration. However, chronic inflammation may play a role together with a number of other players, such as aberrant autophagy, oxidative stress, metabolic disturbances, and autoimmunity, in the neurodegeneration that occurs in MPS IIIB.

1.2 MPS IIIB and enzyme replacement therapy

1.2.2 Enzyme replacement therapy

Hers (Hers, 1961) and de Duve (de Duve, 2005) observed that the majority of LSDs were caused by enzyme deficiencies and noted that replacement of these enzyme had the potential to be therapeutic. The phenomenon of "cross-correction" supported this postulation. It was observed that lysosomal enzymes, when secreted from a cell, could be taken up by nearby cells, often through mannose-6-phophate receptor mediated endocytosis (Kaplan *et al.*, 1977; Neufeld, 1980). This phenomenon was experimentally demonstrated by applying cellular products from a healthy individual to diseased cells from a patient with an LSD and observing the uptake of the deficient enzyme in the diseased cells. In the 1990s, Brady and colleagues developed the first efficacious enzyme replacement therapy (ERT) for a LSD (Barton *et al.*, 1991). Ceredase®, a placentally-derived ß-glucocerebrosidase, was successful at reducing liver and spleen volumes for patients with type I Gaucher disease. Following this therapeutic success, ERTs have been developed and approved by the FDA for seven other LSDs: MPS I, Fabry, MPS VI, MPS II, Pompe, MPS IVa, and Wolman (Platt, 2017).

A major limitation of ERT when it is supplied through its traditional route of administration–intravenous injection–is its restricted bioavailability to certain tissues, especially the tissues of the CNS. The impermeability of blood-brain barrier (BBB) to recombinant enzymes is a significant obstacle for ERT delivery. Therefore, at present, ERT is not an effective at treating LSDs that have CNS involvement. As mentioned above, the neurological pathology of MPS IIIB is the major contributor to the morbidity and mortality of this disease. At present, there is no effective therapy for MPS IIIB, only the management of symptoms. Innovative strategies must be developed to overcome this limitation in BBB delivery so as to create an ERT that can

reach the CNS and effectively treat patients with MPS IIIB.

1.2.3 Brief physiology of the BBB

The capillary network within the human brain has an estimated total length of 600-700km with the distance between adjacent capillaries being approximately 40μm (Zlokovic, 2005). This extensive and vast capillary network within the brain is required to meet the high metabolic demands of the CNS. In addition, the cerebrovascular system is also highly selective. There exists a barrier, known as the blood-brain barrier, that tightly regulates the passage of ions, molecules, and cells between the blood and the brain (Rubin and Staddon, 1999; Gloor *et al.*, 2001; Daneman, 2012). This regulation is necessary to precisely control the CNS environment for proper synaptic transmission and overall neuronal functioning.

Brain endothelial cells (BECs) are the primary component of the BBB (Daneman, Zhou, Agalliu, *et al.*, 2010). BEC's are distinct from endothelial cells of different tissues within the human body in that they lack fenestrations, undergo extremely low rates of transcytosis, and have continuous intracellular tight junctions (Daneman, 2012; Obermeier *et al.*, 2013). These qualities restrict the movement of substances between the blood and the brain via the paracellular and transcellular pathways. Therefore, to gain entry into the brain via the BBB, molecules must interact with specific transport receptors expressed on the luminal and abluminal side of BECs (Gabathuler, 2010a). Furthermore, the BBB contains efflux transporters that can actively pump many substances, in particular lipophilic substances, back out of the brain. Other elements of the neurovascular unit (NVU), such as pericytes (Daneman, Zhou, Kebede, *et al.*, 2010; Winkler *et al.*, 2011), astrocytes (Siegenthaler *et al.*, 2013), and neural progenitor cells, also play key roles in inducing and supporting the BBB. This barrier, essential for the protection and maintenance of the brain environment, is also a formidable obstacle for the delivery of therapeutics to the

brain.

Approximately 100% of large pharmaceutical molecules and 98% of small molecules are unable to enter the CNS due to the restrictive nature of the BBB (Pardridge, 2007). Only a small number of pharmaceutical molecules are able to exploit lipid-mediated free diffusion to cross the BBB. These molecules must have a molecular weight of less than 400 Da and contain no greater than eight hydrogen bonds (Pardridge, 2015). Recombinant enzymes, such as those used in ERT, do not meet the conditions required for lipid-mediated free diffusion across the BBB and efforts to conform would result in significant loss in enzyme activity. At present, there are several novel approaches under development to circumnavigate this therapeutic challenge, which have the potential to be applied to delivery of ERT.

1.2.4 Strategies for BBB delivery of ERT for neuronopathic LSDs

The approaches for BBB delivery that are applicable for ERT can be categorized into mechanical and physiological (Gabathuler, 2010). The mechanical approach involved breaching or bypassing the BBB whereas physiological approach exploits native transport machinery to facilitate delivery to the CNS.

Mechanical approach to BBB delivery

For the mechanical approach, several techniques are currently under development for the delivery of therapeutics across the BBB. Techniques which may be promising for the delivery of ERT include ultrasound mediated blood-brain barrier disruption (BBBD), intrathecal (IT) administration, and convection-enhanced delivery (CED).

Ultrasound mediated blood-brain barrier disruption (BBBD) involves temporarily opening the BBB by subjecting intravenously injected microbubbles to an ultrasound field. These microbubbles oscillate and generate mechanical forces, which disrupt the tight junctions

between brain endothelial cells, allowing for increased paracellular transport (Hynynen *et al.*, 2005). There is also evidence that this induces pore formation and endocytosis, increasing transcellular transport as well (Meijering *et al.*, 2009). This technique has been studied in various animal models and used to successfully deliver a range of therapeutics, including chemotherapy drugs (Treat *et al.*, 2007), antibodies (Kinoshita *et al.*, 2006; Jordão *et al.*, 2013), recombinant proteins (Hsu *et al.*, 2017), and gene vectors (Huang *et al.*, 2012; Lin *et al.*, 2016). A recent study utilized ultrasound mediated BBBD to admit intravenously injected α-L-iduronidase (rhIDU) into the brain in MPS I mice (Hsu *et al.*, 2017). In these mice, the treated side of the brain had 75.84% of normal levels of rhIDU.

Recently, ultrasound mediated BBBD has moved into phase I/II clinical studies for delivery of therapeutics for several neurological diseases (clinicaltrials.gov identifier: NCT03119961, NCT02253212, NCT02986932, NCT03321487, NCT02343991). Additionally, clinical trial NCT02253212 is examining the safety of SonoCloud®, which is an implantable ultrasound device. The advantage of this technology is that it increases the ease of application making it more amendable to a clinic setting and therapeutics that require repeated dosages, like ERT. The volume of disruption is an important limitation for this technique. At present, unfocused ultrasound is only capable of sonicating a brain volume of approximately 5 cm^3, which for may be insufficient for delivering therapeutics to more diffuse CNS pathologies like MPS IIIB (Fu *et al.*, 2012; Carpentier *et al.*, 2016).

IT administration delivers therapeutics to the CNS by infusing them into the cerebrospinal fluid (CSF) of the spinal canal or subarachnoid space via lumbar puncture or cisterna magna injection. IT administration of ERT has been shown to be efficacious in several preclinical models (Kakkis *et al.*, 2004; Dickson *et al.*, 2007; Felice *et al.*, 2011; Xu *et al.*, 2011;

Calias *et al.*, 2012; Chung *et al.*, 2017). A phase I/II clinical trials for IT administration of heparan-N-sulfatase (rhHNS) in patients with MPS IIIA was recently completed. The results indicated that this approach was generally well tolerated but there were high rates of device malfunctions, suggesting a need to improve IT administration. Although the purpose of this study was to assess the safety of IT administrations, it also reported a reduction in HS levels in the CSF. These encouraging results led to the extension of this study for a period of 8 years, during which long term safety and neurocognitive effects will be examined (clinicaltrials.gov identifier: NCT01155778).

Similar to ultrasound mediated BBBD, this approach also has issues with therapeutic biodistribution in the CNS. IT administration relies on diffusion for distribution throughout CNS. While diffusion of substances is extremely effective at small distances (nm-μm) in the CNS, such as between synaptic clefts or cell bodies, for larger distance (mm), diffusion is often slow or entirely limited (Wolak and Thorne, 2013). A study that examined brain perfusion of a chemotherapy agent following IT administration, found the concentration was reduced to only 1% of the concentration in the CSF within 1-2mm from the ependymal surface (Blasberg *et al.*, 1975). Another study administered rhHNS via IT injection to cynomolgus monkeys and reported enzyme concentration 3-4 times lower in white matter and deeper parenchymal regions compared to the gray matter and cortex (Chung *et al.*, 2017).

CED involves sustained infusions of the therapeutic through a cannula into the brain parenchyma. This administration technique has greater biodistribution than diffusion-based strategies because the therapeutic is driven by small amounts of continuous pressure (Bobo *et al.*, 1994). A case study used CED to deliver glucocerebrosidase replacement therapy and an MRI tracer to a patient with type 2 Gaucher disease (Lonser *et al.*, 2007). MRI visualization showed

an increased bioavailability of the glucocerebrosidase therapy throughout the CNS without signs of toxicity in the patient. Although this case study was promising, there needs to be more and larger clinical trials into the efficacy and safety of using CED for ERT administration.

Overall, a major drawback to the majority of techniques that utilize the mechanical approach to BBB delivery is that they are not patient-friendly requiring surgical intervention, often invasive surgeries, and frequent hospitalizations. This is a significant burden for a patient with MPS IIIB when considering the fact that ERT often requires repeat dosages.

Physiological approach to BBB delivery

This approach utilizes native transport machinery for transcellular BBB delivery and therefore, is less invasive and more patient-friendly than the mechanical approach. For this category, there are two distinct transport mechanisms that can be targeted for the delivery of therapeutics across the BBB: receptor-mediated and absorptive-mediated transcytosis.

Receptor-mediated transcytosis (RMT) involves the transport of larger molecules, necessary for CNS function, across the BBB. This includes hormones, growth factors, enzymes, and plasma proteins (Xiao and Gan, 2013). Receptors for this pathway are highly expressed on the luminal side of BECs. The transport pathway can be exploited by fusing specific ligands, modified ligands, and antibodies that target RMT receptors to transport therapeutics. This enables the therapeutic to be ferried across the BBB via RMT. This elegant mechanism of BBB delivery has been coined the molecular trojan horse (MTH) method.

The application of the MTH for ERT delivery has primarily been developed using monoclonal antibodies (MAbs) to target BBB receptors (Pardridge, 2015). The two most predominant MTH are MAbs against the human insulin receptor (HIR) and transferrin receptor (TfR), known as HIRMAb and TfRMAb respectively. One of earliest MTH ERT studies, fused iduroniase

(IDUA) to HIRMAb for BBB delivery in rhesus monkeys (Boado *et al.*, 2009). Brain uptake of the IDUA-HIRMAb was approximately 1% injected dose /brain. Following this study, HIRMAb was fused to enzymes deficient in MPSII, MPSIIIA, and MPS IIIB, which are iduronate 2-sulfatase (IDS), N-sulfoglucosamine sulfohydrolase (SGSH), and Naglu respectively (Ruben J. Boado *et al.*, 2014; Ruben J Boado *et al.*, 2014; Boado *et al.*, 2016). These fusion proteins exhibited similar levels of brain penetration to HIRMAb-IDUA in Rhesus monkeys (1% injected dose /brain). In 2018, a phase I/II clinical trial with MPS I patients determined valanafusp alpha (HIRMAb-IDUA: AGT-181) to be well tolerated (Giugliani *et al.*, 2018). In addition, clinical evidence suggested cognitive and somatic stabilization in patients. The promising results after 52 weeks prompted the extension of this study to 24 months (clinicaltrials.gov identifier: NCT03071341). A phase I clinical trial is also being conducted with MPS II patients to evaluate the safety of HIRMAb-IDS (AGT-182) (clinicaltrials.gov identifier: NCT02262338).

A potential limitation for the MTH is dysregulation of uptake pathways. RMT is a saturable process and chronic high dose administration of molecular Trojan horses may result dysregulation of the targeted pathway throughout the body (Xiao and Gan, 2013). For example, loss of glycemic control upon chronic administration of HIRMabs. In the phase I/II HIRMAb-IDUA clinical trial, there was an 6.4% incidence of transient hypoglycemia. To overcome this limitation, there is ongoing research to discover alternative receptors that are predominantly expressed on BECs and pose a reduced risk for RMT pathway dysregulation (Zuchero *et al.*, 2016).

Absorptive-mediated transcytosis (AMT) can also be exploited for BBB delivery. AMT typically results from electrostatic and other non-specific interactions inducing a combination of endocytic pathways, including micropinocytosis, clathrin- and caveolin-mediated endocytosis.

Cell penetrating peptides (CPPs) are less than 30 amino acids in length and vary in charge, polarity, and structure (Kalafatovic and Giralt, 2017). Their commonality is their ability to target AMT to cross biological membranes, including the BBB. This characteristic of CPPs was initially observed by Frankel and Pabo. They reported that the Trans-activator of transcription (Tat) domain in Human Immunodeficiency Virus possessed the ability to cross cell membranes (Frankel and Pabo, 1988). At present, over a thousand unique CPP sequences have been discovered and a CPP database has been established. The precise mechanism of uptake has not been determined but the current understanding is that CPPs are taken up by a combination of endocytic pathways and direct translocation (Kristensen *et al.*, 2016). Furthermore, the mechanism of uptake is highly dependent on the sequence and concentration of the CPP (Jones and Sayers, 2012a), the cell-type and differentiation status of the receiving cell (Krauss *et al.*, 2004; Zhang *et al.*, 2004), as well as the type of cargo attached to the CPP (Bárány-Wallje *et al.*, 2007).

CPPs are able to facilitate the delivery a fusion partner across biological membranes. This is a promising therapeutic application for CPPs and has significant implications for improving delivery of ERT to the CNS. In 1999, a benchmark preclinical study was conducted that delivered active β-galactosidase fused to Tat to the mouse brain (Schwarze *et al.*, 1999). Recently, a Tat-mediated ERT was tested on a mouse model with lipoamide dehydrogenase (LAD) deficiency (Rapoport *et al.*, 2011). An 80% increase in LAD activity was observed in brain tissue 4 hours after a single injection of Tat-LAD, indicating that Tat-mediated ERT was successful at traversing the BBB.

Immunogenicity and toxicity are possible limitations that have been proposed regarding the use of CPPs (Dinca *et al.*, 2016). CPPs are often foreign to the subject organism and

therefore it is possible CPPs may elicit an immune response. The results of various *in vitro* and *in vivo* studies suggest that these two limitations greatly depend on the CPPs being used and the cargo to which the CPP is fused (El-Andaloussi *et al.*, 2007; Moschos *et al.*, 2007; Suhorutsenko *et al.*, 2011; Carter *et al.*, 2013). Therefore, immunogenicity and toxicity of a given therapeutic CPP must be determined empirically.

1.3 Project background

1.3.1 HIV TAT protein transduction domain

The CPP, Tat has promising implications for the creation of a fusion recombinant ERT that could be transported across the BBB and treat the CNS of neuronopathic LSDs, like MPS IIIB. Furthermore, in addition to its ability to penetrate the BBB, Tat has also shown localization to the lysosome(Zhang *et al.*, 2008). In 2001, the transducibility of Tat was optimized and led to the creation of the PTD4, a synthetic protein transduction domain (Ho *et al.*, 2001). This study optimized the ratio of arginine along the face of the Tat helix and as a result, PTD4 has 33 times more transduction potential compared to wildtype Tat.

Previously, our lab fused PTD4 to Naglu in order to examine the potential of PTD4 to deliver Naglu across biological membranes, specifically the BBB. This was done with the goal of creating an ERT that would reach the CNS and treat the neuropathology of MPS IIIB patients.

1.3.1 Sf9 expression system

The Sf9 insect cell line is derived from the moth, *Spodoptera frugiperda*. This cell line is able to perform most mammalian post-translational modifications, which has made it a popular system for expressing human glycoproteins (Pfeifer *et al.*, 2001). Non-lytic vector systems are commonly used to transfect Sf9 cells for the creation of stable expression lines. This technique involves the integration of the introduced gene into the Sf9 chromosomal DNA. An advantage of

the Sf9 expression system has over mammalian expression lines, is that Sf9 cells are relatively easy and inexpensive to culture. Also, they adapt well to large-scale fermenters, which is beneficial for generating greater quantities of the expressed protein. A notable disadvantage to this system is that Sf9 cells are unable to phosphorylate mannose residues, which are critical for targeting enzymes to the lysosome (Kost *et al.*, 2005). Our lab has selected this expression system because of the advantages listed above despite the significant limitation in lysosomal targeting. The synthetic protein transduction domain, PTD4, that is being investigated by our lab has demonstrated targeting to the lysosome, which mitigates the need for mannose-6-phosphate glycosylation of our lysosomal enzyme by the Sf9 cells.

1.3.2 Cryptic splice site removal

Past research in our lab investigated the expression of human recombinant Naglu in Sf9 cells. Early work on this project found that this expression system produced lower than expected levels of the recombinant enzyme. Expression was approximated to be between 0.129 and 0.210μg/mL based on the assumption that 1μg was equal to 48 unit of activity (Bandsmer, 2004). Real-time polymerase chain reaction (RT-PCR) of Naglu mRNA extracted from transfected Sf9 cells, amplified a small, non-target amplicon of approximately 420bp in length. Sequencing of this amplicon revealed that it shared high sequence identity with positions 1-314 and 2050-2139 in the Naglu cDNA. This led to the conclusion that there was a cryptic splice site in the Naglu cDNA, which closely resembled a consensus sequence for a splice site in Sf9 cells.

In 2011, our lab removed this cryptic splice site by silently mutating the donor and acceptor sites using site-directed PCR mutagenesis (Truelson *et al.*, 2011). The donor site was changed from AGG to CGT (arginine) and the acceptor site from CAG to CAA (glutamine). The mutagenized Naglu cDNA was cloned into a plasmid p2ZoptcxF and expressed in Sf9 cells. RT-

PCR was conducted on the Naglu mRNA, which was isolated from Sf9 cells transfected with the mutagenized Naglu cDNA, and found no evidence of the 420bp band. This indicated that the cryptic site had been successfully abolished in the Naglu cDNA.

To assess whether this had an effect on recombinant Naglu expression in Sf9 cells, Jantzen *et al.* (2013) compared expression levels of the Sf9 transfected with the non-mutagenized and the mutagenized Naglu. Suspension Sf9 cultures transfected with the mutagenized Naglu had a 4.0-fold increase in Naglu activity in comparison to those transfected with the non-mutagenized Naglu. This confirmed that the abolishment of cryptic splice site resulted in an increase in recombinant Naglu expression in Sf9 cells. In addition, Jantzen *et al.* (2013) also successfully expressed mutagenized Naglu with PTD4 fused at the C-terminus in Sf9 cells. The expression levels for Naglu-PTD4 was 2.06 μg/mL, which was significantly higher than previously reported levels (Jantzen *et al.*, 2013).

1.3.2 Protein purification and uptake in human fibroblasts

Following successful purification, our lab investigated developing a procedure for purifying Naglu-PTD4 to homogeneity from Sf9 cells in order to examine the uptake capability of PTD4. Morris (2015) employed Fast Protein Liquid Chromatography (FPLC), which is technique suited for purifying proteins from complex mixtures (GE Healthcare, 2010). A three-step process was developed to purify Naglu-PTD4 based on the capture, intermediate purification, and polishing (CiPP) strategy.

The objective of the capture step was to reduce the sample volume and therefore loading time for subsequent purification steps. The FPLC media used in this step was a multi-modal chromatography (MMC) resin. This resin worked to separate proteins based on electrostatic and

hydrophobic interactions. For this step, Morris (2015) achieved an 82% yield of active Naglu and a 4-fold reduction in sample volume.

The second step was intermediate purification. The objective of this step was to remove the bulk of the impurities from the sample. The FPLC media used in this step was a weak hydrophobic interaction chromatography (HIC), which separates proteins based on their hydrophobicity. Following this step, Morris (2015) achieved a 50% yield of active Naglu and an approximately 150-fold increase in purification.

For the final polishing step, Morris (2015) utilized size exclusion chromatography (SEC) to purify Naglu to homogeneity. In contrast to the previous FPLC media used, this column did not retain specific proteins within the sample to promote purification. Instead this column contained porous beads that filtered proteins based on their hydrodynamic diameter. Using this final column, Morris (2015) purified Naglu-PTD4 to homogeneity with an overall yield of 26% and final protein amount of 0.2 mg. The presence and purify of the purified Naglu-PTD4 sample was confirmed by silver nitrate stain and anti-Naglu immunoblotting analysis.

Uptake studies using the purified Naglu-PTD4 were conducted on MPS IIIB fibroblasts. Preliminary uptake data indicated that there was no detectable increase in intracellular Naglu activity based on fluorogenic 4-Mu Naglu activity assay. Further sequence analysis of the Naglu-PTD4 construct revealed that there was missing stop codon following the PTD4 domain. It was hypothesis that the additional 43 amino acids, which contained a V5 epitope and His tag, following PTD4 likely hindered the uptake of Naglu-PTD4 into the MPS IIIB fibroblasts.

1.3.3 Reintroduction of the missing stop codon

To improve the uptake of Naglu-PTD4-V5/His, our lab re-introduced the missing stop codon using site-directed PCR mutagenesis (Hoitsema and Choy, unpublished data). Sequencing

analysis confirmed the presence of the stop codon following the PTD4 (Supplementary Figure 1). This new construct, Naglu-PTD4X, was used to transfected Sf9 cells based on the method developed by Jantzen *et al.* (2013) (Ashmead, 2011). Following selection, Sf9 cell line, stably expressing Naglu-PTD4 at 1.01 ug/mL, was created.

1.4 Objective

This project can be categorized into four main phases: confirmation of the re-introduction stop codon, purification of Naglu-PTD4X using Morris' (2015) protocol, optimization of Naglu-PTD4X purification, and preliminary uptake studies of Naglu-PTD4X with MPS IIIB fibroblasts.

First, the presence of the re-introduced stop codon following PTD4 will be confirmed. Previously, the *Naglu-PTD4X* insert was sequenced prior to Sf9 transfection and the re-introduced stop codon was confirmed. However, sequencing has not been conducted following incorporation of the *Naglu-PTD4X* insert into the chromosomal Sf9 DNA. Genomic DNA from a stably transfected Sf9 cell line will be extracted and *Naglu-PTD4X* insert will be amplified and sequenced to re-confirm the presence of the stop codon.

Following confirmation of the re-introduced stop, the three-step purification process devised by Morris (2015) will be used to purify Naglu-PTD4X. Although Naglu-PTD4X lacks the V5 epitope and 6xHis tag following PTD4, it is predicted that this protocol will purify Naglu-PTD4X to homogeneity. The purity and presence of Naglu-PTD4X will be assessed using silver nitrate staining and immunoblotting respectively.

The third phase will focus on optimizing the purification of Naglu-PTD4X. Targets for optimization will be identified and multiple parameters will be tested to improve purification values, such as yield, final protein concentration, and purity. Yield will be determined by the amount of active Naglu relative to the crude medium. This will be assessed using a fluorogenic

Naglu activity assay. Final protein concentration will be determined by a Bradford assay and purity by silver nitrate staining.

Finally, uptake studies with purified Naglu-PTD4X on MPS IIIB fibroblasts will be conducted. These uptake studies will be assessed by fluorogenic Naglu activity assay of cellular lysates, immunoblotting, and immunocytochemistry. The results will be compared to uptake studies conducted with Naglu-PTD4-V5/His as well as other uptake studies using fusion proteins.

The overall goal of this project is to create an economical system for the production and purification of human recombinant Naglu that has the potential to be used for enzyme replacement therapy in MPS IIIB.

2. Materials and Methods

2.1 Materials

2.1.1 Chemicals and reagents

Abcam, Toronto, ON: polyclonal rabbit anti-Naglu antibody (ab137685). *ACP Chemicals, Montreal, QC*: sodium acetate. *BioRad, Hercules, CA*: BioRad Protein Assay dye reagent, Precision Plus Protein™ Dual Color Standards, S1000™ Thermal Cycler. *Commercial Alcohols Inc., Brampton, ON*: 95% ethanol. *EMD Millipore, Billerca, MA*: 4-methylumbelliferyl-N-acetyl-α-D-glucosaminide. *Invitrogen, Burlington, ON*: Monoclonal mouse anti-V5-HRP-conjugated antibody, pIZT-V5/His vector system. *Jackson ImmunoResearch Laboratories, West Grove, PA:* Alexa Fluor® 488-conjugated AffiniPure Goat Anti-Rabbit IgG (H+L). *Life Technologies, Burlington, ON*: High Glucose Dulbecco's Modified Eagle Medium (DMEM), Fetal Bovine Serum (FBS), Minimum Essential Media Non-Essential Amino Acids (MEM NEAA) (100X), Ethylenediaminetetracaacetic acid (EDTA). *New England Biolabs, Beverly, MA*: 100x bovine serum albumin (BSA), 1.25 M dithiothreitol (DTT). *New England Peptide, Gardner, MA:* Custom polyclonal rabbit anti-PTD4 antibody. *Pierce Biotechnology, Rockford, IL*: SuperSignal® West Dura chemiluminescent reagent. *Qiagen, Mississauga, ON:* DNeasy Blood & Tissue kit, QIAquick PCR Purification kit. *Sigma-Aldrich, Oakville, ON*: sodium phosphate dibasic (Na_2HPO_4-$7H_2O$), potassium phosphate monobasic (KH_2PO_4), sodium chloride (NaCl), potassium chloride (KCl). Sodium hydroxide (NaOH), Tween® 20. *Thermo Fisher Scientific, Waltham, MA*: goat anti-rabbit horseradish peroxidase (HRP)-conjugated secondary antibody, Gibco™ St-900™ II SFM serum free media, Shandon™ Immuno-Mount™.

2.1.2 Prepared media and solutions

Buffers: *Glycine-NaOH buffer*: 0.5 M glycine-NaOH buffer, pH 10.5. *Methanol SDS transfer buffer*: 10% (v/v) methanol, 0.025% (w/v) SDS, 25 mM tris base, 19.2 mM glycine. *PBS*: 137 mM NaCl, 2.7 mM KCl, 8 mM Na_2HPO_4, 1.44 mM KH_2PO_4, pH 7.4. *PBST*: PBS, 0.2% (v/v) Tween® 20. *Purification buffer A*: 50 mM sodium phosphate, pH 5.8. *Purification buffer B*: 1M NaCl, 50 mM sodium phosphate, pH 7.0. *Purification buffer C*: 2 M NaCl, 50 mM sodium phosphate, pH 5.8. *Purification buffer D*: 150 mM NaCl, 50 mM sodium phosphate, pH 5.8. *Purification buffer E*: 300 mM NaCl, 50 mM sodium phosphate, pH 7. *Purificaiton buffer F:* 300 mM NaCl, 50 mM sodium phosphate, 0.25M methyl-alpha-D-glucopyranoside. *SDS Buffer Mix*: 90% (v/v) 3x SDS sample buffer, 10% (v/v) 30x DTT. *Tris-Glycine electrophoresis buffer*: 0.1% (v/v) SDS, 200 mM glycine, 25 mM Tris base.

Culture Media: *Fibroblast growth medium*: (DMEM High Glucose, NEAA 1% (v/v), FBS 10% (v/v).

Other Prepared Solutions: *4MU-Naglu substrate*: 0.1M sodium acetate, 0.5 mg/ml BSA, 0.2 mM 4-methylumbelliferyl-N-acetyl-α-D-glucosamide, pH 4.3. *Silver stain fixative solution*: 50% (v/v) ethanol, 5% (v/v) acetic acid. *Silver stain developer solution*: 20 mg/mL sodium carbonate, 0.04% (v/v) formaldehyde. *Silver stain pre-drying solution*: 10% (v/v) ethanol, 5% (v/v) glycerol.

2.1.3 Equipment and software

Alpha Innotech Corporation, San Leandro, CA: MultiImage™ Light Cabinet. *Barnstead International, Dubuque, IA*: Sequoia-Turner digital fluorometer (model 450). *BioRad, Hercules, CA*: Immunoblot® polyvinylidene fluoride (PVDF), Mini PROTEAN® Tetra Cell electrophoresis system, Mini Trans-Blot® Cell electrophoretic transfer system. *CodonCode Corporation, Centerville, MA:* CodonCode Aligner. *Eastman Kodak, Rochester, NY*: Kodak® X-

OMAT 2000A processor. Processor. *EMD Millipore, Billerca, MA*: Amicon® Ultra-4 30K centrifugal filter device, Amicon® Ultra-15 30K centrifugal filter device, Stericup®-HV 0.45 µm Durapore PVDF Filter Units. *Forma Scientific, Marietta, ON*: Water-Jacketed Incubator Model 3332. *GE Healthcare Life Sciences, Mississauga, ON*: Äktaprime™ chromatographic system, Capto™ MMC media, HiLoad™ 16/600 Superdex™ 200 prep grade prepacked column, HiScreen™ Capto™ MMC prepacked column, HiScreen™ Butyl-S FF prepacked column, HiTrap™ Butyl-S FF prepacked column, PrimeView 5.0 software, XK 26/50 emtpy column. *New Brunswick Scientific, Edison, NJ*: C24 Incubator Shaker. *Pall Corporation, Mississauga, ON*: 0.2 µm Supor®-200 filtration membranes. *PerkinElmer, Waltham, MA*: Wallac 1420 Victor²™ Microplate Reader. *Pharmacia (now Pfizer), New York City, NY:* P Mono PC3365A13 empty column. *Pierce Biotechnology, Rockford, IL*: CL-X Posure™ film *Sarstedt, Newton, NC*: PE Vented Cap T25, T75, T175, rubber tipped 25 cm cell scrapers. *Thermo Fisher Scientific, Waltham, MA*: 250 mL and 1 L: Fisherbrand® shaker flasks.

2.1.4 Cell lines

Coriell Institute for Medical Research, *Camden, NJ:* GM02391 Sanfilippo Syndrome B skin fibroblasts, GM01426 Sanfilippo Syndrome B skin fibroblasts. *Invitrogen, Burlington, ON*: Gibco™ Spodoptera frugiperda 9 cells. *McGill University Health Centre Cell Repository, Montreal, QC*: MCH064 normal skin fibroblasts.

2.2 Methods

2.2.1 Sf9 cell growth and stable expression of Naglu-PTD4X

Small-scale Sf9 cultures, stably selected to express Naglu-PTD4X, were cultured in vented T25 flasks in 7 mL of SFM media (Thermo Fisher Scientific) at 27°C in a non-humidified water-jacketed incubator. The cells were scaled up in a step-wise manner till they reached

confluency in a T175 flask. The cells were resuspended and transferred into 75 mL of SFM media in a 250 mL unbaffled vented shaker flask. The cultures were continuously shaken at 26-28°C and at 120 rpm. At a cell density of $2x10^6$ cells/mL, 75 mL of the small-scale shaker culture was transferred into 325 mL of SFM media in a 1 L unbaffled shaker flask. After three days of recovery, the culture volume was scaled up to 500 mL. The culture media was harvested and replaced with 450 mL of fresh SFM media every 3-5 days depending on the level of active Naglu present, which was determined by a fluorogenic activity assay. The harvested culture medium was centrifuged at 4000 xg and stored at -20°C.

2.2.2 Sf9 genomic DNA analysis

Genomic DNA from stably transfected Sf9 cells was extracting using DNeasy® Blood & Tissue kit (Qiagen) according to manufacture's instructions. The downstream region of *NNSS-Naglu-PTD4X* insert was PCR amplified using a S1000™ Thermal Cycler (BioRad). Platinum™ Green Hot Start PCR (2X) master mix (Invitrogen), which consisted of Platinum™ Taq, dNTPs and $MgCl_2$, was diluted to a 1X master mix. To this master mix, 1.7mM of each primer, 20% (v/v) Platinum™ GC Enhancer, and 3.7ng of genomic template DNA was added. The final volume was made up to 50μL with nuclease-free dH_2O. The forward primer bound to a sequence within exon six that was 599bp upstream of the PTD4 sequence. The reverse primer bound to the OPIE2 reverse priming site of the pIZT/V5-His vector.

The PCR profile was as follows: PCR reaction mixture was initially denatured at 94°C for 3 min, then it underwent 37 cycles of 94°C (0.5 min), 49°C (0.5 min), 72°C (1 min). This was followed by a final elongation at 72°C for 5 minutes. Samples were stored at 4°C. PCR products

were run on an 2% agarose gel in TBE buffer at 100V. The gel was stained with ethidium bromide and visualized using MultiImage™ Light Cabinet (Alpha Innotech Corporation).

PCR products were purified using QIAquick® PCR purification kit (Qiagen) according to manufacturer's instructions. The concentration of purified PCR products was determined by nanodrop. Sequence analysis of products was conducted by Eurofins Operon (Louisville, KY) and assembled using CodonCode Aligner software (CodonCode Corporation).

2.2.3 Naglu-PTD4Xpurification using Naglu-PTD4-V5/His purification protocol

The following purification protocol was adapted from the Morris (2015) protocol for the purification of Naglu-PTD4-V5/His. All solutions were degassed with 0.2 µm Supor®-200 filtration membranes (Pall) prior to loading on to columns. Purification steps were conducted on ÄktaPrime FPLC system (GE Healthcare Life Sciences) and an in-line UV was used to continuously record UV absorbance at 280 nm for each step of purification This record was saved using PrimeView software.

MMC purification

An XK 26/20 column (GE Healthcare Life Sciences) was custom packed to a final volume of 50 mL with Capto™ MMC media (GE Healthcare Life Sciences). Prior to each purification run, the column was washed with 3 CV of distilled water and equilibrated with 10 CV of buffer A. Purification runs with this column was conducted at a flow rate of 7 mL/min.

Crude, cell-clarified Sf9 culture medium was thawed and centrifuged at 4000 xg for 30 minutes. The pH of the supernatant was adjusted to 5.8 then degassed with a 0.45 µm Durapore PVDF membrane. Prepared medium was loaded on to the column.

Following loading, the MMC was washed with buffer A until the UV profile returned to baseline. To elute Naglu-PTD4X from the column, the pH was increased from 5.8 to 7 and the salt concentration to 1M NaCl. This was accomplished by using an 2 CV linear gradient from buffer A to buffer B followed by an additional 3 CV of buffer B. Fractions of 12 mL were collected and analyzed for Naglu activity with an artificial substrate 4-methylumbelliferyl-N-acetyl-α-D-glucosaminide (4MU-Naglu, EMD Millipore). High activity fractions were pooled and stored at 4°C.

HIC purification

Two pre-packed HiScreen Butyl-S columns (GE Healthcare Life Sciences) were connected in series to produce a single 20 cm, 9.4 mL column. The column was washed with 3 CV of distilled water and equilibrated with 10 CV of buffer C. Purification was conducted at a flow rate of 1 mL/min.

Prior to loading, the salt concentration of the post-MMC sample was adjusted to 2M NaCl and the pH was adjusted to 5.8. Following degassing with a 0.45 μm Durapore PVDF membrane (EMD Millipore), the post-MMC sample was loaded on to the HIC.

After loading, the HIC was washed with buffer C until the UV trace returned to baseline. To elute Naglu-PTD4X from the column, a 5 CV desalting gradient from buffer C to buffer A was used. Fraction of 7 mL were collect and analyzed for Naglu activity with 4-Naglu substrate. High and low activity fractions were pooled separately. Low activity fractions were used to block the Amicon Ultra-15 centrifugal filter device (EMD Millipore) membranes. High activity fractions were concentrated and dialyzed with buffer D to a final volume of 1 mL.

SEC purification

A pre-packed HiLoad Superdex 200 size exclusion column (GE Healthcare Life Sciences) was equilibrated with 2 CV of Buffer A and 3 CV of Buffer D at 1 mL/min. The prepared sample was loaded on to sample loop and then injected onto the column at 0.5 mL/min. Buffer D was run through the column. Fractions of 1 mL were collected and analyzed for activity with the 4MU-Naglu substrate.

2.2.4 Naglu-PTD4X purification optimization

Aside from optimization steps, all other purification steps were conducted based on the protocol outlined above.

Concanavalin A Purification

An P Mono PC3365A13 column (Pharmacia) was custom packed to a final volume of 5.6mL with Con-A Sepharose 4B media (GE Healthcare Life Sciences). The column was equilibrated with 10 CV of Buffer E. The post-MMC sample was diluted to 0.3M NaCl and the pH adjusted to 5.8. Prior to loading, the post-MMC sample was degassed with a 0.45 μm Durapore PVDF membrane. Approximately 45 mL of sample was loaded on to the column then it was washed with 5 CV of buffer E. To elute Naglu-PTD4X, 5 CV of buffer F, which contained a competitively binding sugar, methyl-alpha-D-glucopyranoside, was used. Fractions of 1 mL were collected throughout the run and assayed for Naglu activity using 4MU-Naglu substrate.

HIC Elution Optimization

Crude medium was purified using the capture MMC column according to the above protocol. The HIC purification remained the same as above except for the parameters that were being optimized. For each optimization trial 60 mL of MMC-purified sample was loaded on to the column. A control HIC purification was run according to the above protocol for a baseline comparison. The trials were as follows: in trial #1, the salt concentration of the loading buffer

was decreased to 1.5M of NaCl; in trial #2, the pH of the elution buffer was increased to 7; in trial #3, 0.5M urea was added to the elution buffer; in trial #4, 0.1% (v/v) Triton X-100 was added to the elution buffer; and in trial #5, 0.1% (w/v) sodium cholate was added to the elution buffer. Fraction were collected throughout trial purifications. Fraction from trials #1-3 were assayed for Naglu activity using the 4Mu-Naglu substrate. Fractions from trials #4 and #5 were dialyzed to remove the added detergent using the Amicon Ultra-15 centrifugal filter devices, as described above, before assaying for Naglu activity.

Dialysis Optimization

Crude medium was purified using the MMC and HIC purification protocol as described above. A control sample was dialyzed without passivation of the Amicon Ultra-15 centrifugal filter devices as a baseline for comparison. The Amicon Ultra-15 centrifugal filter device was blocked with 5% (v/v) Triton X-100 for 1 hour. Filters were rinsed with 1.5 L of distilled water then filters were spun with distilled water three times prior to concentrating post-HIC sample according to the above protocol. Samples of pre-dialysis and post-dialysis were taken and assayed for Naglu activity assay using the 4Mu-Naglu substrate.

2.2.5 Bradford Protein Concentration and Naglu Activity Assays

Total protein concentration was determined by a Bradford assay (Bradford, 1976). Bio-Rad Protein Assay concentrated dye was diluted to 50% in water. In a 96-well plate, 80 µL of reagent was mixed with 120 µL of each sample. The plate was incubated shaking at RT for 5 minutes and read at 595 nm using a Wallac 1420 Victor^{2}™ Microplate Reader (PerkinElmer). Protein concentration was calculated using a BSA standard curve ranging from 0 to 50 µg/mL. Samples were diluted to produce values that fell within the linear range of this curve.

Samples were assayed for Naglu activity using the following procedure (Chow and Weissmann, 1981; Zhao and Neufeld, 2000). A reaction mixture of 25 µL sample and 25 µL 4MU-Naglu substrate was incubated at 37°C for 1 hr. The reaction was stopped after an addition of 1.5 mL of glycine-NaOH buffer and the fluorescence was measured using a Novaspec® visible fluorometer (360 nm narrow band excitation filter, 415 nm sharp cut emission detection filer, span fully counter-clockwise). A 4-methylumbelliferone (4-MU) standard curve was used to convert the arbitrary fluorescence unit (AFU) of each sample into units of activity (Supplementary Figure 4 and Supplementary Table 2).

2.2.6 SDS-PAGE protein analysis

Samples were mixed with 3X SDS-PAGE sample buffer and boiled for 5 minutes. The pH of the samples was adjusted using 4M NaOH and the samples were centrifuged for 5 minutes at 16,000 xg. The SDS-PAGE gel was comprised of either a 10% or 8% (v/v) tris-glycine resolving layer with a 4% (v/v) tris-glycine stacking layer. The prepared samples were loaded on the SDS-PAGE gel and run at 100 V in a Mini-Protean® Tetra Cell electrophoresis unit (BioRad). A pre-stained protein ladder (Precision Plus Protein™ Dual Color Standards, BioRad) was loaded alongside samples in order to calculate apparent molecular weights of the sample.

2.2.7 Silver stain analysis

SDS-PAGE gels were visualized using the following silver nitrate stain protocol. The arcylamide gel was submerged in a fixative solution and microwaved for 90 seconds. The gel was placed in a 50% ethanol (v/v) solution and microwaved for 90 seconds then placed in 0.02% (w/v) sodium thiosulfate solution and microwaved for 90 seconds. The gel was rinsed three times in deionized water for 2 minutes before being placed in 0.2% (w/v) silver nitrate solution for 20 minutes at room temperature. The gel was rinsed with deionized water for 90 seconds then added

to a developing solution of 0.04% (v/v) formaldehyde and 2% (w/v) sodium carbonate. The gel was gently shaken until bands developed. A solution of 5% (v/v) glacial acetic acid was added to stop the gel from developing further.

2.2.8 Immunoblot analysis

Following SDS-PAGE, tank electrotransfer was used to transfer proteins from the acrylamide gel to an Immunoblot® polyvinylidene fluoride PVDF membrane (BioRad). Electrotransfer was conducted in 10% (v/v) methanol and 0.025% (w/v) SDS transfer buffer (25 mM tris-HCl, 200 mM glycine) overnight at 20V. Membranes were soaked in 100% methanol, dried at room temperature, and stored at 4°C.

Membranes were placed in 100% methanol and then washed in PBST. Blocking was conducted with 5% (w/v) skim milk in PBST for 1 hour at room temperature, or overnight at 4°C. Membranes were washed with PBST before incubation with various primary antibodies.

For anti-Naglu immunoblotting, a polyclonal rabbit anti-Naglu ab137685 (Abcam) was applied at 1:2000 in PBST and the membrane was incubated for 2 hours at room temperature or overnight at 4°C. For anti-PTD4 immunoblotting, a polyclonal rabbit anti-PTD4 (New England Peptides) was applied at 1:500 in PBST and the membrane was incubated similar to above. The membrane were rinsed three times with PBST for 5 minutes to remove unbound primary antibody. Secondary goat anti-rabbit HRP (Thermo Fisher Scientific) conjugated antibody was applied to membrane at 1:2000 in blocking reagent for 1 hour and then washed three times with PBST for 5 minutes.

SuperSignal® West Dura extended exposure substrate (Pierce) was applied to probed membrane for 5 minutes. Membranes were exposed to CL-X Posure™ film (Pierce) for times varying from 10 seconds to 2 hours and visualized using a Kodak X-OMAT 2000A Processor.

2.2.9 Cellular uptake studies

Survey of incubation length

Human MPS IIIB skin fibroblasts (GM01426, Coriell Institute for Medical Research) were grown on vented T25 cell culture flasks containing fibroblast growth media. At 80-100% confluency, the medium was replaced and reduced to 1 mL and 1000 units of purified Naglu-PTD4X was added. Cells were incubated for various time periods, 1 hr, 4 hrs, or 16 hrs, at 37°C and 5% CO_2. PBS was used to wash cells three times to remove extracellular Naglu-PTD4X. To lyse the cells, 310 μL of M-PER™ was added before cells were gently shaken for 5 minutes. Cells were harvested by mechanical passaging and centrifuged at 16,000 xg for 10 minutes. Supernatant was assayed for Naglu activity using the 4MU-Naglu substrate.

Uptake study with negative and positive control

GM01426 (Coriell Institute for Medical Research) and a wild-type control cell line (MCH064, McGill University Health Centre Cell Repository) were grown on vented T25 cell culture flasks containing fibroblast growth media. At 80-100% confluency, the medium was replaced and reduced to 1 mL and 1000 units of purified Naglu-PTD4X was added. To the controls, PBS was added. Cells were incubated for 16 hours at 37°C and 5% CO_2. PBS was used to wash cells three times to remove extracellular Naglu-PTD4X. To lyse the cells, 310 μL of M-PER™ was added before cells were gently shaken for 5 minutes. Cells were harvested by mechanical passaging and centrifuged at 16,000 xg for 10 minutes. Supernatant was assayed for Naglu activity using the 4MU-Naglu substrate and visualized using anti-Naglu immunoblotting.

Immunocytochemistry

A modified Immunocytochemistry protocol was used to visualize uptake of Naglu-PTD4X (Kan *et al.*, 2014; Litke *et al.*, 2018). GM02931 (Coriell Institute for Medical Research), human MPS IIIB skin fibroblasts with negligible Naglu activity, were cultured on vented T75

flasks in fibroblast medium. To measure viability and overall fluorescence, fibroblasts were passaged on to laminin coated coverslips at 90-100% confluency before 200 units of purified Naglu-PTD4 was added. To measure fluorescence of individual cells, fibroblasts were passaged on to the coverslips at 50% confluency before 200 units of purified Naglu-PTD4X was added. PBS was added to control cells. Cells were incubated for 16 hrs at 37°C and 5% CO_2. PBS was used to wash cells three times before fixing cells using 4% (v/v) paraformaldehyde on a shaker for 15 minutes at room temperature. Cells were washed three times with PBS and then permeabilized with 1% (v/v) Triton X-100 for 10 minutes on a shaker at room temperature. PBS was used to wash cells three times before applying 1:2500 dilution of rabbit anti-Naglu in 0.1% (v/v) Triton X-100 and incubating overnight at 4°C. Cells were washed three times with PBS then 1:500 dilution of Alexa Fluor® 488-conjugated goat anti-rabbit antibody and 0.2 μg of DAPI was applied. The secondary antibody was incubated with the cells for 1 hour at 37°C before washing cells with PBS and mounting with Shandon™ Immuno-Mount™ on microscope slides.

Cells were visualized on a Nikon 2 confocal microscope (Nikon Corp) and NIS-Elements AR software was used to acquire Z-stacks of 2.5 μm thickness. To quantitate fluorescence, FIJI (ImageJ) software was used to create a maximum intensity projection. For these projections, the integrated density of fluorescence for each cell was subtract by the background fluorescence to determine the corrected total fluorescence of each cell.

3. Results

3.1 Isolation and sequencing of stably transfected Sf9 genomic DNA

To verify the presence of the re-introduced stop codon in the *Naglu-PTD4X* insert following stable integration into the Sf9 genome, Sf9 genomic DNA was isolated and the downstream region of the *Naglu-PTD4X* insert was amplified by PCR. The purity and size of the partial *Naglu-PTD4X* insert may be seen in Figure 3.1. Sequence analysis of the insert confirmed the presence of the re-introduced stop codon (TAA) following the PTD4 sequence within the genomic DNA of a stably transfected Sf9 cells. Sequencing results of the downstream region of the *Naglu-PTD4X* insert may be seen in Figure 3.2.

3.2 Purification of Naglu-PTD4X using Naglu-PTD4-V5/His purification protocol

Media was harvested from continuous shaker cultures of Sf9 cells that stably expressed active Naglu-PTD4X. Purification was conducted on a ÄKTAprime™ liquid chromatography system using a three-step column chromatography protocol optimized to purify Naglu-PTD4-V5/His with a yield of 26%. Prior to loading on to the MMC, Sf9 media was adjusted to a pH of 5.8. The protein profile of the MMC may be seen in Figure 3.3A and was measured by in-line UV at 280nm. Approximately, 1100-1300 mL of medium was loaded on to the MMC. To elute Naglu-PTD4X a continuous gradient of increasing salt concentration and pH was employed. The MMC elution occurred over 120 mL with significant Naglu activity occurring in ten 12 mL fractions, which is outlined by a box in Figure 3.3A. This activity was determined by a 4MU Naglu activity assay. The capture step resulted in an 83% yield of active Naglu and a 10-fold

purification, which may be seen in Table 3.1. The pH and salt concentration of the pooled MMC purified fractions was adjusted prior to loading on the HIC column.

Butyl-S, a weak hydrophobic interaction media, was utilized for intermediate purification. Figure 3.3B shows the protein profile of the HIC purification measured with an in-line UV at 280 nm. Approximately 200 mL MMC purified sample was loaded on to the HIC and a continuous gradient of decreasing salt concentration was used to elute Naglu-PTD4X. The HIC column elution occurred over 42 mL with significant Naglu activity detectable in three fractions of 7mL and is outlined by a box in Figure 3.3B. This intermediate step resulted in an 41% yield of active Naglu and a 405-fold purification relative to the crude media, which may be seen in Table 3.1. Prior to the polishing step, the HIC purified fractions were dialyzed in buffer D and concentrated to 1 mL.

A SEC was selected for the polishing step and the SEC purification protein profile, measured by an in-line UV at 280 nm, may be seen in Figure 3.3C. Multiple peaks in the protein profile were centered at approximately 47 mL, 53 mL, and 66 mL. The peak centered at approximately 66mL corresponded to significant Naglu activity levels and is outlined by a box in Figure 3.3C. The purification of Naglu-PTD4X to homogeneity can be visualized in Figure 3.4. This final polishing step resulted in an 11% yield of active Naglu overall and a 551-fold purification relative to the crude media, which may be seen in Table 3.1.

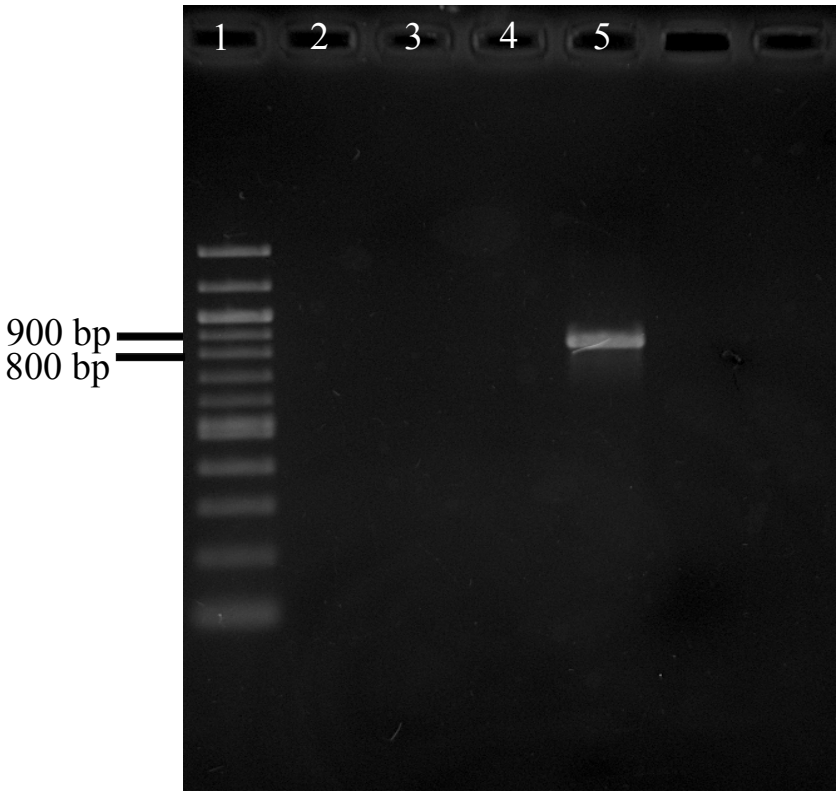

Figure 3.1 Agarose gel analysis of PCR amplification of *Naglu-PTD4X* insert in genomic DNA isolated from stably transfected Sf9 culture

Lane contents: (1) 100bp DNA ladder (2,4) empty (3) negative PCR control: water only (5) PCR amplified genomic Sf9 *Naglu-PTD4X* insert. Genomic DNA was isolated from Sf9 cultures stably expressing Naglu-PTD4Xand the downstream region of Naglu-PTD4Xwas PCR amplified to determine the presence of the re-introduced stop codon following the PTD4 sequence. The expected size for the PCR product was 840bp.

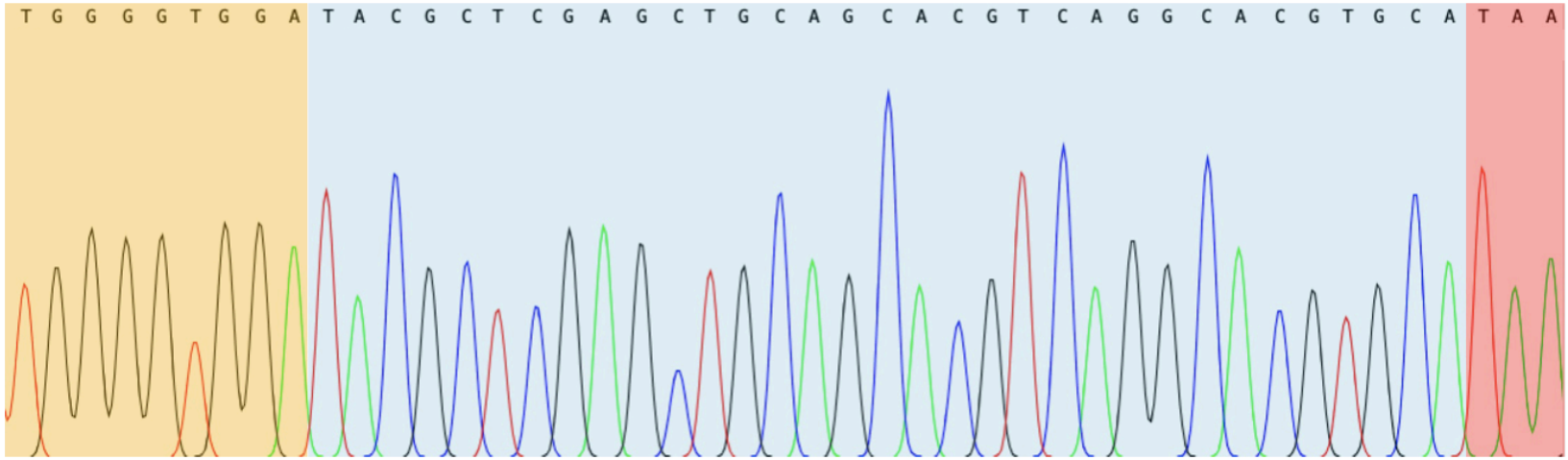

Figure 3.2 DNA chromatograph of the downstream region of Naglu-PTD4X sequenced from genomic DNA that was isolated from a stably transfected Sf9 culture

The 3' end of *Naglu-PTD4X* and following glycine linker is highlighted in yellow, the PTD4 sequence is highlighted in blue and the re-introduced stop codon is highlighted in red. Genomic DNA was isolated from Sf9 cultures stably expressing Naglu-PTD4X. The downstream region of Naglu-PTD4X was PCR amplified and sequenced to verify the presence of the re-introduced stop codon following the PTD4 sequence within the stably transfected Sf9 cell line.

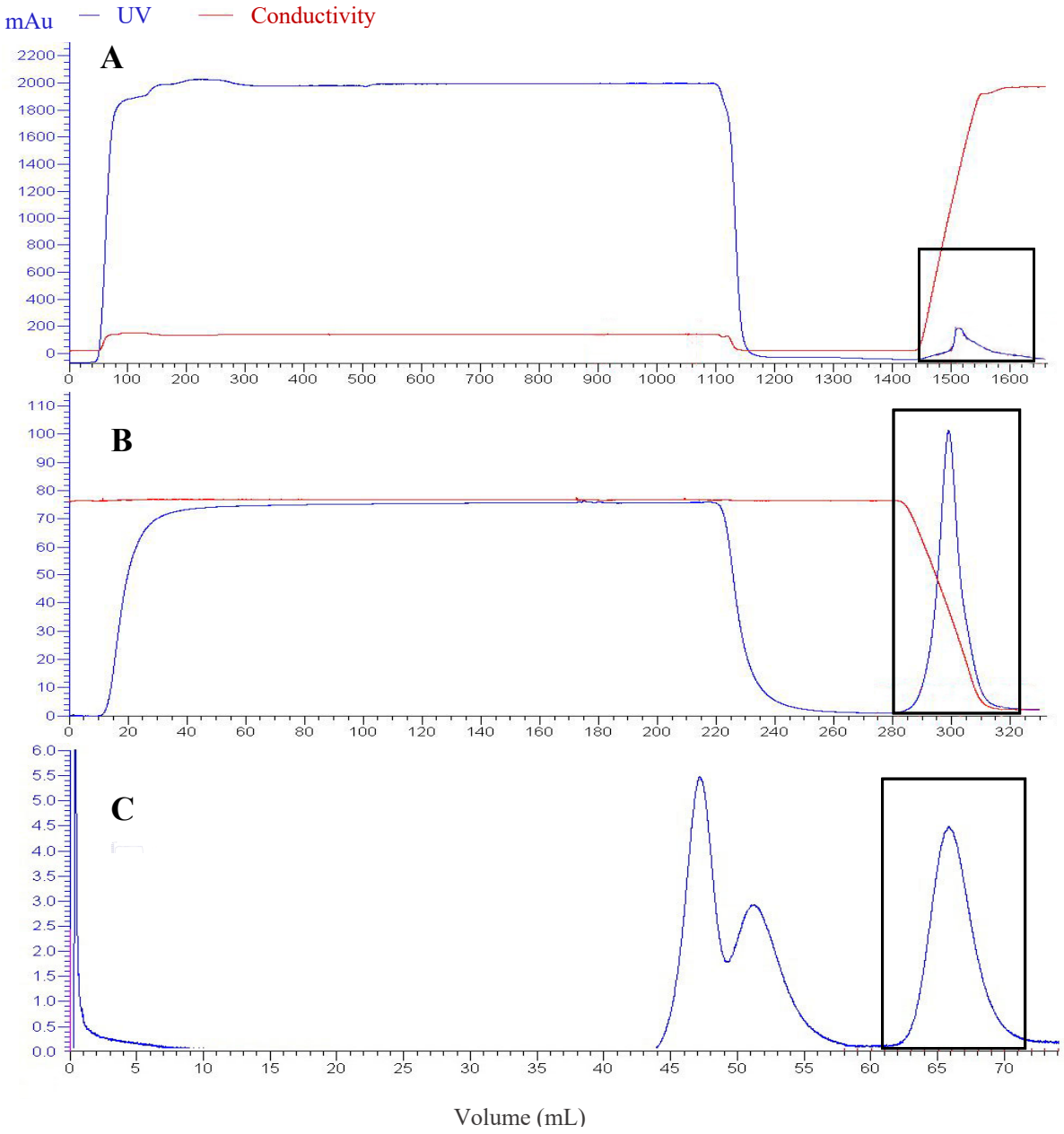

Figure 3.3 Protein profile of Naglu-PTD4X purification using parameters optimized to purify Naglu-PTD4-V5/His

Figures are as follows: A) MMC purification B) HIC purification C) SEC purification. Medium was harvested from Sf9 culture stably expressing Naglu-PTD4X and was purified by a three-stage HiScale Capto™ MMC column, HiTrap Butyl-S column, and HiLoad Superdex 200 column purification protocol previously developed by Morris (2015). Fractions containing Naglu activity, as determined by a 4MU-Naglu assay, are framed by black boxes and were retained and used in subsequent steps. Protein profiles were generated by in-line UV measuring absorbance at 280 nm.

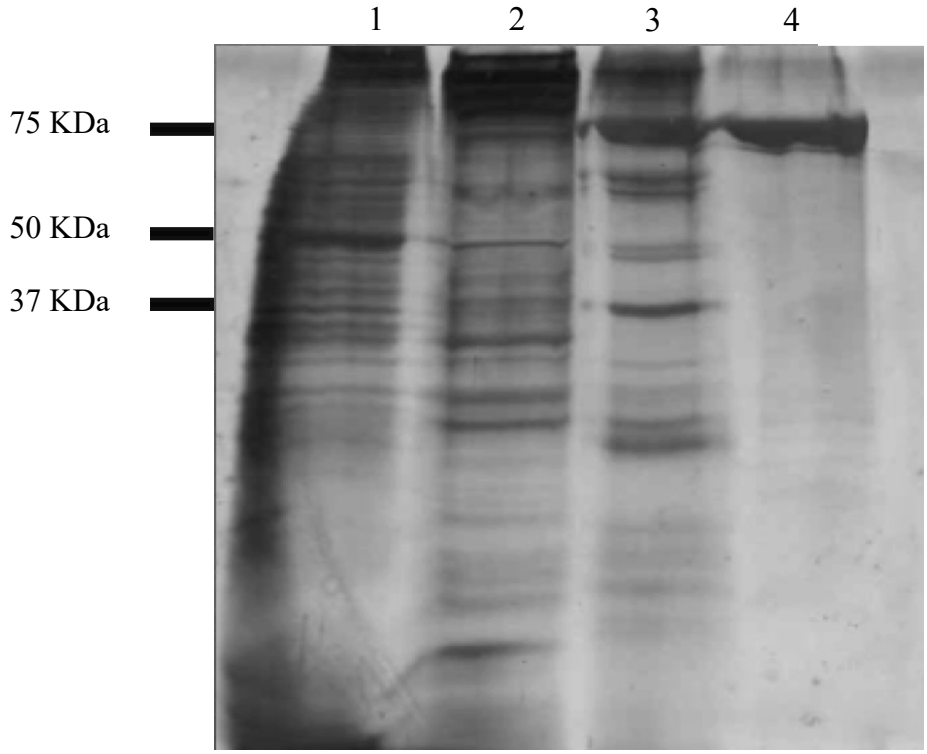

Figure 3.4 SDS-PAGE gel stained with silver nitrate stain to visualize results of preparative purification of Naglu-PTD4X using a protocol designed by Morris (2015) to purify Naglu-PTD4-V5/His.
Lane contents: (1) Crude medium (2) post-MMC (3) post- HIC (4) post-SEC. Culture medium harvested from Sf9 cells stably expressing Naglu-PTD4Xwas purified by a three-stage preparative column purification protocol using a HiScale Capto™ MMC column, HiTrap Butyl-S column, and HiLoad Superdex 200 column. Samples were loaded and separated on a 10% polyacrylamide gel prior to staining with silver nitrate stain.

Table 3.1 Yield of active Naglu through preparative purification of Naglu-PTD4X using a protocol designed by Morris (2015) to purify Naglu-PTD4-V5/His

Step	Volume (mL)	Activity (U)	Protein (mg)	Specific Activity (Units/mg)	Purification (fold)	Yield (%)
Medium	1300	36000	195	185	1	100
Post-MMC	188	30000	15	1985	10	83
Post-HIC	35	15000	0.2	75000	405	41
Post-SEC	7	4080	0.04	102000	551	11

One unit of activity corresponds to 493 arbitrary fluorescent units as measured by the fluorogenic 4MU Naglu activity assay. Protein concentrations was determined by a Bradford protein concentration assay. Equilibrated crude medium was the baseline for comparison to determine percent yield calculations. For the medium and pre-HIC samples, activity values were calculated immediately prior to loading. For the post-HIC and post-SEC sample, activity values were calculated immediately following elution. All values represent the average from three separate purifications.

3.3 Optimization of preparative purification of Naglu-PTD4X

3.3.1 Identification of targets to optimize Naglu-PTD4X purification

Using the purification method developed by Morris (2015), Naglu-PTD4X was purified from Sf9 media with a yield of 11%. This was 15% lower than the yield reported by Morris (2015) for the purification of Naglu-PTD4-V5/His from Sf9 media. Table 3.2 compares the yields throughout purification for Naglu-PTD4X and Naglu-PTD4-V5/His. There was a 25% yield disparity between Naglu-PTD4X and Naglu-PTD4-V5/His following the HIC step and dialysis step. These two steps were identified as potential targets for optimization. For the HIC step, a Naglu activity assay revealed that the majority of the loss in yield was due to incomplete HIC elution: approximately 30-40% of Naglu-PTD4X was not eluted and remained bound to the intermediate column. Another potential target for optimization, was the dialysis step that preceded the polishing column. Approximately 15-20% of Naglu-PTD4X was lost during the centrifugal dialysis step, which was likely due to non-specific binding of Naglu-PTD4X to the centrifugal membranes.

3.3.2 Intermediate purification with Concanavalin A

Con-A was selected as an alternative media to the Butyl-S to potentially improve intermediate purification. Pooled MMC purified fractions were adjusted to pH of 7 and salt concentration of 0.3M. Of this prepared sample, 45 mL was loaded on to the Con-A column. Elution occurred over 53 mL and resulted in a 15% yield of active Naglu relative to the MMC purified sample. No detectable Naglu activity was found in fractions collected during loading or washing of the column. Figure 3.5 shows a significantly higher degree of protein banding in the Con-A purified sample in comparison to the HIC purified sample, indicating that the Con-A was less effective at removing protein impurities in comparison to the HIC.

3.3.3 Optimization of HIC elution

Four different conditions were tested in an attempt to increase elution of Naglu-PTD4X from the intermediate purification column: decreased salt concentration, increased pH, addition of urea, addition of Triton X-100, and addition of sodium cholate. A control HIC purification was conducted based on protocol devised by Morris (2015) and the protein profile and yield calculations may be seen in Figure 3.5A and Table 3.3 respectively. In the first trial, the salt concentration during loading was decreased from 2M to 1.5M. The protein profile of this trial in Figure 3.6 indicates an increase in protein loss during loading: the UV value for loading step of the control HIC was approximately 45-50 mAu whereas trial #1 had a UV value of 55-60 mAu for the loading step. Fractions taken from trial #1 during loading showed an increase in Naglu activity, indicating that Naglu-PTD4X was being lost during the loading step. This was reflected in the decrease in yield from 58% to 28% in this trial compared to the control, which may be seen in Table 3.3.

The second and third trials, which involved increasing the pH to 7 of elution buffer and adding 0.5M urea to the elution buffer respectively, showed little to no effect on elution of the HIC. This is evident in the protein profiles in Figure 3.6, which compares the profiles of these conditions with the profile of the control HIC (Figure 3.6). Table 3.3 shows that the yield of Naglu-PTD4X for these conditions was comparable to the control condition.

The fourth and fifth condition employed detergents to promote increased elution of Naglu-PTD4X from the intermediate column. Triton X-100 and sodium cholate were added with a final concentration of 0.1% to the elution buffer. Figure 3.7 shows that the protein profiles of these conditions were distinct from the control profile. Triton X-100 absorbs in the UV spectrum, which was reflected in the 550 mAu peak at 150 mL in Figure 3.7B. The addition of sodium

cholate resulted in broader elution peak: the elution peak remained above 5 mAu from 135 to 155 mL whereas the elution peak for the control remained above 5 mAu from 145-155 mL. Both Triton X-100 and sodium cholate absorb at the fluorescence emission used to conduct Naglu activity assays, which lead to a distortion in the yield results for these conditions. This can be seen in Table 3.3. The effect of detergent removal on Naglu-PTD4X yield using centrifugal dialysis was analyzed via a Naglu activity assay, which is outlined in Table 3.4. The control, Triton X-100, and sodium cholate condition had a yield of 30%, 5%, and 44% respectively following dialysis.

3.3.4 Optimization of post-HIC dialysis

The dialysis step following HIC and prior to SEC purification was another potential target for optimization. Passivation of the centrifugal membranes using 5% (v/v) Triton X-100 was conducted in order to limit non-specific binding and loss of Naglu-PTD4X during dialysis. The yield of Naglu-PTD4X was determined by a Naglu activity assay and the results can be seen in Table 3.5. Without passivation the yield of Naglu-PTD4X was 72% whereas with passivation it was 86%.

3.3.5 Full-scale optimized preparative purification of Naglu-PTD4X

Optimizing dialysis through passivation was selected to improve the yield of Naglu-PTD4X purification. In addition, the volume of crude media loaded initially on to the MMC column was reduced. Employing these two parameters for optimization, three full-scale replicates of preparative purification of Naglu-PTD4X were conducted.

Figure 3.7 compares the SEC protein profiles of Naglu-PTD4X purification following the parameters for Naglu-PTD4-V5/His purification and the optimized parameters for Naglu-PTD4X purification. The non-optimized purification profile had two peaks proceeding the Naglu-PTD4X

peak centered over 47 mL and 53 mL and they peaked at approximately 5 mAu and 3 mAu respectively. The optimized purification profile had one peak, proceeding the Naglu-PTD4X peak, centered over 47 mL and it peaked at approximately 27 mAu. The Naglu-PTD4X peak for both profiles demonstrated a high degree of similarity: they were centered over approximately 65 mL and measured at 5 mAu.

The purification values, which were averaged from three separate runs of the optimized purification protocol, are highlighted in Table 3.6. The capture step with the MMC had an improved yield, increasing from 83% to 98%, and the final polishing step had an improved yield, increasing from 11% to 26%. Additionally, the overall amount of purified protein increased from 0.04 mg to 0.07 mg. The purification of Naglu-PTD4X to homogeneity was visualized by a silver nitrate stain, which may be seen in Figure 3.10. This silver nitrate stain indicated that the HIC purification step removed the bulk of the protein impurities based on the significant decrease in protein banding. Following the SEC purification, there was only a single distinct band present at approximately 75 kDA, which corresponds to the predicted size of Naglu-PTD4X. This was verified by immunoblotting with antibodies against Naglu and PTD4, which may be seen in Figure 3.11 and Figure 3.12 respectively. Both blots of purification showed a distinct band at 75 kDa for each step throughout purification.

Table 3.2 Comparison of active Naglu yield for the purification of Naglu-PTD4X and Naglu-PTD4-V5/His through a three-step preparative purification protocol designed by Morris (2015).

Step	Overall Yield of Naglu-PTD4-V5/His (Morris, 2015) (%)	Overall Yield of Naglu-PTD4X (%)
Medium	100	100
Pre-HIC	82	83
Post-HIC	-	41
Pre-SEC	50	25
Post-SEC	26	11

Yield was calculated based on active units of Naglu, which were determined from a fluorogenic 4MU-Naglu activity assay. Equilibrated crude medium was the baseline for comparison to determine percent yield calculations. For the medium, pre-HIC, and pre-SEC samples, activity values were calculated immediately prior to loading. For the post- HIC and post-SEC sample, activity values were calculated immediately following elution. All values were averaged from three separate purifications.

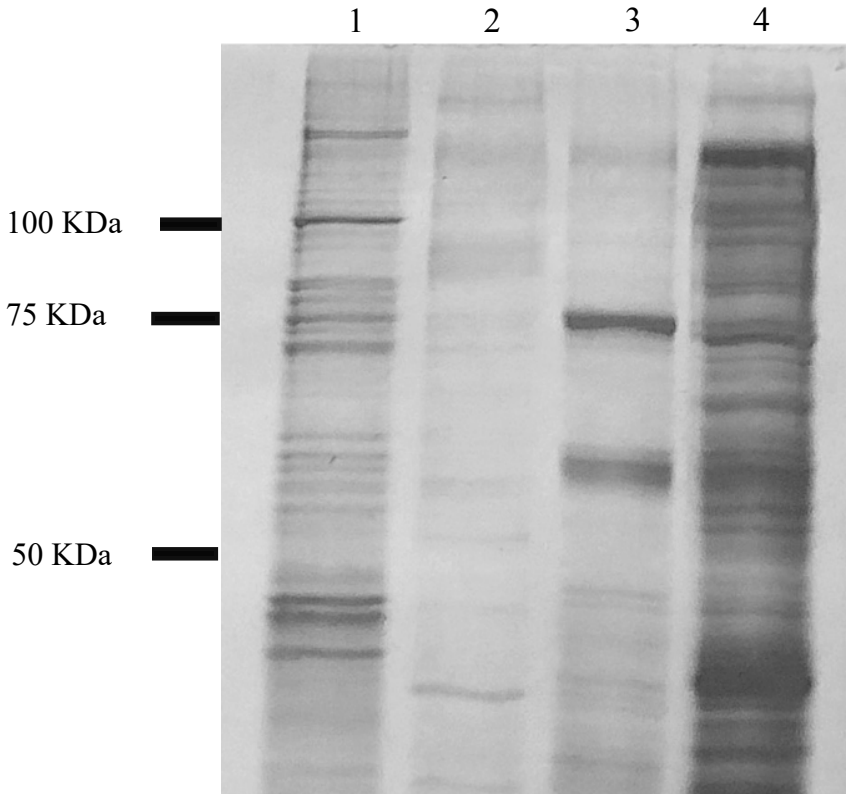

Figure 3.5 SDS-PAGE gel stained with silver nitrate stain to visualize the results Concanavalin A and Butyl-S purification.

Lane contents: (1) Crude medium (2) post-MMC (3) post- HIC (4) post-Con-A. Culture medium harvested from Sf9 cells stably expressing Naglu-PTD4Xwas partially purified by a using a HiScale Capto™ MMC column. The MMC purified sample was divided and one part was purified using an HIC and the other purified using a Con-A column. The samples were loaded and separated on an 8% polyacrylamide gel prior to staining with silver nitrate stain.

Table 3.3 Optimization trials of HIC elution for purification of Naglu-PTD4X

	Pre-HIC Naglu Activity (Units)	Post-HIC Naglu Activity (Units)	Yield (%)
Control	4547	2651	58%
Trial #1: 1.5M NaCl	5298	1465	28%
Trial #2: pH 7.0	1788	926	52%
Trial #3: 0.5M Urea	2210	982	44%
Trial #4: 0.1% Triton X-100	4629	4022	87%
Trial #5: 0.1% Sodium Cholate	6474	8703	134%

Culture medium harvested from Sf9 cells stably expressing Naglu-PTD4Xwas partially purified by a using a HiScale Capto™ MMC column. Approximately 60 mL of Pre-HIC sample was loaded for each purification trial. In Trial #1 the salt concentration of loading conditions was reduced from 2M to 1.5M. In Trial #2 the pH of the elution buffer was increased from 5.8 to 7. In Trial #3-5 0.5M of Urea, 0.1% Triton X-100, and 0.1% sodium cholate respectively were added to elution buffer. Yield was calculated based on active units of Naglu, which were determined from a fluorogenic 4MU Naglu activity assay.

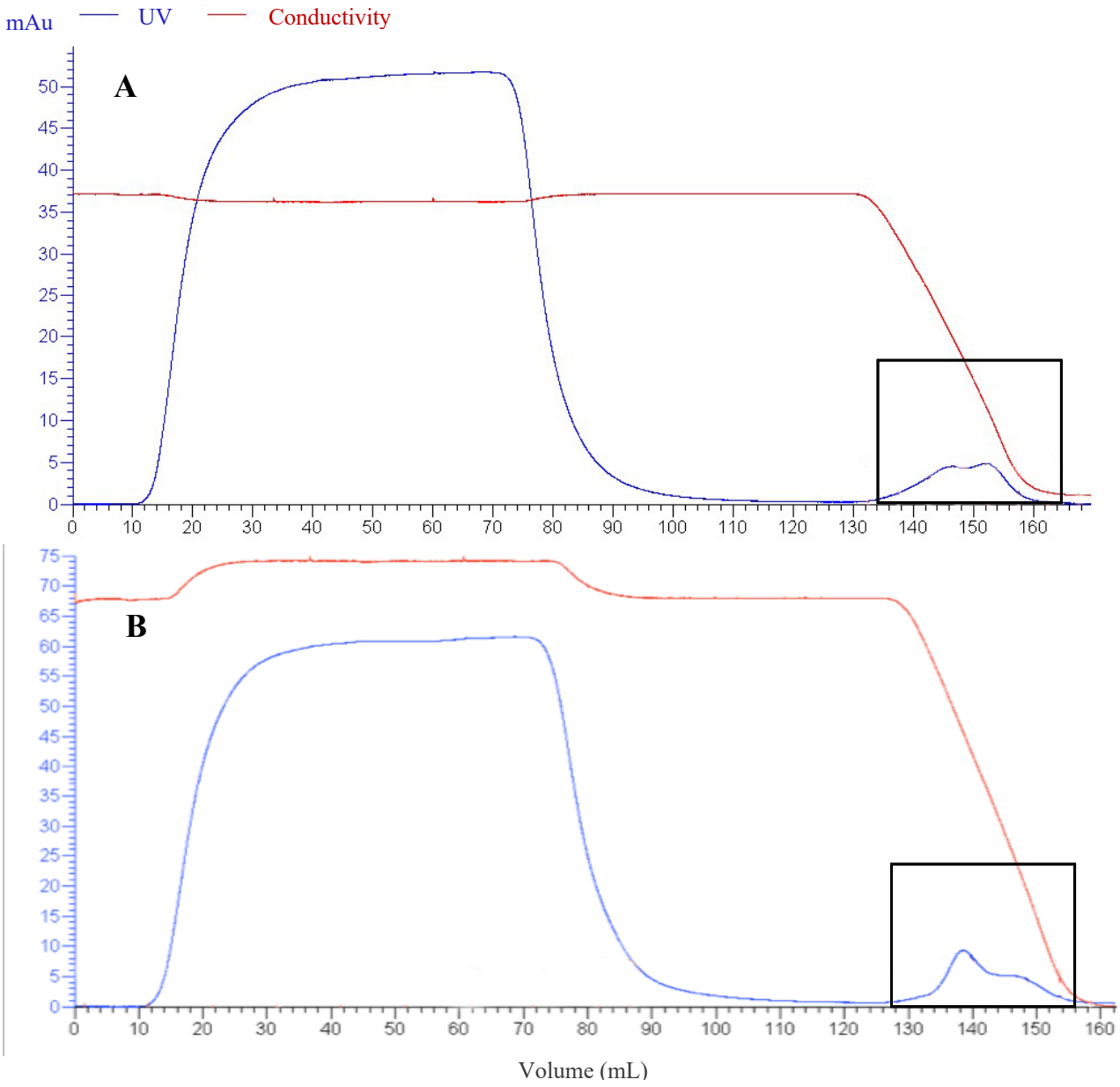

Figure 3.6 Protein profiles of HIC step using various salt concentrations to optimize the purification of Naglu-PTD4X.

Figures are as follow: A) HIC loaded at 2M NaCl (control) B) HIC loaded at 1.5M NaCl (Trial #1). Culture medium harvested from Sf9 cells stably expressing Naglu-PTD4Xwas partially purified by a using a HiScale Capto™ MMC column. Approximately 60 mL of Pre-HIC sample was loaded for control and trial #1 purification run. Column elutions, outlined by black boxes, were analyzed for Naglu activity using 4MU-Naglu activity assay. Protein profiles were generated by in-line UV measuring absorbance at 280 nm.

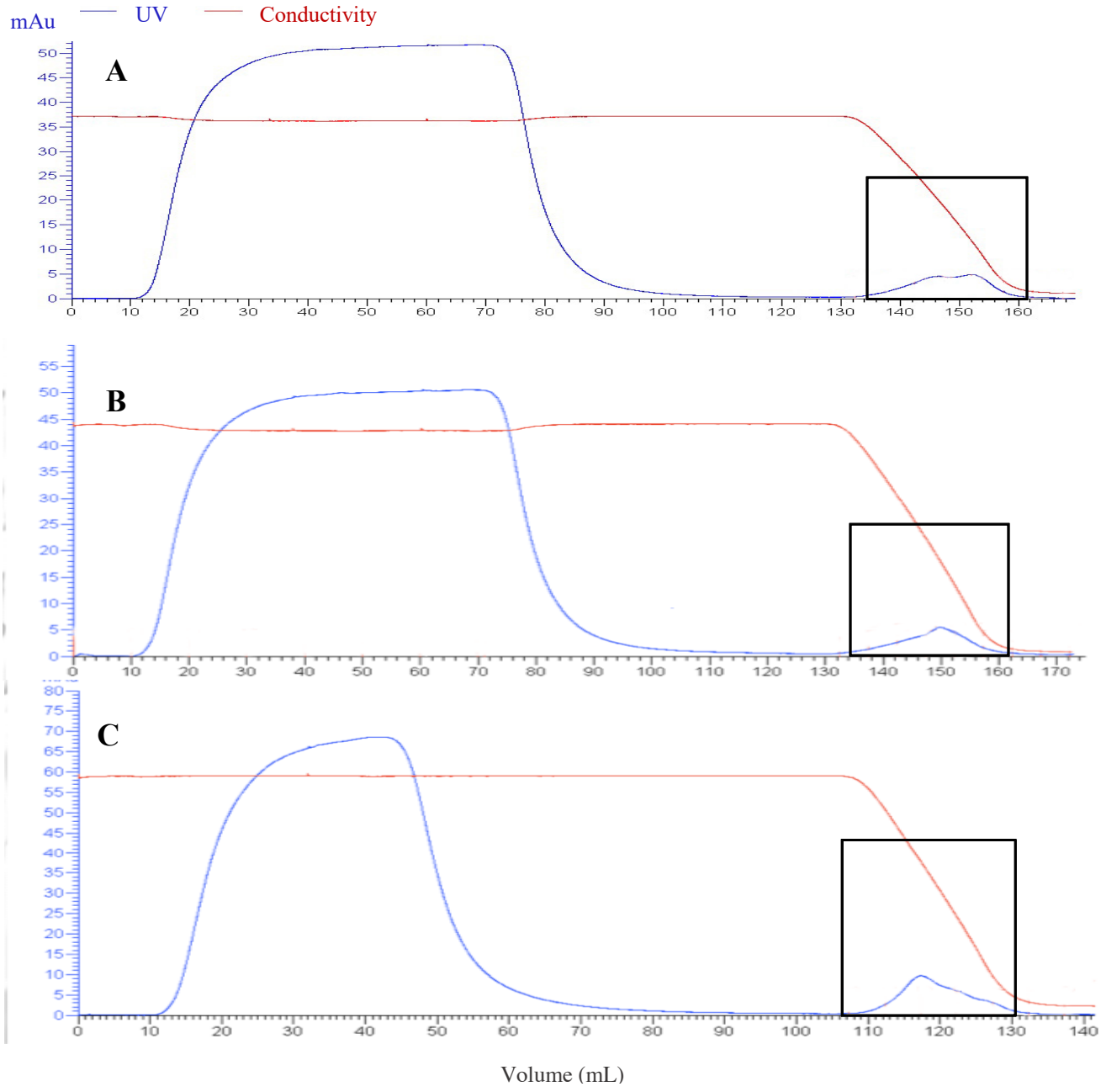

Figure 3.7 Protein profiles of HIC with adjusted elution conditions to optimize purification

Figures are as follow: A) HIC eluted with 50mM sodium phosphate buffer, pH 5.8 (control) B) HIC eluted with 50mM sodium phosphate buffer, pH 7 (Trial #2) C) HIC eluted with 50mM sodium phosphate buffer and 0.5M Urea, pH 5.8 (Trial #3). Culture medium harvested from Sf9 cells stably expressing Naglu-PTD4Xwas partially purified by a using a HiScale Capto™ MMC column. Approximately 60 mL of Pre-HIC sample was loaded for control and trial #2 and #3 purification run. Column elutions, outlined by black boxes, were analyzed for Naglu activity using 4MU-Naglu activity assay. Protein profiles were generated by in-line UV measuring absorbance at 280 nm.

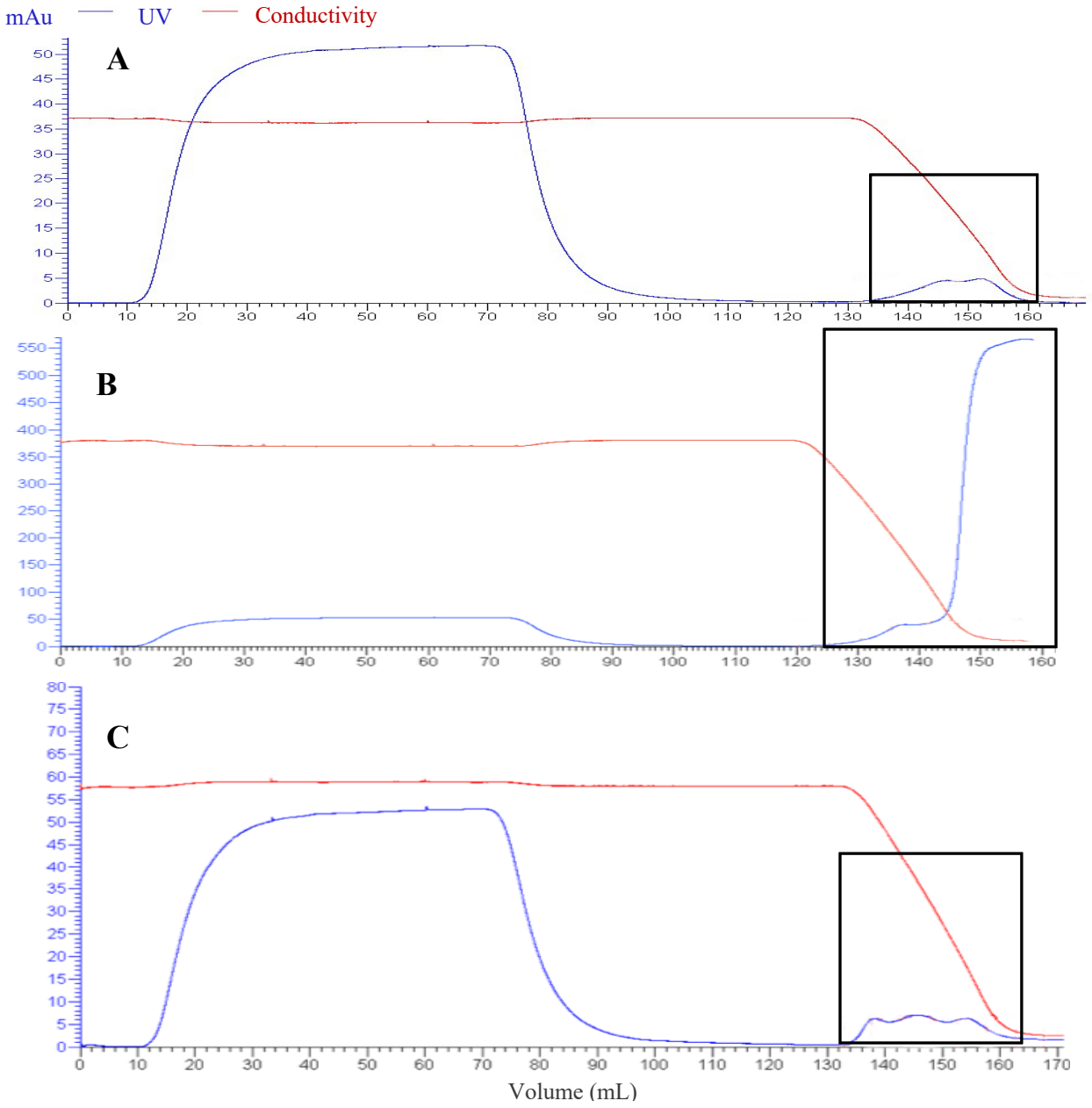

Figure 3.8 Protein profiles of HIC step with detergents in the adjusted elution conditions to optimize the purification of Naglu-PTD4X

Figures are as follow: A) HIC eluted with 50mM sodium phosphate buffer, pH 5.8 (control) B) HIC eluted with 50mM sodium phosphate buffer and 0.1% Triton X-100, pH 5.8 (Trial #4) C) HIC eluted with 50mM sodium phosphate buffer and 0.1% sodium cholate, pH 5.8 (Trial #5). Culture medium harvested from Sf9 cells stably expressing Naglu-PTD4Xwas partially purified by a using a HiScale Capto™ MMC column. Approximately 60mL of Pre-HIC sample was loaded for control and trial #4 and #5 purification run. Column elutions, outlined by black boxes, were analyzed for Naglu activity using 4MU-Naglu activity assay. Protein profiles were generated by in-line UV measuring absorbance at 280nm.

Table 3.4 Detergent removal results, following HIC elution with detergent additive, to optimize purification of Naglu-PTD4X

	Pre-HIC Naglu Activity (Units)	Post-Dialysis Naglu Activity (Units)	Yield (%)
Control	5943	1733	30 %
Trial #4: Elution with 0.1% Triton X-100	1320	72	5%
Trial #5: Elution with 0.1% Sodium cholate	4382	1926	44%

Culture medium harvested from Sf9 cells stably expressing Naglu-PTD4Xwas partially purified by a using a HiScale Capto™ MMC column. Approximately 60 mL of Pre-HIC sample was loaded for each purification run on to the HiTrap Butyl-S column. For elution buffer conditions were as follows: the control was 50mM sodium phosphate buffer, pH 5.8; trial #4 was 50mM sodium phosphate buffer and 0.1% Triton X-100, pH 5.8; and trial #5 was 50mM sodium phosphate buffer and 0.1% sodium cholate, pH 5.8. The eluents for each run were dialyzed separately in 15mL centrifugal devices and concentrated to approximately 1 mL. Yield was calculated based on active units of Naglu, which was determined from a fluorogenic 4MU-Naglu activity assay.

Table 3.5 Passivation trials for optimization of dialysis conditions for purification of Naglu-PTD4X

	Pre-Dialysis Naglu Activity (Units)	Post-Dialysis Naglu Activity (Units)	Yield (%)
Control	2496	1797	72 %
Blocking 5% Triton X-100	8198	7049	86%

Culture medium harvested from Sf9 cells stably expressing Naglu-PTD4Xwas partially purified by a using a HiScale Capto™ MMC column and HiTrap Butyl-S column. Centrifugal dialysis membranes were either blocked with 5% Triton X-100 for an hour or not (control) and then rinsed thoroughly with distilled water. Approximately 30 mL of Pre-HIC sample was loaded and spun down to 1 mL. Yield was calculated based on active units of Naglu, which was determined from a fluorogenic 4MU-Naglu activity assay.

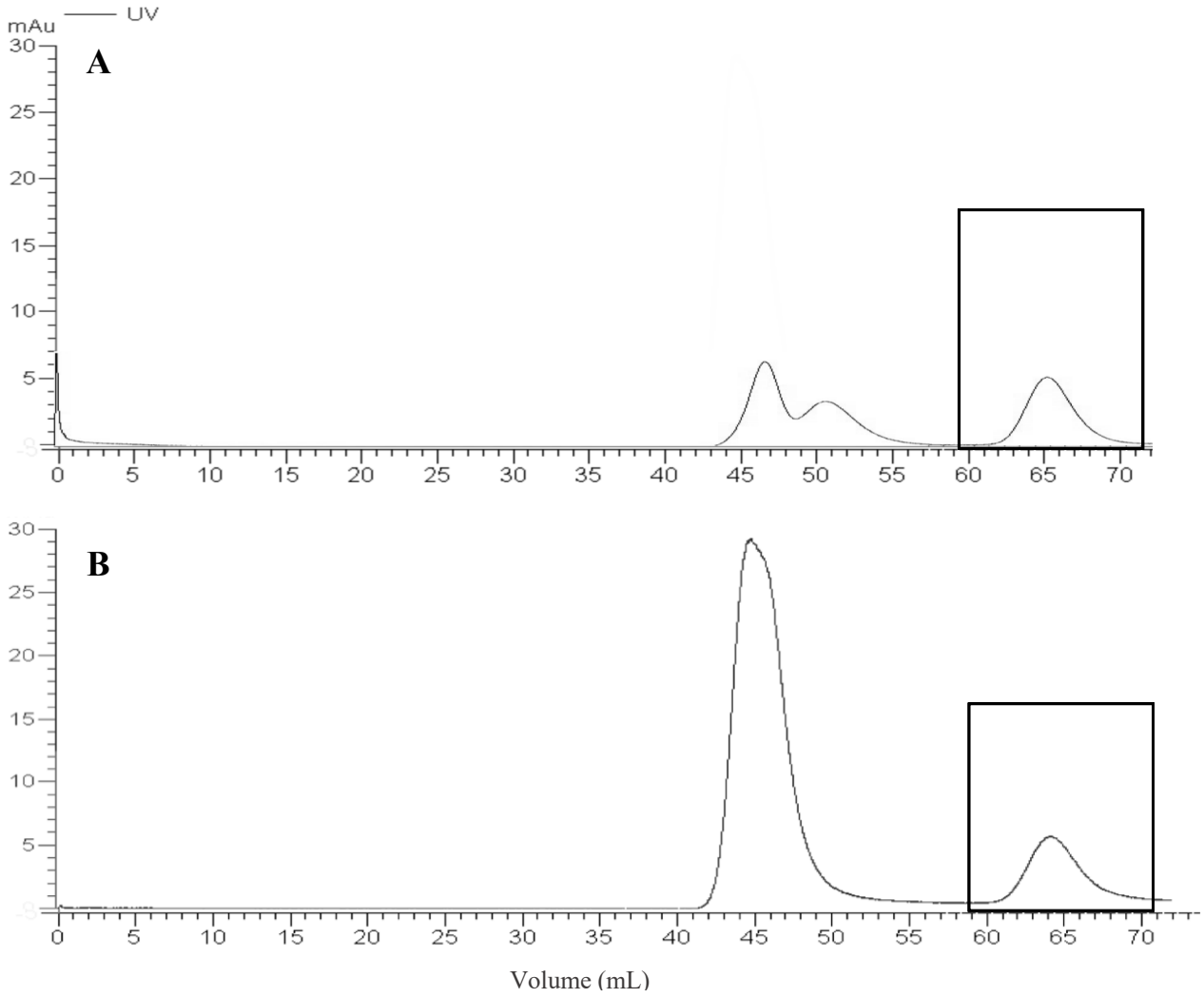

Figure 3.9 Protein profiles of SEC purification of Naglu-PTD4X using Morris (2015) protocol and the optimized protocol

Figures are as follows: (A) Naglu-PTD4X purification using Morris (2015) protocol (B) Naglu-PTD4X purification using the optimized protocol. Medium was harvested from Sf9 culture stably expressing Naglu-PTD4Xand was purified by a three-stage HiScale Capto™ MMC column, HiTrap Butyl-S column, and HiLoad Superdex 200 column. For the optimized protocol, the initial crude volume was reduced, and passivation was introduced prior to dialysis. Protein profiles were generated by in-line UV measuring absorbance at 280 nm.

Table 3.6 Yield of active Naglu through preparative purification of Naglu-PTD4X using an optimized protocol

Step	Volume (mL)	Activity (U)	Protein (mg)	Specific Activity (Units/mg)	Purification (fold)	Yield (%)
Medium	910	21677	132	163	1	100
Post-MMC	128	21345	22	850	5	98
Post-HIC	33	8375	0.4	21915	134	39
Post-SEC	12.5	5565	0.07	84300	517	26

One unit of activity corresponds to 493 arbitrary fluorescent units as measured by the fluorogenic 4MU-Naglu activity assay. Protein concentrations was determined by a Bradford protein concentration assay. Equilibrated crude medium was the baseline for comparison to determine percent yield calculations. For the medium and pre-HIC samples, activity values were calculated immediately prior to loading. For the post-HIC and post-SEC sample, activity values were calculated immediately following elution. All values represent the average from three separate purifications.

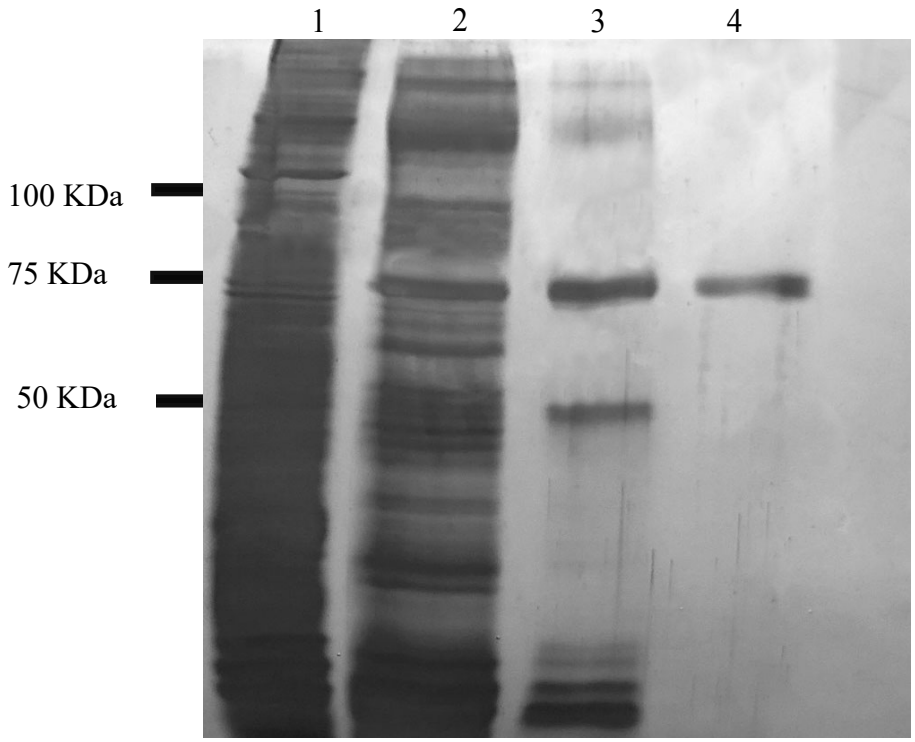

Figure 3.10 SDS-PAGE gel stained with silver nitrate stain to visualize results of preparative purification of Naglu-PTD4X using the optimized protocol

Lane contents: (1) Crude medium (2) post-MMC (3) post- HIC (4) post-SEC. Culture medium harvested from Sf9 cells stably expressing Naglu-PTD4Xwas purified by a three-stage preparative column purification protocol using a HiScale Capto™ MMC column, HiTrap Butyl-S column, and HiLoad Superdex 200 column. Samples were loaded and separated on an 8% polyacrylamide gel prior to staining with silver nitrate stain.

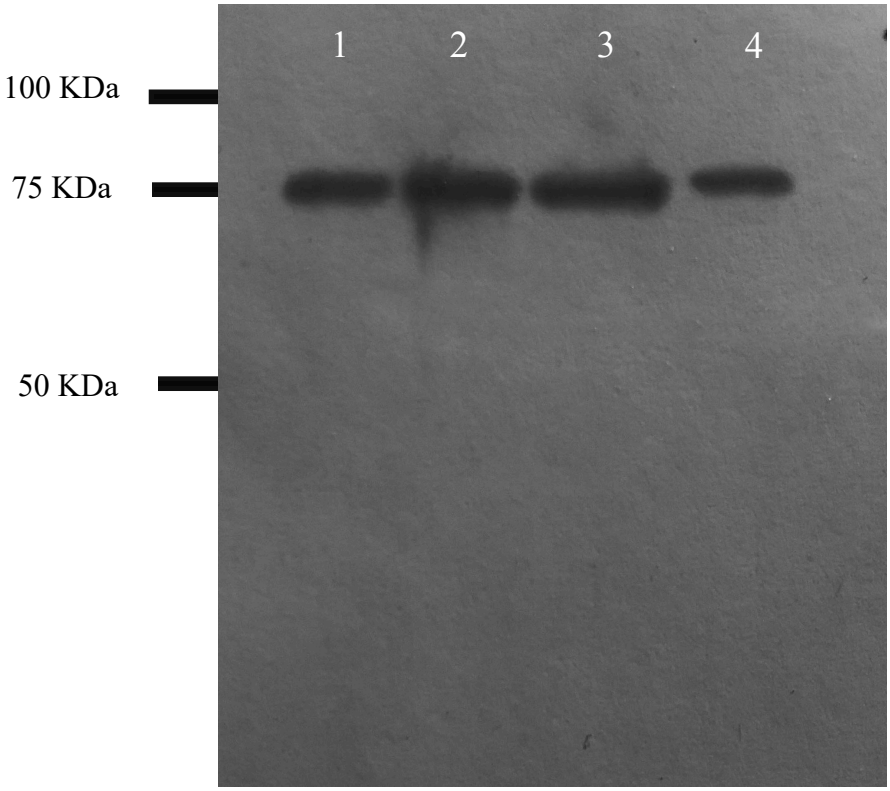

Figure 3.11 Naglu immunoblot of three-step preparative protein purification of Naglu-PTD4X using the optimized protocol

Lane contents: (1) Crude medium (2) post-MMC (3) post- HIC (4) post-SEC. Culture medium harvested from Sf9 cells stably expressing Naglu-PTD4X was purified by a three-stage preparative column purification protocol using a HiScale Capto™ MMC column, HiTrap Butyl-S column, and HiLoad Superdex 200 column. Samples were loaded and separated on an 8% polyacrylamide gel prior to transferring to a PVDF membrane and probing with anti-Naglu antibody. A strong band was seen in all sample lanes at the previously reported size for Naglu-PTD4X.

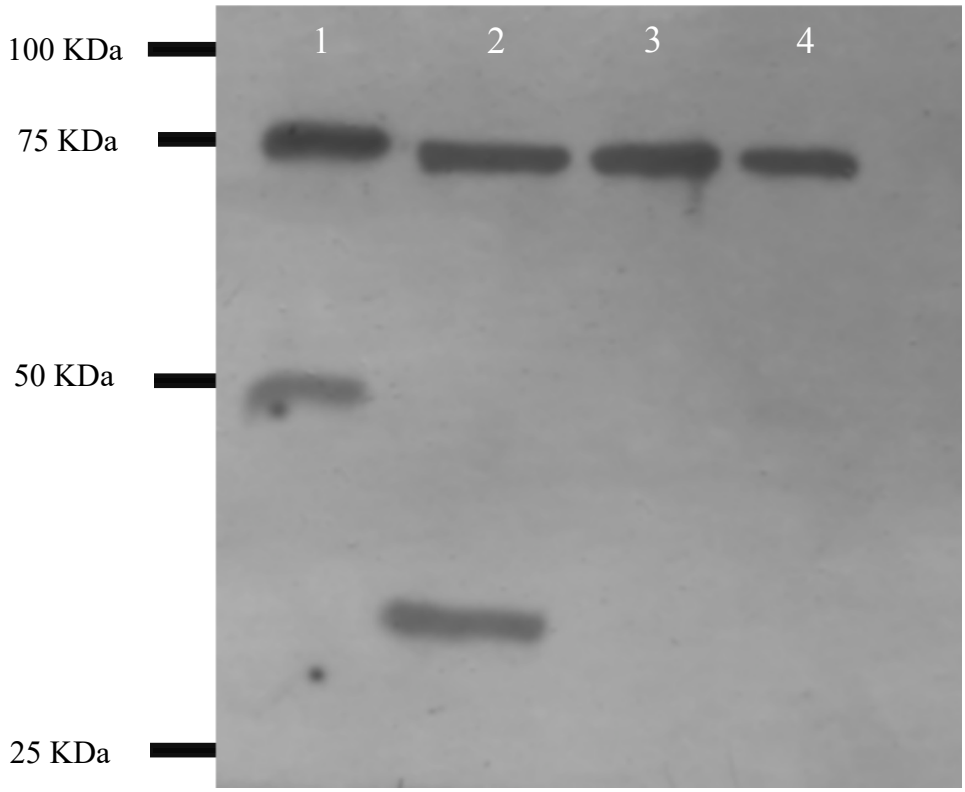

Figure 3.12 PTD4 immunoblot of three-step preparative protein purification of Naglu-PTD4X using the optimized protocol

Lane contents: (1) Crude medium (2) post-MMC (3) post- HIC (4) post-SEC. Culture medium harvested from Sf9 cells stably expressing Naglu-PTD4X was purified by a three-stage preparative column purification protocol using a HiScale Capto™ MMC column, HiTrap Butyl-S column, and HiLoad Superdex 200 column. Samples were loaded and separated on an 8% polyacrylamide gel prior to transferring to a PVDF membrane and probing with anti-PTD4 antibody. A strong band was seen in all sample lanes at the previously reported size for Naglu-PTD4X.

3.4 Uptake of Naglu-PTD4X in MPS IIIB and wildtype fibroblasts

3.4.1 Intracellular Naglu activity

A preliminary uptake study to survey various incubation times was conducted on an MPS IIIB fibroblast cell line, GM01426. Confluent culture dishes were supplied with 1000 units of purified Naglu-PTD4X. Following the various incubation times at 37°C, cells were washed and lysed. Incubation media, washes, and cell lysate were assessed for Naglu activity. Naglu-PTD4X appeared to remain active in incubation media at approximately 900 units, even after lengthy incubation. Naglu activity of cell lysate indicated an increase in intracellular Naglu over time: 1 hr incubation time had the lowest Naglu activity at 1.1 units/mg and 16 hrs incubation time had the highest at 4.3 units/mg (Table 3.7).

An uptake study with purified Naglu-PTD4X was conducted on GM01426 with wildtype control fibroblast cell line, MCH064, as a positive control. Confluent culture dishes were supplied with 1000 units of purified Naglu-PTD4X. Following 16 hrs of incubation at 37°C, cells were washed and lysed. Incubation media, washes, and cell lysate were assessed for Naglu activity. An increase in Naglu activity was detected in experimental conditions in comparison to negative control (Figure 3.13; Table 3.8).

3.4.2 Naglu immunoblotting analysis

An uptake study was conducted on confluent GM01426 and MCH064 cultures using 1000 units of Naglu-PTD4X. After the uptake enzyme was supplied, cultures were incubated for 16 hrs at 37°C. Cells were washed, lysed, and lysates were separated on an SDS-Page gel along with a sample of purified Naglu-PTD4X. The gel was transferred to membrane which was probed for the presence of Naglu. The immunoblotting visualization can be seen in Figure 3.14. The purified Naglu-PTD4X showed a single distinct band at 75 kDA. There was no banding

detected at 75 kDA for cellular lysate samples. For all cellular lysates samples there was a band at approximately 70 kDA, which corresponds to the reported size of endogenous Naglu, and a strong band at 42 kDA. ImageJ software was used to conduct densitometric measurements on the banding at 42 kDA. For the MCH064 cellular lysate, the density of the band at 42 kDA for the control was 72% the density of the experimental. For the GM01426 cellular lysate, the density of the band at 42 kDA for the control was 79% the density of the experimental.

3.4.3 Immunocytochemistry analysis

An uptake study was conducted on confluent GM02931 cultures that had been passaged on to laminin coated coverslips. To the cells, 200 units of Naglu-PTD4X was added before incubating for 16 hrs at 37°C. Cells were fixed and permeabilized then probed with rabbit anti-Naglu antibody. An Alexa Fluor® 488-conjugated goat anti-rabbit antibody and DAPI stain were applied before mounting and visualizing the cells on a confocal microscope (Figure 3.15). No significant cell death was detectable upon incubation with Naglu-PTD4X. Z-stacks of cell images were acquired and corrected total cellular fluorescence was calculated for the entire image. There was no significant difference in corrected total cellular fluorescence between experimental and control samples, which may be seen in Figure 3.16.

To visualize fluorescence in individual cells, an uptake study was conducted on 50% confluent GM02931 cultures that had been passaged on to laminin coated coverslips. To the cells, 200 units of Naglu-PTD4X was added before incubating for 16 hrs at 37°C. Cells were fixed and permeabilized then probed with rabbit anti-Naglu antibody. An Alexa Fluor® 488-conjugated goat anti-rabbit antibody and DAPI stain were applied before mounting and visualizing the cells on a confocal microscope (Figure 3.15). Z-stacks of cell images were acquired and corrected total cellular fluorescence was calculated. The comparison of

fluorescence may be seen in Figure 3.16. There was no significant difference in corrected total cellular fluorescence between experimental and control samples.

Table 3.7 Survey of intracellular Naglu activity following various incubation time periods of Naglu-PTD4X with MPS IIIB fibroblasts

Incubation time (hrs)	Number of replicates (n)	Average Arbitrary Fluorescent Units	Average Total Protein Concentration (ug/uL)	Average Specific Activity (Units/mg)
1hr	3	7	0.5	1.1
4hr	3	14	0.5	2.3
16hr	3	27	0.5	4.3

One unit of activity corresponds to 493 arbitrary fluorescent units as measured by the fluorogenic 4MU Naglu activity assay. Protein concentrations was determined by a Bradford protein concentration assay. GM01426, MPS IIIB fibroblasts, were plated at confluency on T25 flasks and 1000 units of Naglu-PTD4X was added. Cells were incubated for various time periods before being lysed and assayed for Naglu activity.

Table 3.8 Intracellular Naglu activity in wildtype and diseased fibroblasts following Naglu-PTD4X uptake study

Fibroblast cell line	Number of replicates (n)	Naglu-PTD4X added	Average Arbitrary Fluorescent Units	Average Total Protein Concentration (ug/uL)	Average Specific Activity (Units/mg)
GM01426	3	No	03	0.5	0.5± 0.01
GM01426	3	Yes	29	0.4	6.0 ± 0.47
MCH064	3	No	44	0.9	4.4 ± 1.34

One unit of activity corresponds to 493 arbitrary fluorescent units as measured by the fluorogenic 4MU Naglu activity assay. Protein concentrations was determined by a Bradford protein concentration assay. GM01426, MPS IIIB fibroblasts, and MCH064, wildtype fibroblasts, were plated at confluency on T25 flasks and 1000 units of Naglu-PTD4X was added. Cells were incubated 16hrs before being lysed and assayed for Naglu activity.

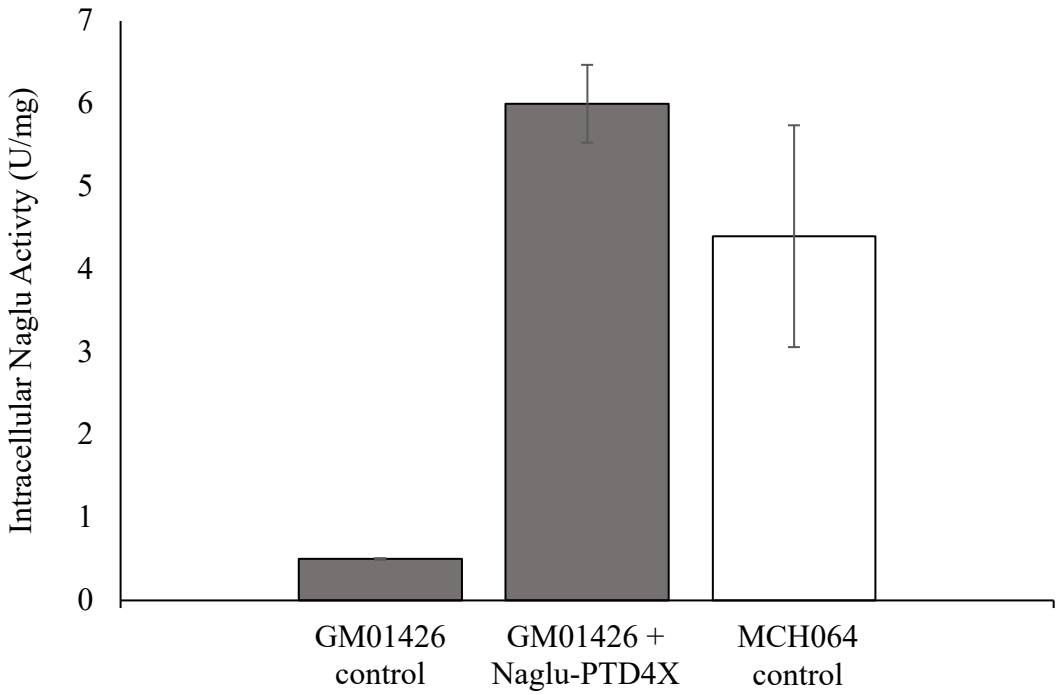

Figure 3.13 Intracellular Naglu activity in wildtype and MPS IIIB fibroblasts following incubation with Naglu-PTD4X

GM01426, MPS IIIB fibroblasts, and MCH064, wildtype fibroblasts, were plated at confluency on T25 flasks and 1000 units of Naglu-PTD4X was added. Cells were incubated 16 hrs before being lysed and assayed for Naglu activity. One unit of activity corresponds to 493 arbitrary fluorescent units as measured by the fluorogenic 4MU Naglu activity assay. Protein concentrations was determined by a Bradford protein concentration assay. Standard error was calculated (n=3).

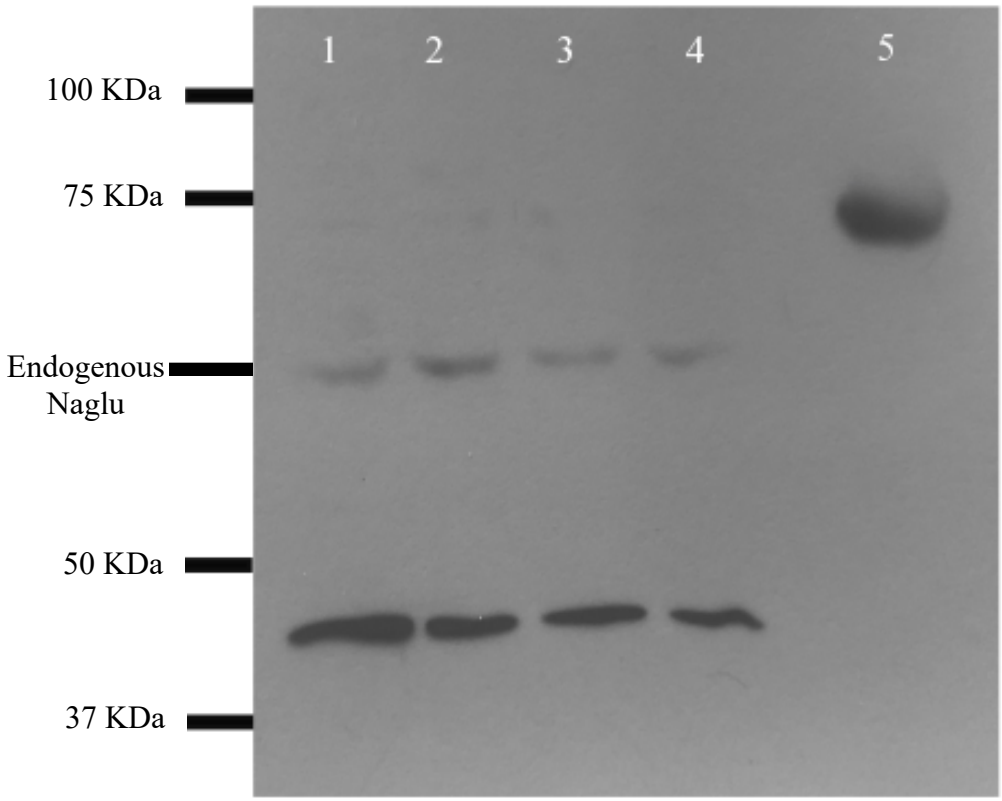

Figure 3.14 Naglu immunoblot of wildtype and MPS IIIB fibroblast lysates following incubation with Naglu-PTD4X

Lane contents: (1) MCH064 + Naglu-PTD4X (2) MCH064 control (3) GM01426 + Naglu-PTD4X (2) GM01426 control. GM01426, MPS IIIB fibroblasts, and MCH064, wildtype fibroblasts, were plated at confluency on T25 flasks and 1000 units of Naglu-PTD4X was added. Cells were incubated 16 hrs before being lysed and resolved on an 10% SDS-PAGE gel. Proteins were transferred on to PVDF membrane and the membrane was probed with anti-Naglu primary antibody.

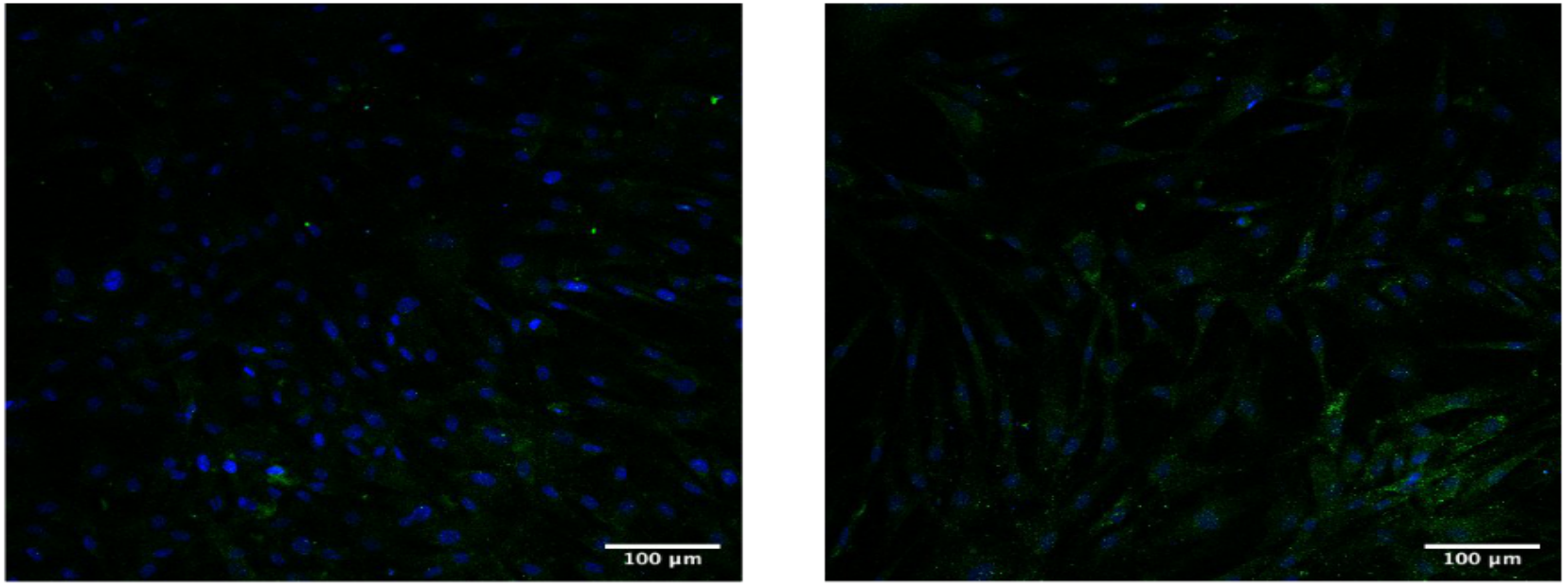

Figure 3.15 Visualization of anti-Naglu immunofluorescence of confluent MPS IIIB fibroblasts following incubation with Naglu-PTD4X

Images are as follows: (A) GM02931 + Naglu-PTD4X (B) GM02931 control. GM02391, MPS IIIB fibroblasts, were plated at 90-100% confluency on laminin coated coverslips and 200 units of Naglu-PTD4X was added. Cells were incubated 16 hrs before being fixed and permeabilized. Cells were probed with anti-Naglu primary antibody and Alexa Fluor® 488-conjugated goat anti-rabbit antibody and stained with DAPI. Cells were mounted and visualized using confocal microscopy at 20x magnification.

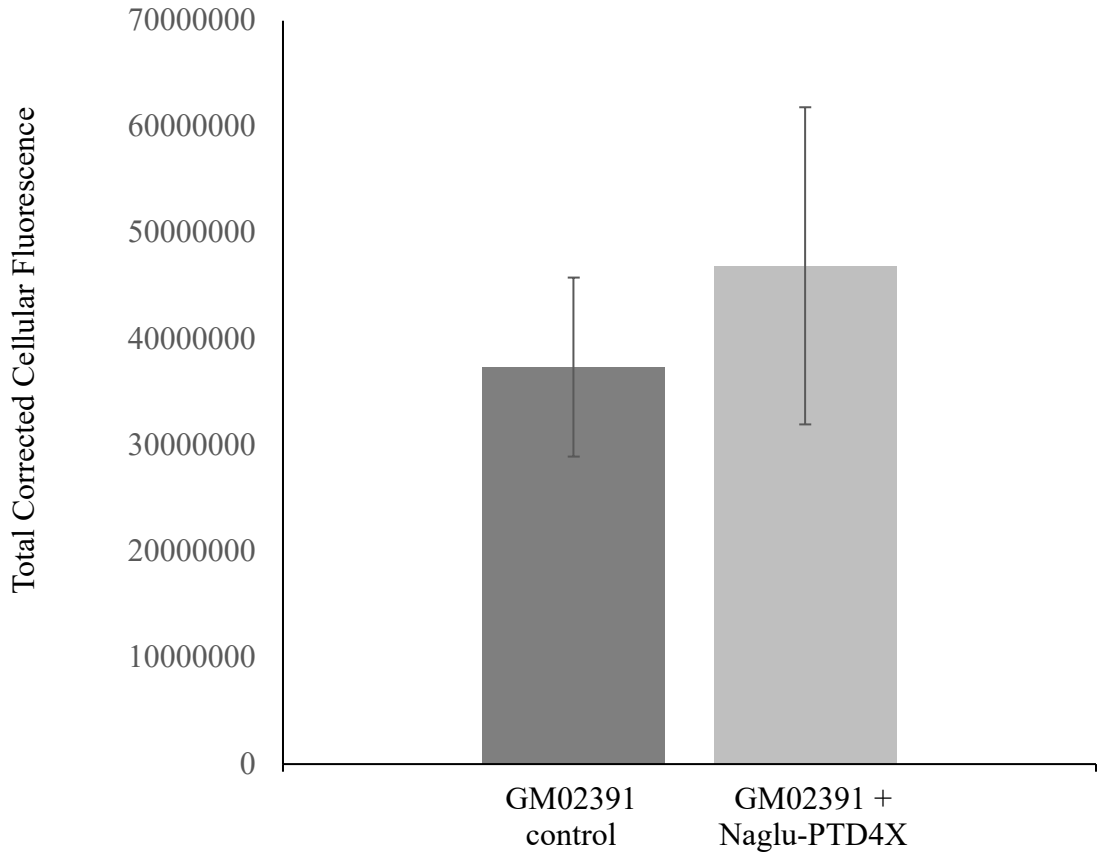

Figure 3.16 Corrected total cellular fluorescence of confluent MPS IIIB fibroblasts following incubation with Naglu-PTD4X

GM02391, MPS IIIB fibroblasts, were plated at confluency on laminin coated coverslips and 200 units of Naglu-PTD4X was added. Cells were incubated 16 hrs before being fixed and permeabilized. Cells were probed with anti-Naglu primary antibody and Alexa Fluor® 488-conjugated goat anti-rabbit antibody and stained with DAPI. Cells were mounted and visualized using confocal microscopy. Z-stacks of images were obtained and corrected total cellular fluorescence was calculated. Standard error was calculated (n=3).

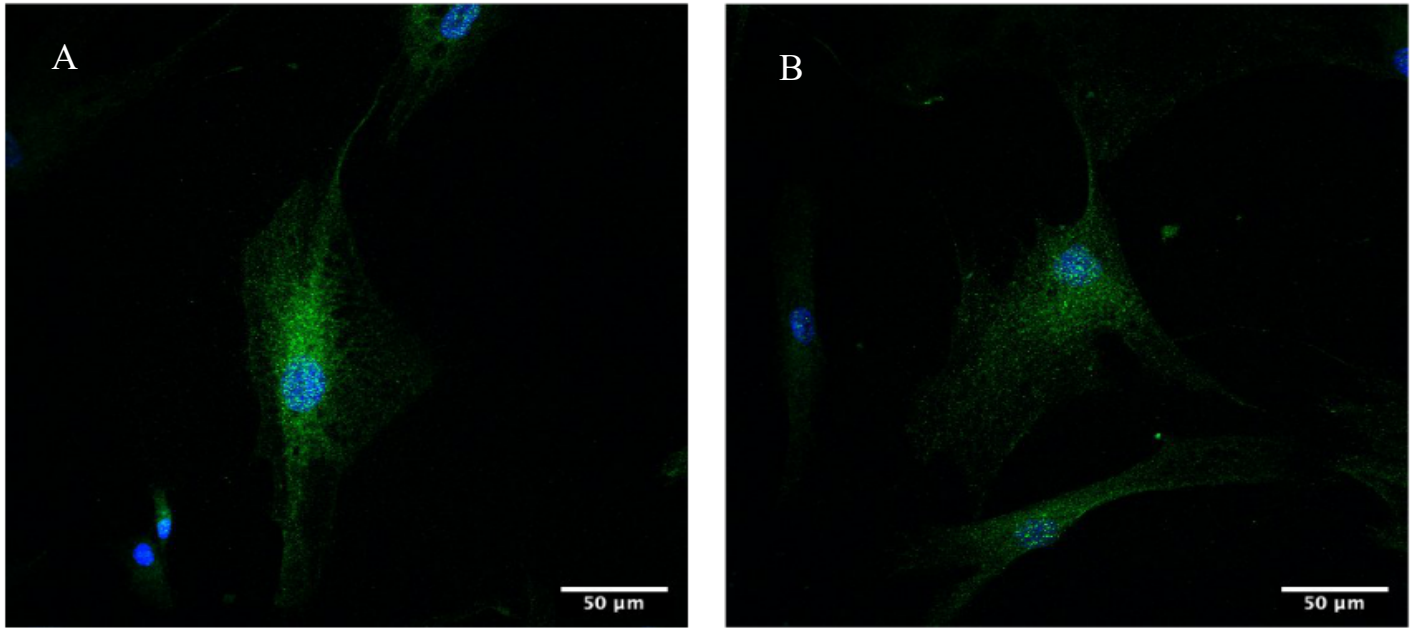

Figure 3.17 Visualization of anti-Naglu immunofluorescence of 50% confluent MPS IIIB fibroblasts following incubation with Naglu-PTD4X

Images are as follows: (A) GM02931 + Naglu-PTD4X (B) GM02931 control. GM02391, MPS IIIB fibroblasts, were plated at 50% confluency on laminin coated coverslips and 200 units of Naglu-PTD4X was added. Cells were incubated 16 hrs before being fixed and permeabilized. Cells were probed with anti-Naglu primary antibody and Alexa Fluor® 488-conjugated goat anti-rabbit antibody and stained with DAPI. Cells were mounted and visualized using confocal microscopy at 40x magnification.

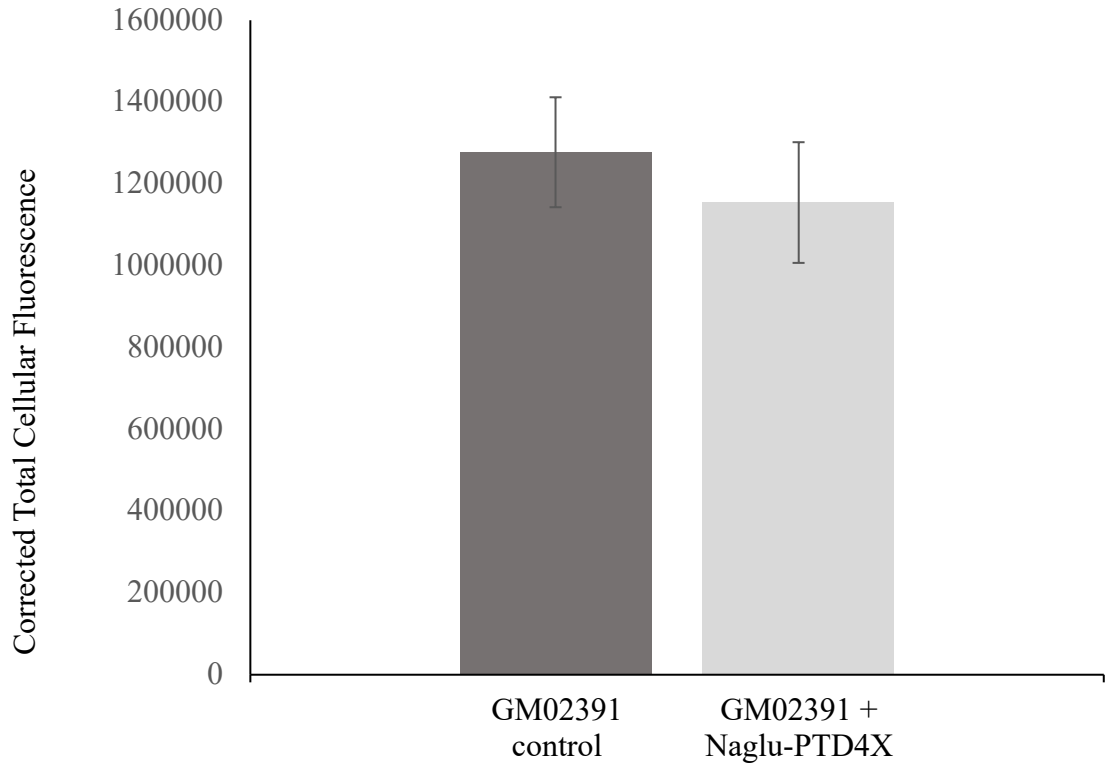

Figure 3.18 Corrected total cellular fluorescence of single MPS IIIB fibroblasts following incubation with Naglu-PTD4X

GM02391, MPS IIIB fibroblasts, were plated at 50% confluency on laminin coated coverslips and 200 units of Naglu-PTD4X was added. Cells were incubated 16hrs before being fixed and permeabilized. Cells were probed with anti-Naglu primary antibody and Alexa Fluor® 488-conjugated goat anti-rabbit antibody and stained with DAPI. Cells were mounted and visualized using confocal microscopy. Z-stacks of images were obtained and corrected total cellular fluorescence was calculated. Standard error was calculated (n=20).

4. Discussion

4.1 Isolation and sequencing of stably transfected Sf9 genomic DNA

Genomic DNA was isolated from transfected Sf9 cells and the downstream region of *Naglu-PTD4X* was amplified and sequenced. Previously, the entirety of this *Naglu-PTD4X* insert was sequenced following cloning but prior to transfection with Sf9 cells (Ashmead, 2016) (Supplementary Figure 1). This further sequencing was conducted to confirm the presence of the re-introduced stop codon after integration into Sf9 chromosomal DNA. The sequencing results indicated that the re-introduced stop codon (TAA) following PTD4 was present after integration into the Sf9 genome. Therefore, this sequencing result, in addition to previous immunoblotting analysis, confirmed that this transfected Sf9 cell line was stably expressing the improved fusion enzyme without the additional protein tags following PTD4 (Morris, 2015; Ashmead, 2016).

4.2 Purification of Naglu-PTD4X using Naglu-PTD4-V5/His purification protocol

The reintroduction of the stop codon following PTD4 resulted in the exemption of the V5 epitope tag (Gly-Lys-Pro-Ile-Pro-Asn-Pro-Leu-Leu-Gly-Leu-Asp-Ser-Thr) and the 6xHis tag from the C-terminus of the Naglu-PTD4X enzyme. The CiPP strategy devised by Morris (2015) for the purification of Naglu-PTD4-V5/His depended on the enzyme's properties, including charge, hydrophobicity, and size. The absence of the hydrophobic V5 epitope tag and charged 6xHis tag was predicted to have an effect on the purification of Naglu-PTD4X using this protocol.

Overall, Naglu-PTD4X was purified to homogeneity using the protocol devised by Morris (2015), which can be seen in Figure 3.4. The protein profile for the purification of Naglu-PTD4X based on silver nitrate stain was similar to the protein profile of Naglu-PTD4-V5/His

(Figure 3.4 and Supplementary Figure 2 respectively). There was little change in protein banding from the crude medium to the post-MMC sample. There was a drastic reduction in banding for the post-HIC sample and only a single band in the post-SEC sample at the expected molecular weight of recombinant Naglu. This aligned well with changes in protein concentration documented in Table 3.1 and the methodology of the CiPP strategy (GE Healthcare, 2010).

Differences between these two enzyme purifications were detected in the UV protein profile recorded during purification (Figure 3.3 and Supplementary Figure 3). Overall, the peaks for the purification of Naglu-PTD4X were smaller, which was expected since the predicted expression of Naglu-PTD4X was lower (1.01 μg/mL) than the predicted expression of Naglu-PTD4-V5/His (2.06 μg/mL) from Sf9 cells. Also, the starting concentration of protein in the crude medium was lower for Naglu-PTD4X purification (195 mg) compared to Naglu-PTD4-V5/His (306 mg).

Another noticeable difference was the Naglu peak for UV profile of SEC purification. The Naglu peak for the purification of Naglu-PTD4-V5/His was centered at 60 mL (Supplementary Figure 3). The Naglu peak for the purification of Naglu-PTD4X was centered at 65 mL. This was likely a reflection of the removal of the V5 epitope and 6xHis tag. These two tags were estimated to add approximately 3 kDa to the size of Naglu-PTD4-V5/His (Life Technologies, 2012). This resulted in the elution of Naglu-PTD4-V5/His from the SEC column earlier than Naglu-PTD4X.

The values of purification were compared for Naglu-PTD4X and Naglu-PTD4-V5/His (Table 3.1 and Supplementary Table 1). Notably, there was a distinct difference in the specific activity values for the purified enzymes: purified Naglu-PTD4-V5/His had a specific activity of 23,000 units/mg and purified Naglu-PTD4X had a specific activity of 102,000 units/mg. One

potential explanation is that the additional protein tags attached to the C-terminus of the fusion enzyme may have interfered with the activity of the enzyme, especially given the outward-facing locations of the active sites (Birrane *et al.*, 2019). Another potential explanation is that the additional protein tags could have reduced the stability of the purified fusion enzyme, resulting in a rapid loss of activity after purification. Enzymatic kinetic studies of Naglu-PTD4X and Naglu-PTD4-V5/His would need to be conducted to determine if there is a significant difference in activity between these two fusion enzymes.

Lastly, the yield of active Naglu and concentration of total purified enzyme was lower for the purification of Naglu-PTD4X. There was 11% of the Naglu activity intact, relative to the crude medium. This was a 15% reduction in yield compared to the purification of Naglu-PTD4-V5/His. The V5 epitope and 6xHis tag may have altered the strength which these two fusion enzymes form hydrophobic interactions. This was evident when comparing the intermediate step of purification for these two enzymes. Naglu-PTD4X formed stronger interactions with the HIC column, resulting in significant amounts of fusion enzyme remaining bound to the column following elution. This step, along with dialysis, were considered targets for optimization of purification for Naglu-PTD4X.

4.3 Optimization of preparative purification of Naglu-PTD4X

The HIC and dialysis steps were selected as optimization targets to increase the overall yield of Naglu-PTD4X. Combined, 58% of the active enzyme was lost during these two steps. Various parameters were tested in order attempt to improve the yield of these intermediate steps and optimize purification of Naglu-PTD4X.

4.3.1 Con-A purification

Con-A was selected as a potential alterative media to Butyl-S for intermediate purification of Naglu-PTD4X. Con-A is an affinity chromatography resin that is designed to capture glycoproteins and other glycosylated biomolecules. In particular, it has a strong affinity for molecules with α-D-glucopyranosyl, α-D-mannopyranosyl or sterically related residues. Elution with this type of column is conducted by introducing a competitive eluent, such as methyl-α-D-mannopyanoside or methyl-α-D-glucopyranoside. Con-A chromatography has previously been used to purify human recombinant Naglu that was fused to an insulin growth factor domain (rhNAGLU-IGF-II) and expressed in CHO cells (Kan *et al.*, 2014).

Preliminary intermediate purification trials with Con-A indicated that this resin was not as effective as Butyl-S for purification of Naglu-PTD4X. This was determined on two factors: yield and removal of bulk impurities. The yield of active enzyme for the Con-A was significantly lower (15%) compared to the Butyl-S (58%). An activity assay of the loading, washing, and elution steps of the Con-A run indicated that the majority of Naglu-PTD4X was retained on the column following elution. Further optimization with more stringent elution conditions would be required to remove the remaining Naglu-PTD4X.

Secondly, the Con-A was less effective at removing bulk impurities from the MMC-purified sample. Silver nitrate stain analysis showed a greater degree of protein banding in the post-Con-A sample compared to the post-HIC sample. Also, further impurities would likely be co-eluted with Naglu-PTD4X under more stringent elution conditions required to improve yield. The removal of bulk impurities is a crucial aspect of the intermediate purification step because the polishing step (SEC) can only resolve a limited number of proteins. For a SEC column, it has been estimated that 10 proteins is the maximum number of proteins that can be resolved (Stellwagen, 2009). Furthermore, resolution is improved when the difference in size between

proteins is greater. Based on the banding for the post-Con-A sample, it would likely be difficult to separate Naglu-PTD4X from the remaining protein impurities using SEC in the final polishing step.

4.3.2 HIC elution optimization

Activity assays of the HIC purification run identified the elution step as the step that required optimization. Naglu-PTD4X remained bound to the column following elution. An array of parameters was tested in an attempt to encourage greater elution of Naglu-PTD4X from the HIC column. These trials were compared to a control HIC purification that used the parameters devised by Morris (2015).

The first trial involved decreasing the concentration of NaCl during loading: the NaCl concentration for the loading buffer and post-MMC sample were reduced to 1.5M. The goal of this trial was to create weaker interactions between the resin and Naglu-PTD4X making Naglu-PTD4X easier to elute (GE Healthcare, 2006). Activity assay of Naglu activity indicated that this reduction in salt concentration did not improve elution and instead resulted in less Naglu-PTD4X binding to the HIC column.

The rest of the trials focused on altering elution conditions to weaken the interactions between Naglu-PTD4X and the resin, forcing the enzyme to elute. Increasing the pH and adding low concentrations of urea were expected to weaken the interactions between Naglu-PTD4X and resin; however, these two parameters had little, to no, discernible effect on the elution of Naglu-PTD4X. The yield after elution was similar to the control yield. More stringent elution conditions were used, and detergents were added to the elution buffer. The detergent's non-polar regions were expected to competitively bind to the hydrophobic residues of the resin, encouraging Naglu-PTD4X to be eluted (GE Healthcare, 2006). Following HIC elution, these

detergents needed to be removed, in order to reduce their interference with downstream applications, such as activity assays and uptake studies (Tiller *et al.*, 1984; Baldridge *et al.*, 2011).

Detergent removal was conducted via centrifugal dialysis. Following centrifugal dialysis, the yield of active Naglu in the 0.1% Triton X-100 trial, was very low. The large reduction in yield was likely due to the concentration of Triton X-100 reaching the critical micelle concentration of 0.22 mM. At the critical micelle concentration, Triton X-100 forms micelles of approximately 80 kDa in size. This excludes them from the 30 kDA cut off of the centrifugal dialysis membranes. Therefore, Triton X-100 was concentrated along with Naglu-PTD4X to levels that rendered Naglu-PTD4 inactive.

Another detergent, sodium cholate was also investigated due to its higher critical micelle concentration of 10mM and smaller micelle size of 13 kDa (Despa *et al.*, 2010). These parameters would make sodium cholate more amenable to removal via centrifugal dialysis than Triton X-100. Following dialysis, the overall yield of Naglu-PTD4X when sodium cholate was added to the HIC elution was 14% higher than the control condition. Therefore, of the HIC parameters tested, the addition of sodium cholate was the most viable candidate for improving the yield of active Naglu-PTD4X.

4.3.3 Dialysis optimization

The dialysis step prior to loading on the SEC was selected as a target for optimization. This dialysis step is necessary for downstream purification resolution. Following HIC purification, the sample volume was approximately 30 mL. For SEC, the resolution between peaks is inversely proportional to sample volume. For the 120 mL HiLoad Superdex 200 column, the max sample volume recommend is 2.4 mL (2% of the CV) to maintain optimal peak

resolution (GE Healthcare, 2010). Therefore, the post-HIC sample needs to be concentrated prior to loading on the SEC column.

The dialysis step for the purification of Naglu-PTD4X resulted in a 15-30% loss in active enzyme. No activity was detected in the filtrate following concentration; therefore, it was determined that the enzyme was likely lost due to non-specific binding to the centrifugal membranes. Previous work in our lab has also reported a similar loss in enzyme when concentrating Naglu-PTD4-V5/His using centrifugal concentrators (Jantzen, 2011). It has been documented that proteins with hydrophobic or charged domain can demonstrate high affinity and irreversible binding to the centrifugal concentrator membranes (Pall Corporation, 2017).

Passivation involves pre-treatment of the membranes of the centrifugal concentrators with a detergent, such as Triton X-100. This blocks potential binding sites that may contribute to enzyme loss during concentration steps. Concentration of Naglu-PTD4X with and without passivation was compared. When passivation was used, the yield of Naglu-PTD4 was increased by approximately 14%.

4.3.4 Optimized purification of Naglu-PTD4X

Passivation was chosen over sodium cholate addition to improve the purification yield of Naglu-PTD4X. There were two determining factors for this selection. Firstly, passivation was an easy, inexpensive, and quick way to improve the yield of purification. Secondly, detergents, like sodium cholate, reduce the life span of HIC resins and result in lowered purification capability over time (GE Healthcare, 2006). Considering the ongoing rate of Naglu-PTD4X purification and the expense of chromatography resins, passivation was selected instead sodium cholate addition.

The SEC profiles in Figure 3.9 for the non-optimized and optimized Naglu-PTD4X purifications were similar with regards to the Naglu-PTD4X peak. The Naglu-PTD4X peak was distinct and centered over 65 mL. Also, the heights of the peaks were relatively the same. It should be noted the starting amount of crude media was reduced for the optimized protocol, which may explain why the SEC peak was not larger.

The yield of active Naglu, relative to the crude medium, increased from 11% to 26%. This is comparable to the yield found by Morris (2015) for the purification of Naglu-PTD4-V5/His (Supplementary Table 1). It is also comparable to other studies that have purified human recombinant Naglu. Zhao and Neufeld (2000) purified human recombinant Naglu with a yield of 10% from CHO cells. Their strategy for purification involved a three-step system using Con-A chromatography, heparin perfusion chromatography, and HIC. In 2001, human recombinant Naglu was purified using a two-step system of heparin affinity and weak anion exchange column with a yield of 18% (Weber *et al.*, 2001).

More recently, Kan *et al.* (2014) purified rhNAGLU-IGF-II from CHO cells. Their yield of active Naglu was 19.4% following purification with two separate affinity columns. In addition, the concentration and specific activity of purified rhNAGLU-IGF-II was 0.08 mg and 127,000 units/mg respectively. This is comparable to the concentration and specific activity of purified Naglu-PTD4X, which was 0.07 mg and 84,300 units/mg respectively.

4.4 Uptake of Naglu-PTD4X in MPS IIIB and Wildtype Fibroblasts

MPS IIIB fibroblasts have extremely low, if not undetectable, levels of endogenous Naglu activity. The two MPS IIIB fibroblasts cell lines, GM01426 and GM02391, in this study have a specific activity of ≤0.3 units/mg (Boado *et al.*, 2016) Therefore, it was assumed that increases in intracellular Naglu activity was a positive indication of uptake of Naglu-PTD4X.

A preliminary uptake study was conducted on MPS IIIB fibroblasts (GM01246) to survey incubation length. 1000 units of purified Naglu-PTD4X was incubated with fibroblasts for 1 hr, 4 hrs, and 16 hrs prior to determining intracellular Naglu activity. An increase in intracellular Naglu activity corresponded with increase in incubation length. The 16 hr incubation had the highest level of intracellular Naglu activity, 4.3 units/mg. For subsequent uptake studies, a 16 hr incubation length was used.

An uptake study with 170 nM of purified Naglu-PTD4 was conducted with MPS IIIB and wildtype (MCH064) fibroblasts. The untreated MPS IIIB and wildtype fibroblasts acted as a negative and positive control respectively. The MPS IIIB fibroblasts that were treated with Naglu-PTD4X showed a detectable increase in intracellular Naglu activity. In comparison to the wildtype, the treated MPS IIIB fibroblasts show equal, if not higher, levels of intracellular Naglu activity. These activity results were comparable to previous research that conducted uptake studies with fusion enzymes on MPS IIIB fibroblasts. Boado *et al.* (2016) detected an increase in Naglu intracellular activity in MPS IIIB from ≤0.3 units/mg to 5.41 units/mg after incubation with 30 nM of Naglu-HIRMab for 30 hrs.

To confirm the uptake of Naglu-PTD4X, anti-Naglu immunoblotting of cell lysates were conducted following uptake. A purified Naglu-PTD4X sample was included in the immunoblot as a positive control. There was no banding present that corresponded to Naglu-PTD4X in the cellular lysate samples. The cellular lysate samples did contain a faint band at approximately 70 kDA, which corresponded reported weight of native Naglu. There was also a smaller, more intense band at approximately 42 kDa for all cellular lysate samples. These results were unable to confirm the presence of Naglu-PTD4X within the fibroblasts following uptake. It was

theorized that the absence of Naglu-PTD4X banding and intense banding at 42 kDa may have been due to proteolytic enzymes rapidly degrading Naglu-PTD4X following lysis.

Immunocytochemistry of uptake samples was conducted in order to limit the rate of potential Naglu degradation and improve the visualization of Naglu-PTD4X. For immunocytochemistry there was no lysis step instead cells were rapidly fixed on a coverslip and permeabilized. Uptake studies with 200 units of Naglu-PTD4X on MPS IIIB (GM02931) were conducted prior to immunocytochemistry analysis. At lower magnification, immunofluorescence images of uptake samples did not show any evidence of increased cell death for experimental conditions. This indicated that a 16 hr incubation with Naglu-PTD4X did not result in significant level of visible toxicity to the fibroblasts. For the higher magnification, the fluorescence of individual cells was calculated and compared between the experimental and control conditions. There was no detectable difference in the total corrected cellular fluorescence between the control MPS IIIB fibroblasts and the MPS IIIB fibroblasts treated with Naglu-PTD4X. Similar to immunoblotting, immunocytochemistry was unable to confirm the uptake of Naglu-PTD4X into human fibroblasts.

Experimental sensitivity may be a possible explanation for the disparity between the intracellular activity assay and the immunodetection analyses. The fluorogenic Naglu activity assay is capable of detecting nano- to pico-moles of Naglu activity whereas immunodetection requires 20-30 μg of protein (Supplementary Figure 4 and Supplementary Table 2) (Abcam, 2017). For uptakes studies, approximately 12.5 μg of Naglu-PTD4X is applied fibroblast culture medium. The analysis of GAG storage is an alternative secondary confirmation to immunodetection. Kan *et al.* (2014) labeled fibroblast cultures with $H_2{}^{35}SO_4$ and investigated the reduction in GAGs following incubation with rhNAGLU-IGF-II. This analysis should also be

explored with Naglu-PTD4X since it reveals whether Naglu-PTD4X addresses the root cause of pathology, the HS accumulation in the lysosome.

Furthermore, studies conducted with tat and tat-fusion proteins have noted that uptake was concentration dependent (Zhang *et al.*, 2008; Jones and Sayers, 2012). The immunodection protcol for Naglu-PTD4X was adapted from Kan *et al.* (2014) uptake studies with rhNAGLU-IGF-II. The uptake mechanism for rhNAGLU-IGF-II, however, is distinct since it exploits receptor-mediated pathways instead of absorptive-mediated transcytosis. Therefore, higher concentrations of Naglu-PTD4X may be required in order to detect uptake using immunodetection. In a study by Zhang *et al.* (2008), 2000 to 50,000 units of β-glucuronidase-Tat was added to fibroblasts to study uptake of the fusion enzyme. Future research should scale up purification in order to investigate using higher concentration levels of Naglu-PTD4X for uptake studies in MPS IIIB fibroblasts.

Conclusion and Future Directions

The re-introduced stop codon following PTD4 was confirmed in the *Naglu-PTD4X* insert that was stably integrated into Sf9 chromosomal DNA. The three-step purification system devised by Morris (2015) was used to purify Naglu-PTD4X to homogeneity. Naglu-PTD4X was purified 551-fold with 11% of the active Naglu remaining, relative to the crude medium. The final amount of purified Naglu-PTD4X was 0.04 mg and the specific activity was 102,000 units/mg. These purification values were lower than those reported by Morris (2015) using this purification system to purify Naglu-PTD4-V5/His. The purification system was optimized by introducing a passivation step during dialysis to reduce the loss of Naglu-PTD4X due to non-specific binding. The purification values for the optimized protocol were as follows. Naglu-PTD4X was purified 500-fold with 26% of the active Naglu remaining, relative to the crude medium. The final amount of purified Naglu-PTD4X was 0.07 mg and the specific activity was 84,300 units/mg. These improved purification values were comparable other studies which purified human recombinant Naglu (Zhao and Neufeld, 2000; Weber *et al.*, 2001; Kan *et al.*, 2014; Morris, 2015). Uptake studies with purified Naglu-PTD4X were conducted with MPS IIIB fibroblasts. Intracellular Naglu activity assay indicated a detectable increase in Naglu activity following incubation with Naglu-PTD4X for 16 hrs; however, immunodetection techniques were unable to confirm the presence of Naglu-PTD4X within the fibroblasts. Future research should focus on optimizing the uptake conditions of Naglu-PTD4X. Higher concentration of Naglu-PTD4X should be investigated since uptake of tat-derived domains are concentration dependent. This may allow for the secondary confirmation using immunodetection. In addition, other

methods of secondary confirmation should be explored, such GAG storage reduction analysis using $H_2{}^{35}SO_4$ labelled fibroblasts.

Bibliography

Abcam. 2017. Protocols book. Eugene, OR: Abcam plc. Available online at www.abcam.com.

Andrade, F., L. Aldámiz-Echevarría, M. Llarena and M. L. Couce. **2015**. Sanfilippo syndrome: Overall review: Mucopolysaccharidosis type III. *Pediatr. Int.* **57**: 331–338.

Ashmead, R. 2016. Expression of Recombinant Human α -N-Acetylglucosaminidase in Sf9 Insect Cells following Stop Codon Addition. Honours Thesis. University of Victoria, Victoria, BC.

Ausseil, J., N. Desmaris, S. Bigou, R. Attali, S. Corbineau, S. Vitry, M. Parent, D. Cheillan, M. Fuller, I. Maire, *et al.* 2008. Early Neurodegeneration Progresses Independently of Microglial Activation by Heparan Sulfate in the Brain of Mucopolysaccharidosis IIIB Mice. *PLoS ONE* **3**: e2296.

Baldridge, A., A. Amador and L. M. Tolbert. **2011**. Fluorescence Turn On by Cholate Aggregates. *Langmuir* **27**: 3271–3274.

Bame, K. J. 2001. Heparanases: endoglycosidases that degrade heparan sulfate proteoglycans. *Glycobiology* **11**: 91R-98R.

Bandsmer, J. C. 2004. Expression of alpha-N-acetylglucosaminidase fused to the HIV-1 protein transduction domain and a modified protein transduction domain. University of Victoria, Victoria, BC.

Bárány-Wallje, E., J. Gaur, P. Lundberg, Ü. Langel and A. Gräslund. **2007**. Differential membrane perturbation caused by the cell penetrating peptide Tp10 depending on attached cargo. *FEBS Lett.* **581**: 2389–2393.

Barton, N. W., R. O. Brady, J. M. Dambrosia, A. M. Di Bisceglie, S. H. Doppelt, S. C. Hill, H. J. Mankin, G. J. Murray, R. I. Parker and C. E. Argoff. **1991**. Replacement Therapy for Inherited Enzyme Deficiency — Macrophage-Targeted Glucocerebrosidase for Gaucher's Disease. *N. Engl. J. Med.* **324**: 1464–1470.

Birrane, G., A.-L. Dassier, A. Romashko, D. Lundberg, K. Holmes, T. Cottle, A. W. Norton, B. Zhang, M. F. Concino and M. Meiyappan. **2019**. Structural characterization of the α-N-acetylglucosaminidase, a key enzyme in the pathogenesis of Sanfilippo syndrome B. *J. Struct. Biol.* **205**: 65–71.

Blasberg, R. G., C. Patlak and J. D. Fenstermacher. **1975**. Intrathecal chemotherapy: Brain tissue profiles after ventriculocisternal perfusion. *J Pharmacol Exp Ther* **195**: 73–83.

Boado, R. J., E. K. W. Hui, J. Z. Lu and W. M. Pardridge. **2009**. AGT-181: Expression in CHO cells and pharmacokinetics, safety, and plasma iduronidase enzyme activity in Rhesus monkeys. *J. Biotechnol.* **144**: 135–141.

Boado, Ruben J., E. Ka-Wai Hui, J. Zhiqiang Lu and W. M. Pardridge. **2014**. Insulin receptor antibody-iduronate 2-sulfatase fusion protein: Pharmacokinetics, anti-drug antibody, and safety pharmacology in Rhesus monkeys. *Biotechnol. Bioeng.* **111**: 2317–2325.

Boado, R. J., J. Z. Lu, E. K. W. Hui, H. Lin and W. M. Pardridge. **2016**. Insulin Receptor Antibody-α-N-Acetylglucosaminidase Fusion Protein Penetrates the Primate Blood-Brain Barrier and Reduces Glycosoaminoglycans in Sanfilippo Type B Fibroblasts. *Mol. Pharm.* **13**: 1385–1392.

Boado, Ruben J, Z. Lu, E. K. Hui and W. M. Pardridge. **2014**. Insulin Receptor Antibody − Sulfamidase Fusion Protein Penetrates the Primate Blood − Brain Barrier and Reduces Glycosoaminoglycans in San fi lippo Type A Cells. *Mol. Pharm.* **11**: 2928–34.

Bobo, R. H., D. W. Laske, A. Akbasak, P. F. Morrison, R. L. Dedrick and E. H. Oldfield. **1994**. Convection-enhanced delivery of macromolecules in the brain. *Proc. Natl. Acad. Sci.* **91**: 2076–2080.

Bradford, M. M. 1976. A Rapid and Sensitive Method for the Quantitation of Microgram Quantities of Protein Utilizing the Principle of Protein-Dye Binding. *Anal. Biochem.* **72**: 248–254.

Calias, P., M. Papisov, J. Pan, N. Savioli, V. Belov, Y. Huang, J. Lotterhand, M. Alessandrini, N. Liu, A. J. Fischman, *et al.* 2012. CNS penetration of intrathecal-lumbar idursulfase in the monkey, dog and mouse: Implications for neurological outcomes of lysosomal storage disorder. *PLoS ONE* **7**.

Carpentier, A., M. Canney, A. Vignot, V. Reina, K. Beccaria, C. Horodyckid, C. Karachi, D. Leclercq, C. Lafon, J.-Y. Chapelon, *et al.* 2016. Clinical trial of blood-brain barrier disruption by pulsed ultrasound. *Sci. Transl. Med.* **8**: 1–6.

Carter, E., C. Y. Lau, D. Tosh, S. G. Ward and J. M. Randal. **2013**. Cell penetrating peptides fail to induce an innate immune response in epithelial cells in vitro: Implications for continued therapeutic use. *Eur. J. Pharmaeutics Biopharm.* **85**: 12–19.

Chow, P. and B. Weissmann. **1981**. 4-Methylumbelliferyl 2-Acetamido-2-Deoxy-Alpha-D-Glucopyranoside, a Fluorogenic Substrate for N-Acetyl-Alpha-D-Glucosaminidase. *Carbohydr. Res.* **96**: 87–93.

Chung, J. K., L. Pan, K. Palmieri, A. S. Youssef and T. G. McCauley. **2017**. Whole body and CNS biodistribution of rhHNS in cynomolgus monkeys after intrathecal lumbar administration: Treatment implications for patients with MPS IIIA. *Int. J. Mol. Sci.* **18**: 1–16.

Clark, W. T., G. K. Yu, M. Aoyagi-Scharber and J. H. LeBowitz. **2018**. Utilizing ExAC to assess the hidden contribution of variants of unknown significance to Sanfilippo Type B incidence. *PLOS ONE* **13**: e0200008.

Daneman, R. 2012. The blood-brain barrier in health and disease. *Ann. Neurol.* **72**: 648–672.

Daneman, R., L. Zhou, D. Agalliu, J. D. Cahoy, A. Kaushal and B. A. Barres. **2010**. The mouse blood-brain barrier transcriptome: A new resource for understanding the development and function of brain endothelial cells. *PLoS ONE* **5**: 1–16.

Daneman, R., L. Zhou, A. A. Kebede and B. A. Barres. **2010**. Pericytes are required for blood-brain barrier integrity during embryogenesis. *Nature* **468**: 562–566.

de Duve, C. 2005. The lysosome turns fifty. *Nat. Cell Biol.* **7**: 847–849.

De Pasquale, V., A. Pezone, P. Sarogni, A. Tramontano, G. G. Schiattarella, V. E. Avvedimento, S. Paladino and L. M. Pavone. **2018**. EGFR activation triggers cellular hypertrophy and lysosomal disease in NAGLU-depleted cardiomyoblasts, mimicking the hallmarks of mucopolysaccharidosis IIIB. *Cell Death Dis.* **9**.

Despa, F., J. T. Luo, J. Li, Y. Duan and K. S. Lam. **2010**. Cholic acid micelles—controlling the size of the aqueous cavity by PEGylation. *Phys. Chem. Chem. Phys.* **12**: 1589–1594.

Dickson, P., M. McEntee, C. Vogler, S. Le, B. Levy, M. Peinovich, S. Hanson, M. Passage and E. Kakkis. **2007**. Intrathecal enzyme replacement therapy: Successful treatment of brain disease via the cerebrospinal fluid. *Mol. Genet. Metab.* **91**: 61–68.

Dinca, A., W. M. Chien and M. T. Chin. **2016**. Intracellular delivery of proteins with cell-penetrating peptides for therapeutic uses in human disease. *Int. J. Mol. Sci.* **17**.

El-Andaloussi, S., P. Järver, H. J. Johansson and Ü. Langel. **2007**. Cargo-dependent cytotoxicity and delivery efficacy of cell-penetrating peptides: a comparative study. *Biochem. J.* **407**: 285–292.

Felice, B. R., T. L. Wright, R. B. Boyd, M. T. Butt, R. W. Pfeifer, J. Pan, J. A. Ruiz, M. W. Heartlein and P. Calias. **2011**. Safety evaluation of chronic intrathecal administration of idursulfase-IT in cynomolgus monkeys. *Toxicol. Pathol.* **39**: 879–892.

Ficko-Blean, E., K. A. Stubbs, O. Nemirovsky, D. J. Vocadlo and A. B. Boraston. **2008**. Structural and mechanistic insight into the basis of mucopolysaccharidosis IIIB. *Proc. Natl. Acad. Sci.* **105**: 6560–6565.

Frankel, A.D., and C.O. Pabo. **1988**. Cellular uptake of the tat protein from human immunodeficiency virus. *Cell* **55**: 1189–1193.

Fu, H., J. D. Bartz, R. L. Stephens and D. M. McCarty. **2012**. Peripheral Nervous System Neuropathology and Progressive Sensory Impairments in a Mouse Model of Mucopolysaccharidosis IIIB. *PLoS ONE* **7**: e45992.

Fu, H., A. S. Meadows, R. J. Pineda, R. P. Mohney, S. Stirdivant and D. M. McCarty. **2017**. Serum global metabolomics profiling reveals profound metabolic impairments in patients with MPS IIIA and MPS IIIB. *Metab. Brain Dis.* **32**: 1403–1415.

Fu, H., A. S. Meadows, T. Ware, R. P. Mohney and D. M. McCarty. **2017**. Near-Complete Correction of Profound Metabolomic Impairments Corresponding to Functional Benefit in MPS IIIB Mice after IV rAAV9-hNAGLU Gene Delivery. *Mol. Ther.* **25**: 792–802.

Gabathuler, R. 2010a. Approaches to transport therapeutic drugs across the blood-brain barrier to treat brain diseases. *Neurobiol. Dis.* **37**: 48–57. Elsevier Inc.

Gabathuler, R. 2010b. Approaches to transport therapeutic drugs across the blood-brain barrier to treat brain diseases. *Neurobiol. Dis.* **37**: 48–57. Elsevier Inc.

GE Healthcare Bio-Sciences. 2006. Hydrophobic interaction and reversed phased chromatography: principles and methods. Pittsburgh, PA: General Electric. Report nr 11-0012-69. Available online at www.gelifesciences.com

GE Healthcare Bio-Sciences. 2010. Strategies for protein purification. Pittsburgh, PA: General Electric. Report nr 28-9833-31AA. Available online at www.gelifesciences.com

Giugliani, R., L. Giugliani, F. de Oliveira Poswar, K. C. Donis, A. D. Corte, M. Schmidt, R. J. Boado, I. Nestrasil, C. Nguyen, S. Chen, *et al.* 2018. Neurocognitive and somatic stabilization in pediatric patients with severe Mucopolysaccharidosis Type I after 52 weeks of intravenous brain-penetrating insulin receptor antibody-iduronidase fusion protein (valanafusp alpha): an open label phase 1-2 trial. *Orphanet J. Rare Dis.* **13**.

Gloor, S. M., M. Wachtel, M. F. Bolliger, H. Ishihara, R. Landmann and K. Frei. **2001**. Molecular and cellular permeability control at the blood – brain barrier. *Brain Res. Rev.* **36**: 258–264.

Hers, H. G. 1961. a-Glucosidase Deficiency in Generalized Glycogen-Storage Disease (Pompe ' s Disease). *Biochem J* **86**: 11–16.

Ho, A., S. R. Schwarze, S. J. Mermelstein, G. Waksman and S. F. Dowdy. **2001**. Synthetic Protein Transduction Domains : Enhanced Transduction Potential in Vitro and in Vivo Advances in Brief Synthetic Protein Transduction Domains : Enhanced Transduction Potential in Vitro. *Cancer Res.* **61**: 474–477.

Hsu, Y.-H., R.-S. Liu, W.-L. Lin, Y.-S. Yuh, S.-P. Lin and T.-T. Wong. **2017**. Transcranial pulsed ultrasound facilitates brain uptake of laronidase in enzyme replacement therapy for Mucopolysaccharidosis type I disease. *Orphanet J. Rare Dis.* **12**: 109. Orphanet Journal of Rare Diseases.

Huang, Q., J. Deng, F. Wang, S. Chen, Y. Liu, Zhibiao Wang, Zhigang Wang and Y. Cheng. **2012**. Targeted gene delivery to the mouse brain by MRI-guided focused ultrasound-induced blood–brain barrier disruption. *Exp. Neurol.* **233**: 350–356.

Hynynen, K., N. McDannold, N. A. Sheikov, F. A. Jolesz and N. Vykhodtseva. **2005**. Local and reversible blood–brain barrier disruption by noninvasive focused ultrasound at frequencies suitable for trans-skull sonications. *NeuroImage* **24**: 12–20.

Jantzen, R. R. 2011. Expression of Human α-N-Acetylglucosaminidase in Sf9 Insect Cells: Effect of Cryptic Splice Site Removal and Native Secretion-Signaling Peptide Addition. MSc Thesis. University of Victoria, Victoria, BC.

Jantzen, R. R., S. N. Truelson and F. Y. M. Choy. **2013**. Human α-N-acetylglucosaminidase: CDNA cryptic site removal and native secretion signal addition significantly enhance enzyme expression and secretion. *Process Biochem.* **48**: 1197–1202. Elsevier Ltd.

Jones, A. T. and E. J. Sayers. **2012a**. Cell entry of cell penetrating peptides: Tales of tails wagging dogs. *J. Controlled Release* **161**: 582–591. Elsevier B.V.

Jones, A. T. and E. J. Sayers. **2012b**. Cell entry of cell penetrating peptides: Tales of tails wagging dogs. *J. Controlled Release* **161**: 582–591. Elsevier B.V.

Jordão, J. F., E. Thévenot, K. Markham-Coultes, T. Scarcelli, Y.-Q. Weng, K. Xhima, M. O'Reilly, Y. Huang, J. McLaurin, K. Hynynen, *et al.* 2013. Amyloid-β plaque reduction, endogenous antibody delivery and glial activation by brain-targeted, transcranial focused ultrasound. *Exp. Neurol.* **248**: 16–29.

Kakkis, E., M. McEntee, C. Vogler, S. Le, B. Levy, P. Belichenko, W. Mobley, P. Dickson, S. Hanson and M. Passage. **2004**. Intrathecal enzyme replacement therapy reduces lysosomal storage in the brain and meninges of the canine model of MPS I. *Mol. Genet. Metab.* **83**: 163–174.

Kalafatovic, D. and E. Giralt. **2017**. *Cell-penetrating peptides: Design strategies beyond primary structure and amphipathicity*.

Kan, S., M. Aoyagi-Scharber, S. Q. Le, J. Vincelette, K. Ohmi, S. Bullens, D. J. Wendt, T. M. Christiansen, P. M. N. Tiger, J. R. Brown, *et al.* 2014. Delivery of an enzyme-IGFII fusion protein to the mouse brain is therapeutic for mucopolysaccharidosis type IIIB. *Proc. Natl. Acad. Sci. U. S. A.* **111**: 14870–14875.

Kaplan, A., D. T. Achord and W. S. Sly. **1977**. Phosphohexosyl components of a lysosomal enzyme are recognized by pinocytosis receptors on human fibroblasts. *Proc. Natl. Acad. Sci. U. S. A.* **74**: 2026–30.

Killedar, S., J. DiRosario, E. Divers, P. G. Popovich, D. M. McCarty and H. Fu. **2010**. Mucopolysaccharidosis IIIB, a lysosomal storage disease, triggers a pathogenic CNS autoimmune response. 8.

Kinoshita, M., N. McDannold, F. A. Jolesz and K. Hynynen. **2006**. Noninvasive localized delivery of Herceptin to the mouse brain by MRI-guided focused ultrasound-induced blood-brain barrier disruption. *Proc. Natl. Acad. Sci.* **103**: 11719–11723.

Kornfeld, S. 1986. Trafficking of lysosomal enzymes in normal and disease states. *J. Clin. Invest.* **77**: 1–6.

Kost, T. A., J. P. Condreay and D. L. Jarvis. **2005**. Baculovirus as versatile vectors for protein expression in insect and mammalian cells. *Nat. Biotechnol.* **23**: 567–575.

Krauss, U., G. Annette, H. P. Merkle and M. Hanne. **2004**. Cellular Uptake but Low Permeation of Human Calcitonin – Derived Cell Penetrating Peptides and Tat (47-57) Through Well-Differentiated Epithelial Models. *Pharm. Res.* **21**: 1248–1256.

Kristensen, M., D. Birch and H. M. Nielsen. **2016**. Applications and challenges for use of cell-penetrating peptides as delivery vectors for peptide and protein cargos. *Int. J. Mol. Sci.* **17**.

Li, H. H., H.-Z. Zhao, E. F. Neufeld, Y. Cai and F. Gómez-Pinilla. **2002**. Attenuated plasticity in neurons and astrocytes in the mouse model of Sanfilippo syndrome type B: Attenuated Plasticity in MPS III B Mouse. *J. Neurosci. Res.* **69**: 30–38.

Li, J.-P. and M. Kusche-Gullberg. **2016**. Heparan Sulfate: Biosynthesis, Structure, and Function. In: *International Review of Cell and Molecular Biology*, pp. 215–273. Elsevier.

Lin, C.-Y., H.-Y. Hsieh, C.-M. Chen, S.-R. Wu, C.-H. Tsai, C.-Y. Huang, M.-Y. Hua, K.-C. Wei, C.-K. Yeh and H.-L. Liu. **2016**. Non-invasive, neuron-specific gene therapy by focused ultrasound-induced blood-brain barrier opening in Parkinson's disease mouse model. *J. Controlled Release* **235**: 72–81.

Litke, A. M., S. Samuelson, K. R. Delaney, Y. Sauvé and R. L. Chow. **2018**. Investigating the Pathogenicity of *VSX1* Missense Mutations and Their Association With Corneal Disease. *Investig. Opthalmology Vis. Sci.* **59**: 5824.

Lonser, R. R., R. Schiffman, R. A. Robison, J. A. Butman, Z. Quezado, M. L. Walker, P. F. Morrison, S. Walbridge, G. J. Murray, D. M. Park, *et al.* 2007. Image-guided, direct convective delivery of glucocerebrosidase for neuronopathic Gaucher disease. *Neurology* **68**: 254–261.

McGlynn, R., K. Dobrenis and S. U. Walkley. **2004**. Differential subcellular localization of cholesterol, gangliosides, and glycosaminoglycans in murine models of mucopolysaccharide storage disorders. *J. Comp. Neurol.* **480**: 415–426.

Meijering, B. D. M., L. J. M. Juffermans, A. van Wamel, R. H. Henning, I. S. Zuhorn, M. Emmer, A. M. G. Versteilen, W. J. Paulus, W. H. van Gilst, K. Kooiman, *et al.* 2009. Ultrasound and Microbubble-Targeted Delivery of Macromolecules Is Regulated by Induction of Endocytosis and Pore Formation. *Circ. Res.* **104**: 679–687.

Morris, G. 2015. Purification and Uptake Studies of Recombinant Human N-α-D-Acetylglucosaminidase from Sf9 Insect Cells. MSc Thesis. University of Victoria.

Moschos, S. A., S. W. Jones, M. M. Perry, A. E. Williams, J. S. Erjefalt, J. J. Turner, P. J. Barnes, B. S. Sproat, M. J. Gait and M. A. Lindsay. **2007**. Lung delivery studies using siRNA conjugated to TAT(48-60) and penetratin reveal peptide induced reduction in gene expression and induction of innate immunity. *Bioconjug. Chem.* **18**: 1450–1459.

Neufeld, E. F. 1980. The uptake of enzymes into lysosomes: an overview. *Birth Defects Orig. Artic. Ser.* **16**: 77–84.

Obermeier, B., R. Daneman and R. M. Ransohoff. **2013**. Development, maintenance and disruption of the blood-brain barrier. *Nat. Med.* **19**: 1584–1596.

Ohmi, K., D. S. Greenberg, K. S. Rajavel, S. Ryazantsev, H. H. Li and E. F. Neufeld. **2003**. Activated microglia in cortex of mouse models of mucopolysaccharidoses I and IIIB. *Proc. Natl. Acad. Sci.* **100**: 1902–1907.

Pall. 2017. Protein purification and handling. Port Washington, NY: Pall Corporation. Available online at www.pall.com.

Pardridge, W. M. 2007. Blood-brain barrier delivery. *Drug Discov. Today* **12**: 54–61.

Pardridge, W. M. 2015. Targeted delivery of protein and gene medicines through the blood-brain barrier. *Clin. Pharmacol. Ther.* **97**: 347–361.

Parenti, G., G. Andria and A. Ballabio. **2015**. Lysosomal Storage Diseases: From Pathophysiology to Therapy. *Annu. Rev. Med.* **66**: 471–486.

Pfeifer, T. A., M. M. Guarna, E. M. Kwan, G. Lesnicki, D. A. Theilmann, T. A. Grigliatti and D. G. Kilburn. **2001**. Expression Analysis of a Modified Factor X in Stably Transformed Insect Cell Lines. *Protein Expr. Purif.* **23**: 233–241.

Platt, F. M. 2017. Emptying the stores: lysosomal diseases and therapeutic strategies. *Nat. Rev. Drug Discov.* **17**: 133–150.

Rapoport, M., L. Salman, O. Sabag, M. S. Patel and H. Lorberboum-Galski. **2011**. Successful TAT-mediated enzyme replacement therapy in a mouse model of mitochondrial E3 deficiency. *J. Mol. Med.* **89**: 161–170.

Roy, E., J. Bruyère, P. Flamant, S. Bigou, J. Ausseil, S. Vitry and J. M. Heard. **2012**. GM130 gain-of-function induces cell pathology in a model of lysosomal storage disease. *Hum. Mol. Genet.* **21**: 1481–1495.

Rubin, L. L. and J. M. Staddon. **1999**. the Cell Biology of the. *Annu. Rev. Neurosci.* **22**: 11–28.

Ryazantsev, S., W.-H. Yu, H.-Z. Zhao, E. F. Neufeld and K. Ohmi. **2007**. Lysosomal accumulation of SCMAS (subunit c of mitochondrial ATP synthase) in neurons of the mouse model of mucopolysaccharidosis III B. *Mol. Genet. Metab.* **90**: 393–401.

Schroder, B. A., C. Wrocklage, A. Hasilik and P. Saftig. **2010**. The proteome of the lysosomes. *Proteomics* **10**: 4053–4076.

Schwarze, S. R., A. Ho, A. Vocero-akbani, S. F. Dowdy, S. R. Schwarze, A. Ho and A. Vocero-akbani. **1999**. In vivo Protein Transduction : Delivery of a Biologically Active Protein into the Mouse. **285**: 1569–1572.

Settembre, C., A. Fraldi, L. Jahreiss, C. Spampanato, C. Venturi, D. Medina, R. de Pablo, C. Tacchetti, D. C. Rubinsztein and A. Ballabio. **2008**. A block of autophagy in lysosomal storage disorders. *Hum. Mol. Genet.* **17**: 119–129.

Settembre, C., A. Fraldi, D. L. Medina and A. Ballabio. **2013**. Signals from the lysosome: a control centre for cellular clearance and energy metabolism. *Nat. Rev. Mol. Cell Biol.* **14**: 283–296.

Shriver, Z., I. Capila, G. Venkataraman and R. Sasisekharan. **2012**. Heparin and Heparan Sulfate: Analyzing Structure and Microheterogeneity. In: *Heparin - A Century of Progress* (R. Lever, B. Mulloy, and C. P. Page, eds), pp. 159–176. Springer Berlin Heidelberg, Berlin, Heidelberg.

Siegenthaler, J. A., F. Sohet and R. Daneman. **2013**. "Sealing off the CNS": Cellular and molecular regulation of blood-brain barriergenesis. *Curr. Opin. Neurobiol.* **23**: 1057–1064. Elsevier Ltd.

Stellwagen, E. 2009. Gel Filtration. In: *Methods in Enzymology*, pp. 373–385. Elsevier Inc.

Suhorutsenko, J., N. Oskolkov, P. Arukuusk, K. Kurrikoff, E. Eriste, D. M. Copolovici and Ü. Langel. **2011**. Cell-penetrating peptides, PepFects, show no evidence of toxicity and immunogenicity in vitro and in vivo. *Bioconjug. Chem.* **22**: 2255–2262.

Tiller, G. E., T. J. Mueller, M. E. Dockter and W. G. Struve. **1984**. Hydrogenation of Triton X-l 00 Eliminates Its Fluorescence and Ultraviolet Light Absorption while Preserving Its Detergent Properties. *Anal. Biochem.* **141**: 262–266.

Treat, L. H., N. McDannold, N. Vykhodtseva, Y. Zhang, K. Tam and K. Hynynen. **2007**. Targeted delivery of doxorubicin to the rat brain at therapeutic levels using MRI-guided focused ultrasound. *Int. J. Cancer* **121**: 901–907.

Truelson, S. N., R. R. Jantzen and F. Y. M. Choy. **2011**. Sanfilippo syndrome: Identification and removal of a cryptic splice site in α-N-acetylglucosaminidase cDNA for potential improved expression and enzyme replacement therapy. *J. Biochem. Mol. Biol. Post Genomic Era* **1**: 131–136.

Truxal, K. V., H. Fu, D. M. McCarty, K. A. McNally, K. L. Kunkler, N. A. Zumberge, L. Martin, S. C. Aylward, L. N. Alfano, K. M. Berry, *et al.* 2016. A prospective one-year natural history study of mucopolysaccharidosis types IIIA and IIIB: Implications for clinical trial design. *Mol. Genet. Metab.* **119**: 239–248.

Uttara, B., A. Singh, P. Zamboni and R. Mahajan. **2009**. Oxidative Stress and Neurodegenerative Diseases: A Review of Upstream and Downstream Antioxidant Therapeutic Options. *Curr. Neuropharmacol.* **7**: 65–74.

Valstar, M. J., H. T. Bruggenwirth, R. Olmer, R. A. Wevers, F. W. Verheijen, B. J. Poorthuis, D. J. Halley and F. A. Wijburg. **2010**. Mucopolysaccharidosis type IIIB may predominantly present with an attenuated clinical phenotype. *J. Inherit. Metab. Dis.* **33**: 759–767.

Valstar, M. J., G. J. G. Ruijter, O. P. van Diggelen, B. J. Poorthuis and F. A. Wijburg. **2008**. Sanfilippo syndrome: A mini-review. *J. Inherit. Metab. Dis.* **31**: 240–252.

Villani, G. R. D., C. D. Domenico, A. Musella, F. Cecere, D. D. Napoli and P. D. Natale. **2009**. Mucopolysaccharidosis IIIB: Oxidative damage and cytotoxic cell involvement in the neuronal pathogenesis. *Brain Res.* **1279**: 99–108.

Villani, G. R. D., N. Gargiulo, R. Faraonio, S. Castaldo, E. Gonzalez y Reyero and P. Di Natale. **2007**. Cytokines, neurotrophins, and oxidative stress in brain disease from mucopolysaccharidosis IIIB. *J. Neurosci. Res.* **85**: 612–622.

Watson, H. A., R. J. Holley, K. J. Langford-Smith, F. L. Wilkinson, T. H. van Kuppevelt, R. F. Wynn, J. E. Wraith, C. L. R. Merry and B. W. Bigger. **2014**. Heparan Sulfate Inhibits Hematopoietic Stem and Progenitor Cell Migration and Engraftment in Mucopolysaccharidosis I. *J. Biol. Chem.* **289**: 36194–36203.

Weber, B. 1996. Cloning and expression of the gene involved in Sanfilippo B syndrome (mucopolysaccharidosis III B). *Hum. Mol. Genet.* **5**: 771–777.

Weber, B., J. J. Hopwood and G. Yogalingam. **2001**. Expression and Characterization of Human Recombinant and α-N-Actylglucosaminidase. *Protein Expr. Purif.* **21**: 251–259.

Whitelock, J. M. and R. V. Iozzo. **2005**. Heparan Sulfate: A Complex Polymer Charged with Biological Activity. *Chem. Rev.* **105**: 2745–2764.

Wilkinson, F. L., R. J. Holley, K. J. Langford-Smith, S. Badrinath, A. Liao, A. Langford-Smith, J. D. Cooper, S. A. Jones, J. E. Wraith, R. F. Wynn, *et al.* 2012. Neuropathology in Mouse Models of Mucopolysaccharidosis Type I, IIIA and IIIB. *PLoS ONE* **7**: e35787.

Winkler, E. A., R. D. Bell and B. V. Zlokovic. **2011**. Central nervous system pericytes in health and disease. *Nat. Neurosci.* **14**: 1398–1405.

Wolak, D. J. and R. G. Thorne. **2013**. Diffusion of Macromolecules in the Brain: Implications for Drug Delivery. *Mol. Pharm.* **10**: 1492–1504.

Xiao, G. and L.-S. Gan. **2013**. Receptor-mediated endocytosis and brain delivery of therapeutic biologics. *Int. J. Cell Biol.* **2013**: 703545.

Xu, S., L. Wang, M. El-Banna, I. Sohar, D. E. Sleat and P. Lobel. **2011**. Large-volume intrathecal enzyme delivery increases survival of a mouse model of late infantile neuronal ceroid lipofuscinosis. *Mol. Ther.* **19**: 1842–1848.

Yamaguchi, Y. 2001. Heparan sulfate proteoglycans in the nervous system: their diverse roles in neurogenesis, axon guidance, and synaptogenesis. *Semin. Cell Dev. Biol.* **12**: 99–106.

Yogalingam, G. and J. J. Hopwood. **2001**. Molecular genetics of mucopolysaccharidosis type IIIA and IIIB: Diagnostic, clinical, and biological implications. *Hum. Mutat.* **18**: 264–281.

Zhang, X., L. Wan, S. Pooyan, Y. Su, C. R. Gardner, M. J. Leibowitz, S. Stein and P. J. Sinko. **2004**. Quantitative Assessment of the Cell Penetrating Properties of RI-Tat-9: Evidence for a Cell Type-Specific Barrier at the Plasma Membrane of Epithelial Cells. *Mol. Pharm.* **1**: 145–155.

Zhang, X.-Y., A. Dinh, J. Cronin, S.-C. Li and J. Reiser. **2008**. Cellular uptake and lysosomal delivery of galactocerebrosidase tagged with the HIV Tat protein transduction domain. *J. Neurochem.* **104**: 1055–1064.

Zhao, H. G., H. H. Li, G. Bach, A. Schmidtchen and E. F. Neufeld. **1996**. The molecular basis of Sanfilippo syndrome type B. *Proc. Natl. Acad. Sci.* **93**: 6101–6105.

Zhao, K.-W. and E. F. Neufeld. **2000**. Purification and Characterization of Recombinant Human α-N-Acetylglucosaminidase Secreted by Chinese Hamster Ovary Cells. *Protein Expr. Purif.* **19**: 202–211.

Zlokovic, B. V. 2005. Neurovascular mechanisms of Alzheimer's neurodegeneration. *Trends Neurosci.* **28**: 202–208.

Zuchero, Y. J. Y., X. Chen, N. Bien-Ly, D. Bumbaca, R. K. Tong, X. Gao, S. Zhang, K. Hoyte, W. Luk, M. A. Huntley, *et al.* 2016. Discovery of Novel Blood-Brain Barrier Targets to Enhance Brain Uptake of Therapeutic Antibodies. *Neuron* **89**: 70–82. Elsevier Inc.

Appendix

```
                                                                                                                ACC ATG
01    GAC GAG GCC CGG GAG GCG GCG GCC GTG CGG GCG CTC GTG GCC CGG CTG CTG GGG CCA GGC
61    CCC GCG GCC GAC TTC TCC GTG TCG GTG GAG CGC GCT CTG GCT GCC AAG CCG GGC TTG GAC
121   ACC TAC AGC CTG GGC GGC GGC GGC GCG GCG CGC GTG CGG GTG CGC GGC TCC ACG GGC GTG
181   GCG GCC GCC GCG GGG CTG CAC CGC TAC CTG CGC GAC TTC TGT GGC TGC CAC GTG GCC TGG
241   TCC GGC TCT CAG CTG CGC CTG CCG CGG CCA CTG CCA GCC GTG CCG GGG GAG CTG ACC GAG
301   GCC ACG CCC AAC CGT TAC CGC TAT TAC CAG AAT GTG TGC ACG CAA AGC TAC TCC TTC GTG
361   TGG TGG GAC TGG GCC CGC TGG GAG CGA GAG ATA GAC TGG ATG GCG CTG AAT GGC ATC AAC
421   CTG GCA CTG GCC TGG AGC GGC CAG GAG GCC ATC TGG CAG CGG GTG TAC CTG GCC TTG GGC
481   CTG ACC CAG GCA GAG ATC AAT GAG TTC TTT ACT GGT CCT GCC TTC CTG GCC TGG GGG CGA
541   ATG GGC AAC CTG CAC ACC TGG GAT GGC CCC CTG CCC CCC TCC TGG CAC ATC AAG CAG CTT
601   TAC CTG CAG CAC CGG GTC CTG GAC CAG ATG CGC TCC TTC GGC ATG ACC CCA GTG CTG CCT
661   GCA TTC GCG GGG CAT GTT CCC GAG GCT GTC ACC AGG GTG TTC CCT CAG GTC AAT GTC ACG
721   AAG ATG GGC AGT TGG GGC CAC TTT AAC TGT TCC TAC TCC TGC TCC TTC CTT CTG GCT CCG
781   GAA GAC CCC ATA TTC CCC ATC ATC GGG AGC CTC TTC CTG CGA GAG CTG ATC AAA GAG TTT
841   GGC ACA GAC CAC ATC TAT GGG GCC GAC ACT TTC AAT GAG ATG CAG CCA CCT TCC TCA GAG
901   CCC TCC TAC CTT GCC GCA GCC ACC ACT GCC GTC TAT GAG GCC ATG ACT GCA GTG GAT ACT
961   GAG GCT GTG TGG CTG CTC CAA GGC TGG CTC TTC CAG CAC CAG CCG CAG TTC TGG GGG CCC
1021  GCC CAG ATC AGG GCT GTG CTG GGA GCT GTG CCC CGT GGC CGC CTC CTG GTT CTG GAC CTG
1081  TTT GCT GAG AGC CAG CCT GTG TAT ACC CGC ACT GCC TCC TTC CAG GGC CAG CCC TTC ATC
1141  TGG TGC ATG CTG CAC AAC TTT GGG GGA AAC CAT GGT CTT TTT GGA GCC CTA GAG GCT GTG
1201  AAC GGA GGC CCA GAA GCT GCC CGC CTC TTC CCC AAC TCC ACC ATG GTA GGC ACG GGC ATG
1261  GCC CCC GAG GGC ATC AGC CAG AAC GAA GTG GTC TAT TCC CTC ATG GCT GAG CTG GGC TGG
1321  CGA AAG GAC CCA GTG CCA GAT TTG GCA GCC TGG GTG ACC AGC TTT GCC GCC CGG CGG TAT
1381  GGG GTC TCC CAC CCG GAC GCA GGG GCA GCG TGG AGG CTA CTG CTC CGG AGT GTG TAC AAC
1441  TGC TCC GGG GAG GCC TGC AGG GGC CAC AAT CGT AGC CCG CTG GTC AGG CGG CCG TCC CTA
1501  CAG ATG AAT ACC AGC ATC TGG TAC AAC CGA TCT GAT GTG TTT GAG GCC TGG CGG CTG CTG
1561  CTC ACA TCT GCT CCC TCC CTG GCC ACC AGC CCC GCC TTC CGC TAC GAC CTG CTG GAC CTC
1681  ACT CGG CAG GCA GTG CAG GAG CTG GTC AGC TTG TAC TAT GAG GAG GCA AGA AGC GCC TAC
1741  CTG AGC AAG GAG CTG GCC TCC CTG TTG AGG GCT GGA GGC GTC CTG GCC TAT GAG CTG CTG
1801  CCG GCA CTG GAC GAG GTG CTG GCT AGT GAC AGC CGC TTC TTG CTG GGC AGC TGG CTA GAG
1861  CAG GCC CGA GCA GCG GCA GTC AGT GAG GCC GAG GCC GAT TTC TAC GAG CAG AAC AGC CGC
1921  TAC CAG CTG ACC TTG TGG GGG CCA GAA GGC AAC ATC CTG GAC TAT GCC AAC AAG CAG CTG
1981  GCG GGG TTG GTG GCC AAC TAC TAC ACC CCT CGC TGG CGG CTT TTC CTG GAG GCG CTG GTT
2041  GAC AGT GTG GCC CAG GGC ATC CCT TTC CAA CAG CAC CAG TTT GAC AAA AAT GTC TTC CAA
2101  CTG GAG CAA GCC TTC GTT CTC AGC AAG CAG AGG TAC CCC AGC CAG CCG CGA GGA GAC ACT
2161  GTG GAC CTG GCC AAG AAG ATC TTC CTC AAA TAT TAC CCC GGC TGG GTG GCC GGC TCT TGG
2221  GGT GGA ***TAC GCT CGA GCT GCA GCA CGT CAG GCA CGT GCA*** TAA
```

Supplementary Figure 1. Human recombinant α-N-acetylglucosaminidase cDNA sequence (Ashmead, 2016)

Numbering corresponds to base pairs encoding Naglu-PTD4X. The re-introduced stop codon (underlined) follows the synthetic protein transduction domain, PTD4 (33bp, bold and italics).

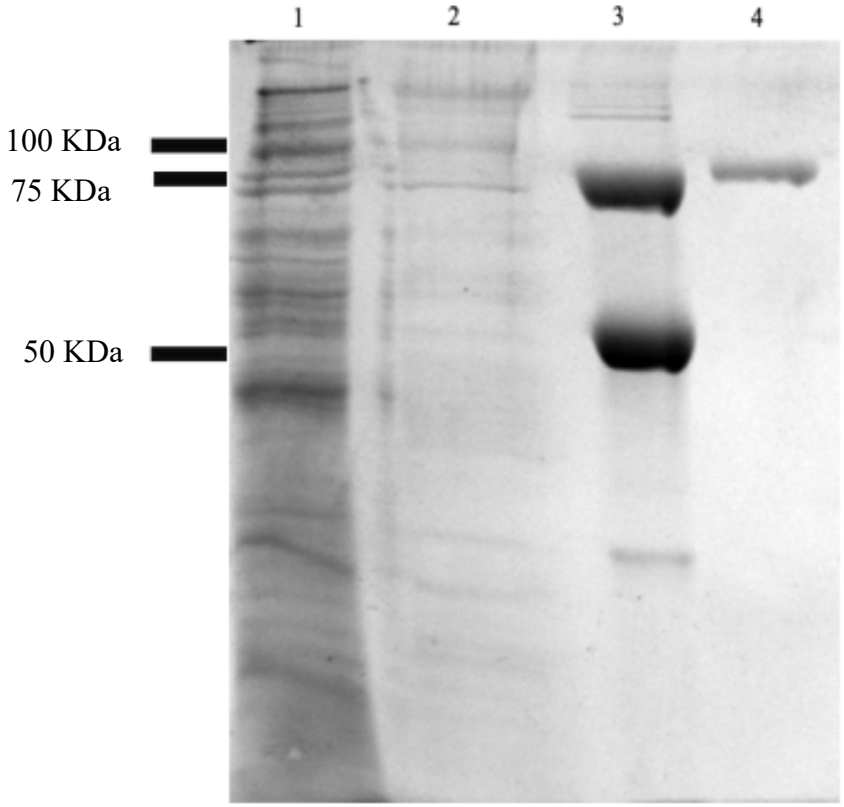

Supplementary Figure 2 SDS-PAGE gel visualizing results of three-step preparative-scale purification of Naglu-PTD4-V5/His by Coomassie blue stain (Morris, 2015)
Lane contents: (1) Crude medium (2) post-MMC (3) pre- SEC (4) post-SEC. Naglu-PTD4-V5/His was purified to homogeneity from Sf9 media by a three-stage protocol with a custom packed XK 26/20 Capto™ MMC column, HiPrep Butyl-S columns, and HiLoad Superdex 200 column. The apparent molecular weight of Naglu-PTD4-V5/His was 75kDa, which was confirmed by anti-Naglu immunoblotting.

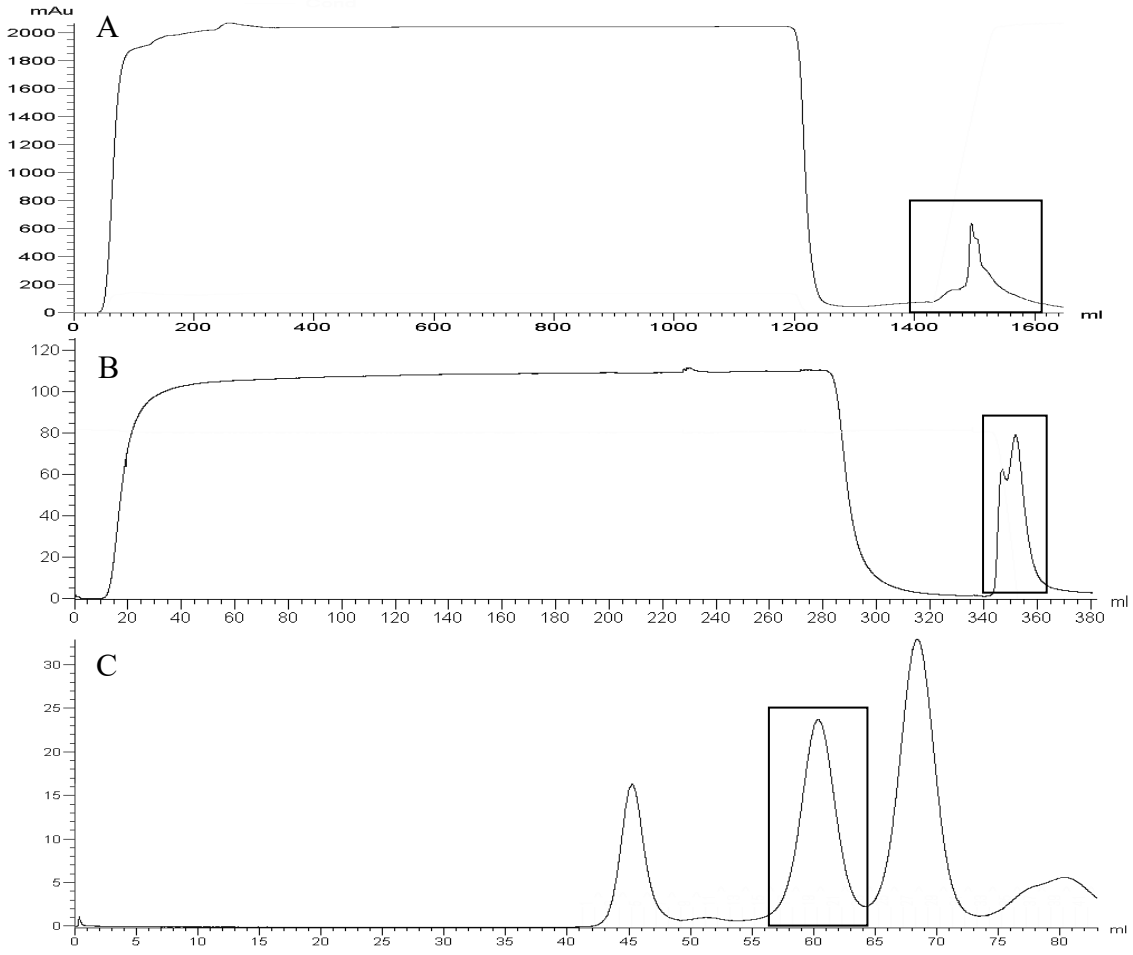

Supplementary Figure 3 Protein elution profiles of preparative-scale purification of Naglu-PTD4-V5/His (Morris, 2015)

Figures are as follows: A) MMC purification B) HIC purification C) SEC purification. Naglu-PTD4-V5/His was purified to homogeneity from Sf9 media by a three-stage protocol with a custom packed XK 26/20 Capto™ MMC column, HiPrep Butyl-S columns, and HiLoad Superdex 200 column. Peaks framed by black boxes indicate fractions of high Naglu activity. These fractions were carried forward to proceeding steps.

Supplementary Table 1 Yield of active Naglu through three-step preparative-scale purification of Naglu-PTD4-V5/His (Morris, 2015)

Step	Volume (mL)	Activity (units)	Protein (mg)	Specific Activity (units/mg)	Purification (fold)	Yield (%)
Medium	1068	34900	306	114	1	100
Pre-HIC	288	28600	86	333	3	82
Pre-SEC	1	17600	1	17600	150	50
Post-SEC	8	9100	0.4	23000	200	26

One unit of activity corresponds to 493 arbitrary fluorescent units as measured by the fluorogenic 4MU Naglu activity assay. Protein concentrations was determined by a Bradford protein concentration assay. Equilibrated crude medium was the baseline for comparison to determine percent yield calculations. For the medium, pre-HIC, and pre-SEC samples, activity and protein values were calculated immediately prior to column loading. For the post-SEC sample, activity and protein values were calculated immediately following column elution. All values represent the average from three separate purification runs.

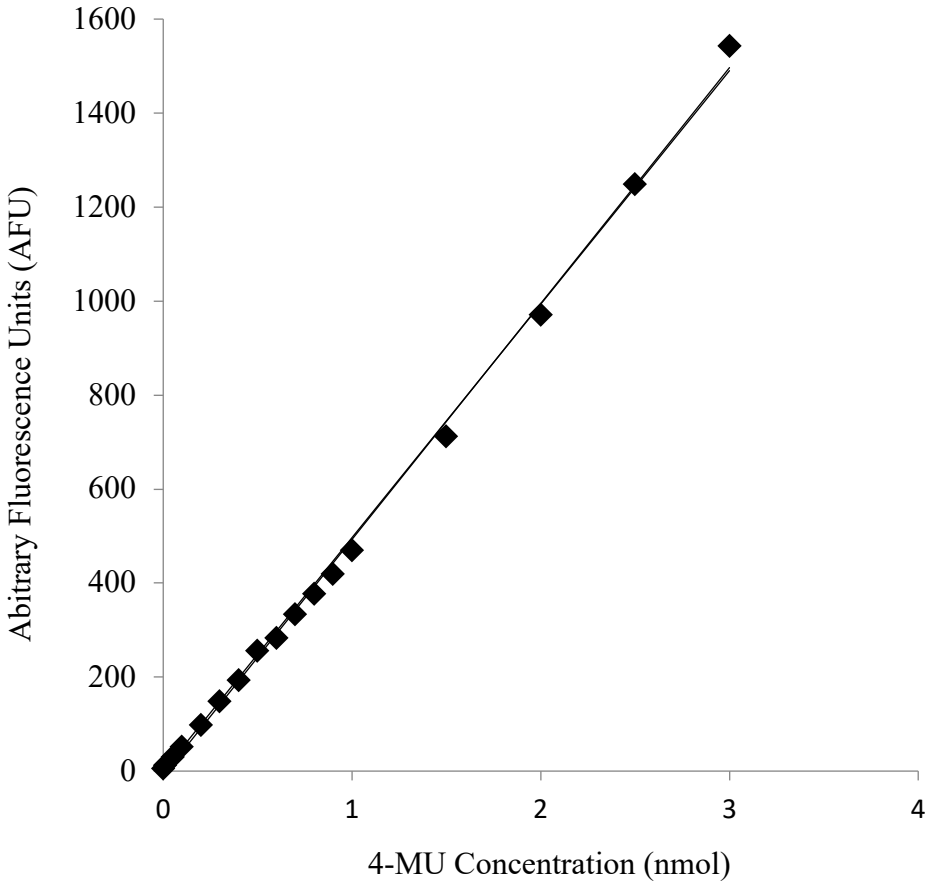

Supplementary Figure 4 4-MU standard curve for calculation of active units of Naglu
A stock solution of 1 mM 4-MU in 50:50 ddH_2O: methanol was prepared. The 4-MU stock was diluted 1:100 with 0.5M glycine NaOH (pH 10.5). The arbitrary fluorescence of a range of 4-MU concentrations was measured on a Novaspec® visible fluorometer (360 nm narrow band excitation filter, 415 nm sharp cut emission detection filer, span fully counter-clockwise). One unit of activity corresponded to 493 arbitrary fluorescent units based on the equation of the line.

Supplementary Table 2 Values for 4-MU standard curve for calculation of active units of Naglu

Concentration of 4-MU (nmol)	Experimental replicates (Arbitrary Fluorescence Units; AFU)			Average
0	5	5	5	5
0.01	12	13	12	12
0.05	34	29	26	30
0.1	51	53	50	51
0.2	103	92	99	98
0.3	150	148	150	149
0.4	204	187	191	194
0.5	286	241	240	256
0.6	289	275	286	283
0.7	351	320	330	334
0.8	380	376	376	377
0.9	426	412	419	419
1	472	469	468	470
1.5	715	709	715	713
2	971	977	967	972
2.5	1309	1218	1218	1248
3	1489	1493	1649	1544

A stock solution of 1 mM 4-MU in 50:50 ddH_2O: methanol was prepared. The 4-MU stock was diluted 1:100 with 0.5M glycine NaOH (pH 10.5). The arbitrary fluorescence of a range of 4-MU concentrations was measured on a Novaspec® visible fluorometer (360 nm narrow band excitation filter, 415 nm sharp cut emission detection filer, span fully counter-clockwise).